Effects of Stress History of Sand on the Shaft Resistance of Large Displacement Piles

Fabrizio Di Camillo

A Thesis

in

The Department

of

Building, Civil and Environmental Engineering

Presented in Partial Fulfilment of the Requirements for the Degree of Master of Applied Science at Concordia University
Montreal, Quebec, CANADA

March 2014

CONCORDIA UNIVERSITY
Department of Building, Civil and Environmental Engineering

This is to certify the thesis prepared

By: **Fabrizio Di Camillo**

Entitled: **Effects of Stress History of Sand on the Shaft Resistance of Large Displacement Piles**

and submitted in partial fulfilment of the requirements for the degree of

Master of Applied Science (Civil Engineering)

complies with the regulations of the University and meets with the accepted standards with respect to originality and quality.

Signed by the final examining committee:

_____ Chair
Dr. A. Zsaki

_____ Examiner
Dr. L. Lin

_____ Examiner
Dr. S. Williamson

_____ Supervisor
Dr. A. Hanna

Approved by _____
Dr. M. Zaheeruddin, Chair, Department of Building, Civil & Environmental Engineering

_____2014 _____
Dr. C. Trueman
Dean, Faculty of Engineering and Computer Science

ABSTRACT

Effects of Stress History of Sand on the Shaft Resistance of Large Displacement Piles

An experimental investigation on the coefficient of earth pressure of overconsolidated cohesionless soil developed around displacement piles was conducted. An instrumented prototype set-up and model pile was developed in the laboratory. The set-up was capable of measuring the total load, the shaft resistance acting on the pile and the overconsolidation ratio in the sand mass. Overconsolidated sand was prepared by placing the sand in the testing tank in layers, each subjected to a predetermined compaction effort. The stresses in the sand mass were measured by means of pressure transducer units placed in selected locations in the testing tank. The model piles were driven into the sand mass to a selected depth. Pile load tests were conducted at a constant rate of penetration at different depths.

The pile capacity was determined from load-displacement curves. The shaft resistance and, hence, the coefficient of earth pressure around the pile were determined. The results showed that the coefficient of earth pressure is heavily dependent on the stress history of the sand mass. A theoretical model was developed to incorporate the effects of overconsolidation of the sand on the shaft resistance of driven piles in cohesionless soils.

ACKNOWLEDGEMENTS

Foremost, I would like to express my sincere gratitude to my supervisor, Professor A. M Hanna, for his valuable guidance, patience, constant support and dear encouragement throughout the course of this work. His insight and wisdom shaped the setting which provided the means to complete this research.

I would like to thank my friend and colleague, Rouzbeh Vakili, for many inspiring and fruitful discussions throughout the duration of this program.

I am thankful to the technical staff at Concordia University, including Mr. Joseph Hrib, Mr. Jaime Yeargans, Mr. Luc Demers and Mr. Brian Cooper for the many hours of consultation and technical assistance.

My return to school would not have been possible without my wife, Johanna Ballhaus, to whom I am sincerely indebted for her utter support and patience.

TO MY MOTHER

TABLE OF CONTENTS

List of Figures

List of Tables

List of Symbols

K_a = Active coefficient of earth pressure

K_p = Passive coefficient of earth pressure

K_o = Coefficient of earth pressure at rest

K' = Intercept corresponding to an overconsolidation ratio of 1 on a log p vs. log OCR plot

K_{rb}^{o} = Rebound coefficient of earth pressure

$K_{o(ocr)}$ = Coefficient of earth pressure at rest for overconsolidated soils

$K_{o(nc)}$ = Coefficient of earth pressure at rest for normally consolidated soils

OCR = Overconsolidation Ratio

K_z = Lateral earth pressure coefficient at depth z

K_s = Lateral average earth pressure coefficient developed around driven shafts

ϕ' = Effective soil friction angle

δ' = Angle of friction between the soil and the wall

α = Slope of the backfill surface

θ = Inclination angle of the back face of the wall

σ_h = Horizontal stresses acting on a soil element

σ_v = Vertical stresses acting on a soil element

h = Slope of the line

λ = A factor which depends on the mechanical properties of sand

μ = Poisson's ratio

Q_u = Ultimate pile bearing capacity

Q_s = Shaft resistance

Q_t = Tip resistance

τ = Shear stress at the pile-sand interface

σ'_h = Lateral effective stress

δ_z = Mobilized angle of friction on the pile-sand interface at depth z

σ'_{vz} = Effective vertical stress

D = Pile diameter

L = Pile embedment length

f_s = Average unit shaft resistance over the embedment length

A_s = The surface area of the shaft embedded in sand

f_s = Average skin friction along the pile shaft

τ = Average shear stress on the outer surface of the soil annulus

r = Radius of the pile

n = Factor indicating the magnitude of the outer radius of the soil annulus

N_c, N_q, N_γ = Bearing capacity factors

q_p = Unit point resistance

$\gamma_1 D$ = Pressure at the pile tip level (Terzaghi)

D_f = Embedment length

c = Soil cohesion

$\gamma' h$ = Overburden effective stress

D_r = Relative density

α_T = Coefficient dependent on the relative depth and friction angle

A_k and B_k = Capacity factors

B = Pile diameter

Q_{test} = Shaft resistance measured experimentally

Q_{calc} = Calculated shaft resistance by the beta method

P_p = Passive earth pressure acting on the pile shaft

W_p = Weight of the pile

δ = Friction angle between the pile and the sand mass

$P_{u\alpha}$ = Uplift coefficient for batter piles

P_u = Pullout capacity of piles

γ = Unit weight of sand

R= Radius of influence as proposed by Berezantzev (1965)

$\Delta\zeta$ = Angle of rotation in radian

F_1 = Resultant earth pressure force acting on the rectangle ahde

F_2 = Resultant earth pressure force acting on the triangle ahc

β = Angle segment AC makes with the horizontal at pile tip measured positive in the downward direction.

E_{i+1} and E_i = Normal forces acting on slice *i*

ω_{i+1} and ω_i = Tilt of the sides of slice *i*

ϕ_{Bi} = Mobilized angle of friction at mid-point of the base of slice i

ϕ_{Si+1} and ϕ_{Si} = Average mobilized friction angle along the sides of slice i

W_i = Weight of slice i

F_i = Resultant of other external forces acting on slice i

FH_i and FV_i = Horizontal and vertical components of F_i

G_s = Specific gravity of soil solids

W_s = Weight of soil solids

W_w = Weight of water

Chapter 1

Introduction

1.1 Preface

Pile foundations are used around the world on a wide range of applications where shallow foundations fail to provide the capacity needed to support the structure. The skin friction developed along the pile's shaft is a function of the horizontal stresses acting on the shaft which, in turn, depend on the coefficient of earth pressure of the surrounding soil. For driven piles in sand, the earth pressure developed around the shaft, and hence the friction resistance depend on many factors such as the method of installation, the relative depth, the friction angle between the pile and the sand mass, relative density and the stress history of the soil. The latter, represented by the term overconsolidation ratio (OCR) of the sand mass, is at large excluded from conventional design theories for predicting the skin resistance of driven piles and accordingly the pile capacity. This is due to the complexity of the mechanisms which govern the stresses surrounding the pile's shaft.

1.2 Motivation

Innovation and efficiency have structure advances in science and engineering through paradigms of collective effort in pursuit of understanding and foresight. The motivation behind the work presented herein is led by the desire to contribute to the above mentioned joint effort.

The effects of stress history in foundation design in cohesionless soils are difficult to quantify because sampling of undisturbed sands, and hence laboratory testing is challenging. When a sand mass undergoes loading, stresses in the sand mass increase and remain locked in the soil fabric after loading. When a pile is driven into such sand mass, the resistance is influenced by the stresses locked in the sand mass. This effect can significantly improve the performance of the pile

and result in a more efficient and economical design. The research herein is intended to promote the progress of efficient design.

1.3 Research Objectives

The main objectives of this research program are as follows:

1. To conduct a thorough review of the pertinent literature and to discuss the limitations of the existing earth pressure theories and its application to the prediction of the shaft resistance of driven piles in sand.
2. To conduct an experimental investigation to measure the shaft resistance in a sand mass subject to different levels of overconsolidation.
3. To develop a design theory that incorporates the stress history of the sand mass a given relative depth of driven piles in the prediction of shaft resistance.

1.4 Organization of Thesis

Chapter one introduces the subject of study and the research objectives of the thesis. Chapter two reports a review of the literature pertinent to the subject. The experimental set-up, testing program and experimental results are presented in chapter three. Analyses of the test results are presented in chapter four. Finally, the conclusions and recommendations are given in chapter five.

Chapter 2

Literature Review

2.1 General

The load-carrying capacity of pile foundations is generally determined by two different methods of analysis: the static approach which relates the soil properties to the load-carrying capacity of the pile; and the dynamic approach where the ultimate bearing capacity is estimated from field data. In this investigation, the static approach will be considered. Although numerous studies have been reported in the literature over the years pertaining to earth pressure theories, the question on the effects of overconsolidation on the earth pressure developed around the shaft of a driven pile remains unanswered. This is mainly due to the complexity of the mechanism in hand. The average coefficient of earth pressure, K_s, developed around the shaft of driven piles depends on many factors such as the relative density of the sand mass, the initial state of overconsolidation of the sand mass prior to installation, and the pile diameter. In order to present a model that incorporates the above mentioned factors, it is prudent to begin with a review of the earth pressure theories reported in the literature followed by a historical account of various theoretical models capable of predicting pile capacity.

2.2 Historical Developments of Earth Pressure Theories

Coulomb, F (1776) presented a theory for active and passive earth pressures behind retaining walls. His theory was based on the following assumptions: the presence of friction forced between the wall and the soil; the rupture surface is a plane surface; the failure wedge is a rigid body undergoing translation; the soil is isotropic and homogeneous and the frictional resistance is distributed uniformly along the rupture surface. For cohesionless backfill, Coulomb's active and passive earth pressure coefficients are as follows:

$$K_a = \frac{\cos^2(\phi'-\theta)}{\cos^2\cos(\delta'+\theta)\left[1+\sqrt{\frac{\sin(\delta'+\phi')\sin(\phi'-\alpha)}{\cos(\delta'+\theta)\cos(\theta-\alpha)}}\right]^2} \tag{2.1}$$

$$K_p = \frac{\cos^2(\phi'+\theta)}{\cos^2\cos(\delta'-\theta)\left[1-\sqrt{\frac{\sin(\delta'-\phi')\sin(\phi'+\alpha)}{\cos(\delta'-\theta)\cos(\theta-\alpha)}}\right]^2} \tag{2.2}$$

Where

$\phi' =$ soil friction angle.

$\delta' =$ angle of friction between the soil and the wall.

$\alpha =$ slope of the backfill surface

$\theta =$ inclination angle of the back face of the wall

Rankine (1857) considered the soil in a state of plastic equilibrium. With a Mohr-Coulomb construction for the case of vertical frictionless wall, cohesionless soil and

horizontal backfill, Rankine's active and passive coefficients of earth pressure are as follows:

$$K_a = \tan^2(45 - \frac{\phi'}{2}) \tag{2.3}$$

$$K_p = \tan^2(45 + \frac{\phi'}{2}) \tag{2.4}$$

Donath (1891) was first to introduce the concept of the coefficient of earth pressure at rest K_o. It is defined for the condition where no lateral movement exists between soil elements. According to Donath, it is defined as the ratio of horizontal (σ_h) to vertical (σ_v) stresses acting on a soil element and is given in Eq. (2.5)

$$K_o = \frac{\sigma_h}{\sigma_v} \tag{2.5}$$

Jaky (1944) derived a theoretical expression for the coefficient of earth pressure at rest (K_o) from the analysis of the stress field in a wedge prism of granular material inclined at an angle of repose (ϕ) to the horizontal and asserted that the vertical plane *OC* in Figure 2.1 is the pressure at rest. Region *ABO* is assumed to have a state of stress shown by a Coulomb element whereas the stress distributions on region BCO are assumed parabolic. Solving the two differential equations of equilibrium and setting $x = 0$ yields the following:

$$K_o = \frac{\sigma_x}{\sigma_y} = (1 - \sin\phi)\frac{1 + 2/3\sin\phi}{1 + \sin\phi} \tag{2.6}$$

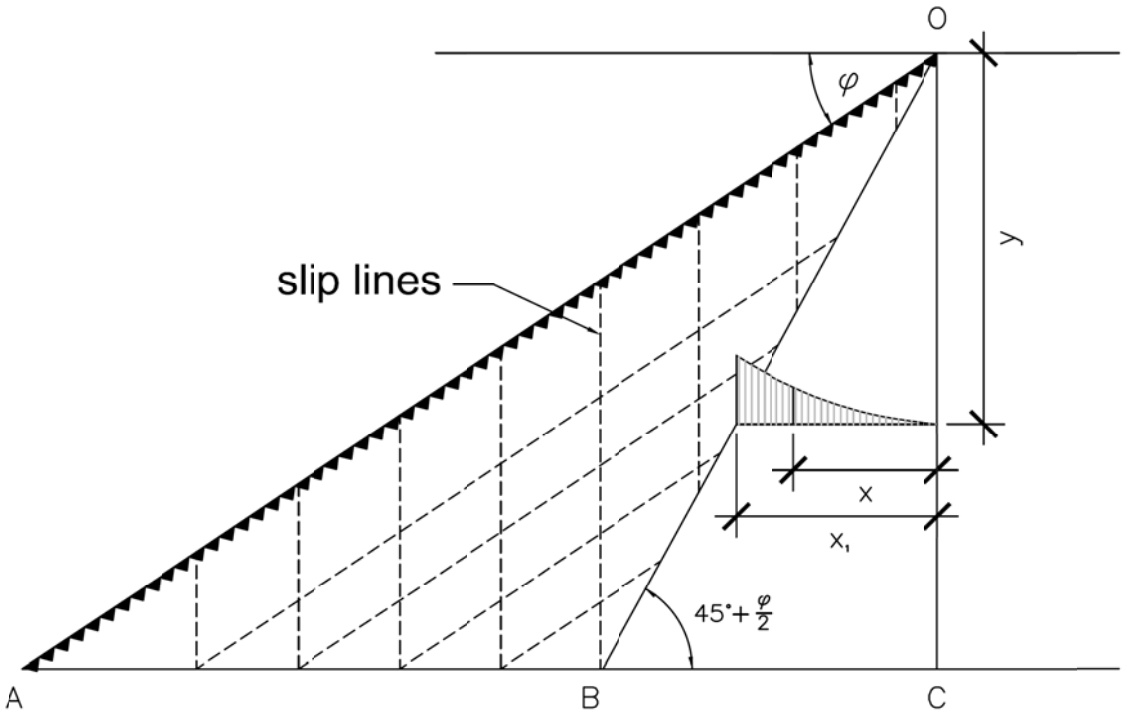

Figure 2.1 Distribution of stresses in Jaky's at rest earth pressure solution (after Jaky, 1944)

Jaky (1948) simplified Eq. (2.6) by dropping the fraction term resulting in the widely accepted form of Eq. (2.7).

$$K_o = 1 - \sin\phi \tag{2.7}$$

Hendron (1963) designed and improved oedometer and presented the results of uniaxial compression tests on sand. He indicated that the value of K_o increased as the angle as shear resistance decreased down to $\phi = 20°$ and thereafter, the value of for a given overconsolidation ratio (OCR) decreased. He conducted a series of recompression test and indicated that the values of K_o for the recompression curves with OCR=2 and

OCR = 4 were greater than the values of K_o for the rebound curves at all times, even at the end of the rebound curve. He also reported that values of K_o for rounded sand where lower than the values of K_o for angular sand with the same values of the angle of friction. Hendron suggested that K_o may not be a function of the angle of shear resistance alone. However he proposed the following expression for K_o as a function of ϕ:

$$K_o = \frac{1}{2}\left[\frac{1+\frac{\sqrt{5}}{8}-3\frac{\sqrt{5}}{8}(\sin\phi)}{1-\frac{\sqrt{5}}{8}+3\frac{\sqrt{5}}{8}(\sin\phi)}\right] \tag{2.8}$$

Brooker and Ireland (1965) investigated the effects of stress history on the coefficient of earth pressure at rest of remoulded cohesive soils in one dimensional compression tests. They concluded that the stress history of soil governs the value of the coefficient of earth pressure at rest. They stated that for values of the overconsolidation ratio OCR>20, the values of K_o appear to asymptotically approach the values of K_p. They presented their findings in charts of K_o vs. OCR for five types of clay.

Schmidt (1966) discussed the validity of Jaky's equation for K_o and presented a formula based on the work reported by **Brooker and Ireland (1965)** and **Hendron (1963)**. The following expression was proposed:

$$K_{rb}^{o} = K'\left(\frac{\sigma_{v-\max}}{\sigma_v}\right)^h \approx (1-\sin\phi)\left(\frac{\sigma_{v-\max}}{\sigma_v}\right)^h \tag{2.9}$$

From the plots of $Log(OCR)$ vs. $Log(\frac{\sigma_h}{\sigma_v})$, Schmidt found a straight line relationship on which *h* is the slope of the line and only varies with sand type, and K' is the intercept corresponding to an overconsolidation ratio $\frac{\sigma_{1(\max)}}{\sigma_1} = 1$

Alpan (1967) proposed the following empirical relationship for overconsolidated sands after analysing the experimental data presented by **Brooker and Ireland (1965)** and proposed the following empirical expression:

$$\frac{K_{o(ocr)}}{K_{o(nc)}} = (OCR)^{\lambda} \tag{2.10}$$

Where λ is a factor which depends on the mechanical properties of sand, namely the angle of shear resistance and found that λ increases with a decrease in the angle of friction of the soil.

Wroth (1975) presented an assessment of insitu stress measurement and deformation characteristics and proposed the following relationship for the coefficient of earth pressure at rest in overconsolidated soils:

$$K_{o(ocr)} = K_{o(nc)} OCR - \left[\frac{\mu}{1-\mu}\right](OCR - 1) \tag{2.11}$$

where $K_{o(nc)}$ is given by Jaky (Eq. 2.7) and μ is Poisson's ratio.

Meyerhof (1976) proposed the following equation after **Schmidt (1966)** and stated that for most soils, a value of 0.5 for the parameter *h* in Schmidt's equation is suitable.

$$K_{o(ocr)} = (1 - \sin\phi)\sqrt{OCR} \tag{2.12}$$

Sherif and Mackey (1977) studied the pressures applied on retaining walls during compaction and stated that 40-90% of the induced lateral pressures exerted on the walls due to compaction remain in the soil mass as residual stresses.

Mayne and Kulhawy (1982) conducted extensive research in clays and sands by way of statistical analysis and presented the following expression for normally consolidated sands:

$$K_{o(nc)} = 1 - 0998\sin\phi \tag{2.13}$$

Furthermore, from linear regression analysis, they presented the following expressions for clays and dense sands:

$$K_{o(nc)} = 1 - 1.003\sin\phi \tag{2.14}$$

and

$$K_{o(oc)} = (1 - \sin\phi)\left(\frac{OCR}{OCR_{\max}^{(1-\sin\phi)}}\right) + \frac{3}{4} \times \left(1 - \frac{OCR}{OCR_{\max}}\right) \tag{2.15}$$

The authors stated that the value of $OCR_{\max} = OCR$ during rebound and the expression above reduces to the following:

$$K_{o(oc)} = (1 - \sin\phi)OCR^{(1-\sin\phi)} \tag{2.16}$$

Mayne (1995) conducted research with results of CPT tests and propose the following expression for the coefficient of earth pressure at rest in overconsolidated sands:

$$K_{o(oc)} = 0.192(q_c / p_a)^{0.22}(\sigma'_{vo} / p_a)^{-0.31} OCR^{(0.27)} \quad (2.17)$$

Duncan and Seed (1986) studied the effects of compaction induced stresses and presented hysteric analytical models and procedures generated by multiple cycles of loading and unloading in order to evaluate the earth pressures resulting from the compaction of soil. They stated that the strength of a sand mass is dependent to a large extent on the stress level within the sand mass, and compaction can significantly increase these stresses. They concluded that compaction represents a form of overconsolidation to the extent that transient loading conditions induces stresses that remain in the sand mass, to some extent, after the removal of the load.

Hanna and Al-Romheim (2008) conducted an experimental investigation on the at-rest earth pressure of overconsolidated cohesionless backfill acting on retaining walls. The results of the experiments were used to examine the empirical formulations available in the literature and presented earlier in this section. The authors reported that the experimental results agreed well with the formulations in the literature up to OCR values of 3. A new empirical formula was proposed by the authors, which corresponded well with the experimental results for a wide range of overconsolidation values. The following empirical formula was presented:

$$K_{o(oc)} = (1 - \sin\phi) OCR^{(\sin\phi - 0.18)} \quad (2.18)$$

2.3 Pile Capacity and Shaft Resistance

The load carrying capacity of pile foundations is conventionally divided into two components: the load carried by the shaft and the load at the pile tip. The basic pile problem is depicted in Figure 2.1.

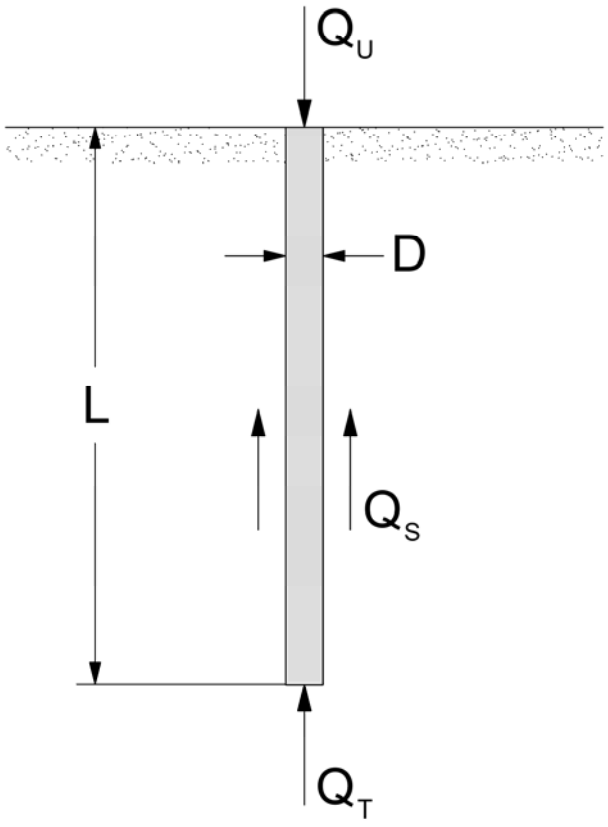

Figure 2.2 Loading mechanism for a single pile under axial compression

Thus,

$$Q_u = Q_s + Q_p \tag{2.19}$$

where

Q_u = ultimate pile bearing capacity

Q_s = shaft resistance

Q_t = tip resistance

The shaft resistance of pile foundations is conventionally estimated by integrating the pile-sand shear stress τ over the surface of the shaft as proposed by **Dorr (1922)** and given on Eq. 2.23. Dorr assumed that the frictional resistance developed at the surface of a pile is proportional to the lateral effective stress σ'_h. Thus, the shear stress τ at the soil-pile interface at a given depth as a function of lateral stress can be expressed as follows:

$$\tau = \sigma'_h \tan\delta_z \tag{2.20}$$

where

$\delta_z =$ the mobilized angle of friction on the pile-sand interface at depth z.

The ratio of the effective normal stress σ'_h to the effective vertical stress σ'_{vz} is usually referred to as the lateral earth pressure coefficient K_z.

Thus,

$$\sigma'_h = K_z \sigma'_{vz} \tag{2.21}$$

Combining Eq. (2.2) and (2.3)

$$\tau = K_z \sigma'_{vz} \tan\delta_z \tag{2.22}$$

Assuming symmetry about the pile's axis at a given depth, Q_s can be obtained by integrating the following expression over the pile depth,

$$Q_s = \pi D \int_0^L (\tau) dz \tag{2.23}$$

$$Q_s = \pi D \int_0^L \sigma'_{vz} K_z \tan\delta_z dz \tag{2.24}$$

Where

$D =$ pile diameter.

$L =$ pile embedment length.

In practice, the values of K_z and δ_z are generally averaged over the embedment depth and are denoted by K_s and δ, respectively. The effective vertical stress σ_{vz} is conventionally assumed to be the overburden effective stress $\gamma' h$ at a given depth. With these simplifications, Eq. 2.24 becomes:

$$Q_s = \pi D K_s \tan\delta \int_0^L \gamma' L dz \tag{2.25}$$

$$Q_s = \pi D K_s \tan\delta \gamma' \frac{L^2}{2} \tag{2.26}$$

$$Q_s = (\frac{1}{2} K_s \tan\delta \gamma' L) A_s = f_s A_s \tag{2.27}$$

Where

$f_s =$ The average unit shaft resistance over the embedment length.

$A_s =$ The surface area of the shaft embedded in sand.

The difficulty associated with the estimation of shaft resistance using Eq. (2.27) comes from the estimation of the value of K_s for a given soil condition. The magnitude of K_s

has been found to depend on many factors, such as the angle of shear resistance of the sand mass, pile shape, pile installation method, loading conditions, deformation characteristics of the sand mass, and the initial state of stress of the soil **(McClelland et el, 1967).**

Terzaghi (1943) was among the first authors to present a solution for the bearing capacity of a single pile. The failure mechanism involves the downward movement of the cone shaped region below the pile tip displacing the soil outward and upward with the failure surface ending at the level of the pile tip. Terzaghi stated that the only difference between cylindrical pears and pile foundation is the method of construction. Hence, the formulation for pile capacity follows from Figures 2.3, 2.4 and 2.5, on which the failure mechanism is shown. Terzaghi suggested that the point resistance of a single pile in sand can be estimated from an extension of his solution for shallow foundations as follows:

$$q_p = 1.3cN_c + \gamma_1 D_f N_q + 0.6\gamma B N_\gamma \qquad (2.28)$$

Where

N_c, N_q, N_γ = bearing capacity factors

D_f = embedment length

c = soil cohesion

γ = soil unit weight

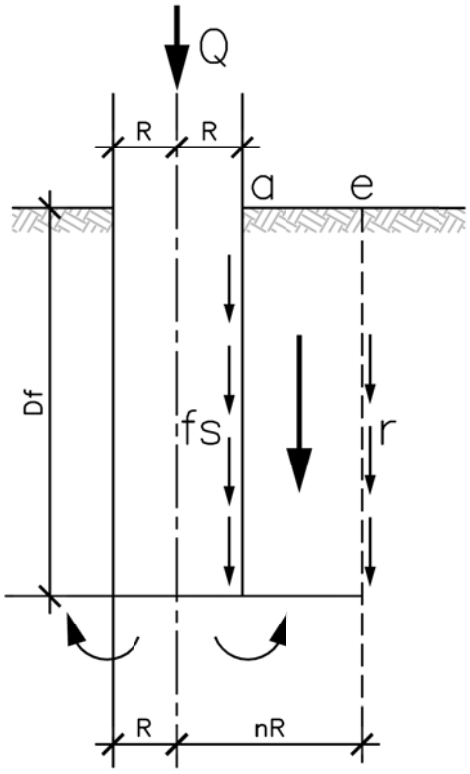

Figure 2.3 Failure mechanism for cylindrical piers (after from Terzaghi, 1943)

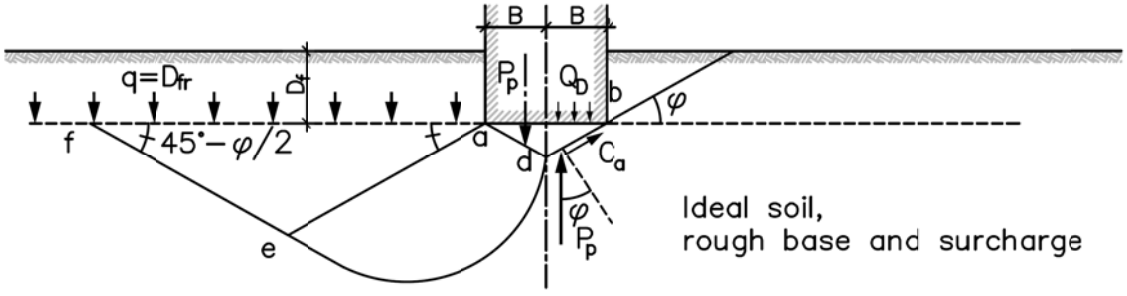

Figure 2.4 Failure mechanism at the tip of cylindrical piers (after from Terzaghi, 1943)

The difference between Eq. 2.28 and that for circular shallow foundations is in the term ($\gamma_1 D$) which here represents the pressure at the pile tip level exerted by the resultant

effect of the weight of the soil annulus D'B'B DEAA'E', the pile shaft resistance, f_s, and the shear forces on the outer surface of the soil annulus (Figure 2.5).

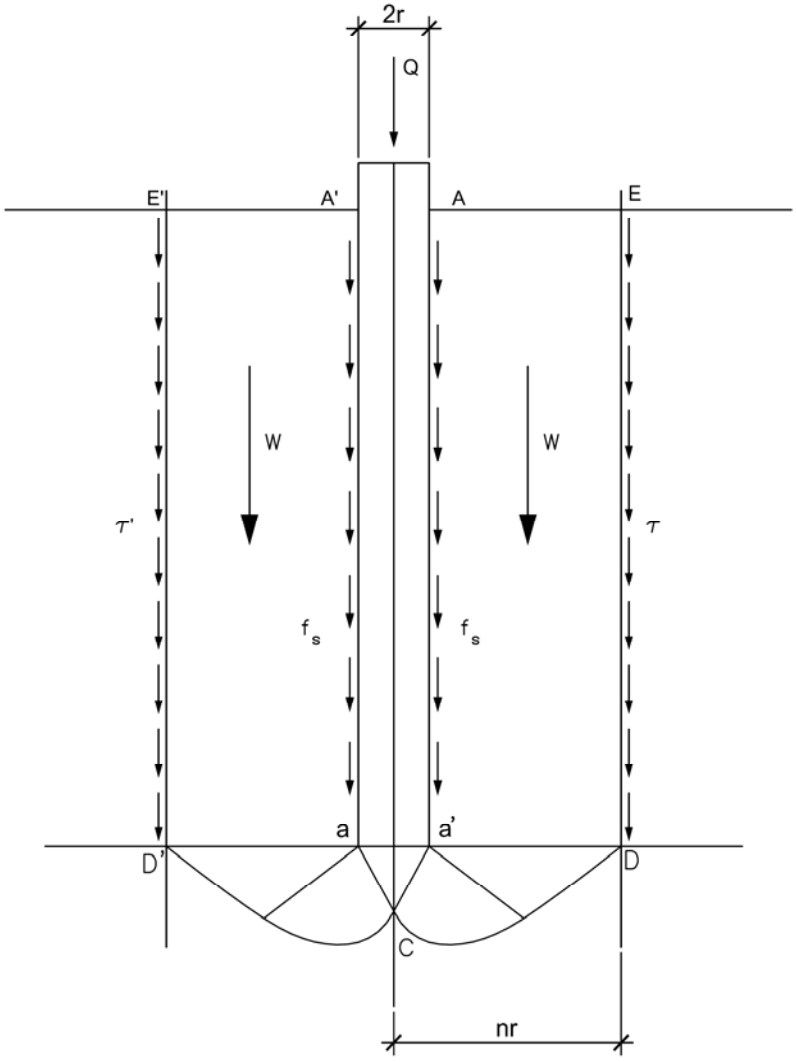

Figure 2.5 Terzaghi's failure mechanism (after Terzaghi, 1943)

The magnitude of the term γ_1 is given by:

$$\gamma_1 = \gamma + 2\frac{f_s + n\tau}{(n^2 - 1)r} \tag{2.29}$$

where

γ = soil unit weight

f_s = average skin friction along the pile shaft

τ = average shear stress on the outer surface of the soil annulus

r = the radius of the pile

n = a factor indicating the magnitude of the outer radius of the soil annulus

The limitations of Terzaghi's theory in practical application rise from the fact that he did not offer a method of solution for determining the skin friction nor the shear stress developed along the outer surface of the soil annulus in order to determine γ_1.

Meyerhof (1951) presented a general bearing capacity theory where the assumed failure mechanism in contrast with that assumed by Terzaghi for shallow and deep foundations are shown in Figures 2.6 and 2.7, respectively. Three failure zones are identified: wedge ABC which is a zone in an elastic state of equilibrium acting as part of the foundation; a zone BCD of radial shear, and a zone of mixed shear BDEF. Figure 2.7 shows the mechanism for the case of deep foundations where the failure surface reverts back onto the foundation shaft. Both Terzaghi's model as well as Meyerhof's model attempt to incorporate the effects of shaft resistance into ultimate bearing capacity formulations of a strip footing at any depth. In Meyerhof's approach, the earth coefficient at the shaft, K_s, must be assumed in advance (K_s=0.5 for loose sand and 1.0 for dense sand).

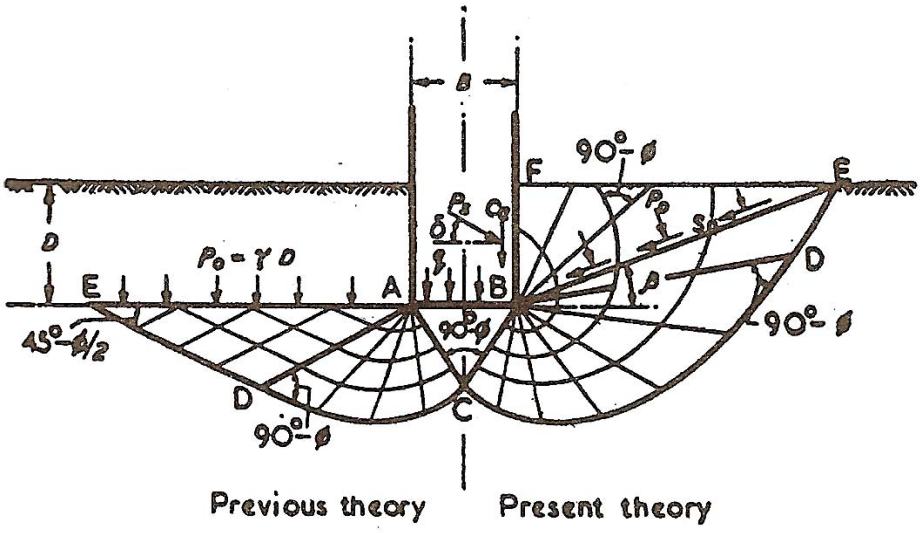

Figure 2.6 Meyerhof's assumed failure mechanism for shallow foundations (adapted from Meyerhof, 1951)

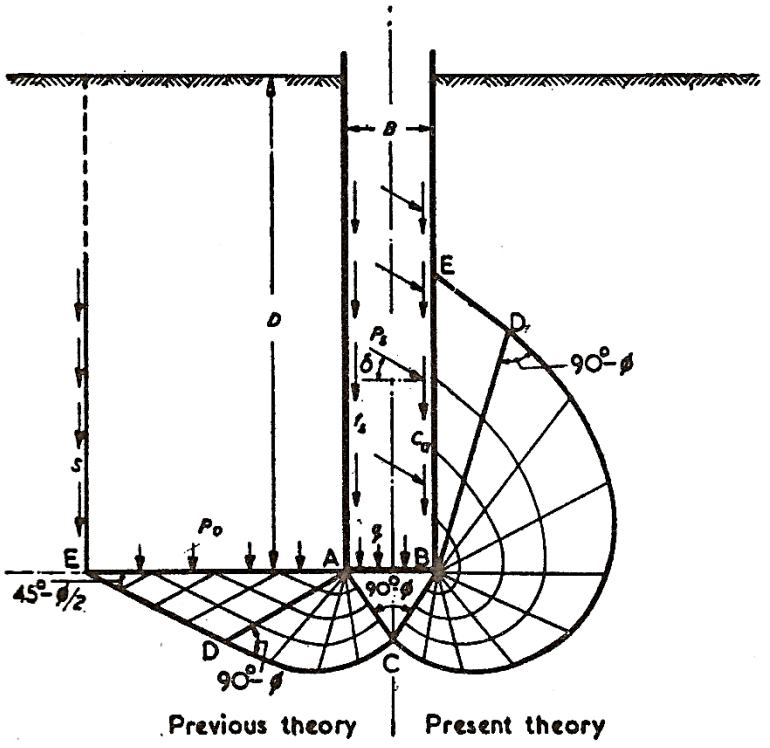

Figure 2.7 Meyerhof's assumed failure mechanism for deep foundations (adapted from Meyerhof, 1951)

Skempton et al. (1953) presented an analytical model for estimating the bearing capacity of a single pile in cohesionless soil. The failure mechanism included curved surfaces with circles as their vertical cross sections. From equilibrium conditions and many trial calculations with the circle center assuming different positions, the capacity factor N_q with minimal value is obtained. The author stated that the shear stress along the outer vertical surface of the model depends on both the friction angle and the relative density of the soil. The mechanism is shown in Figure 2.8.

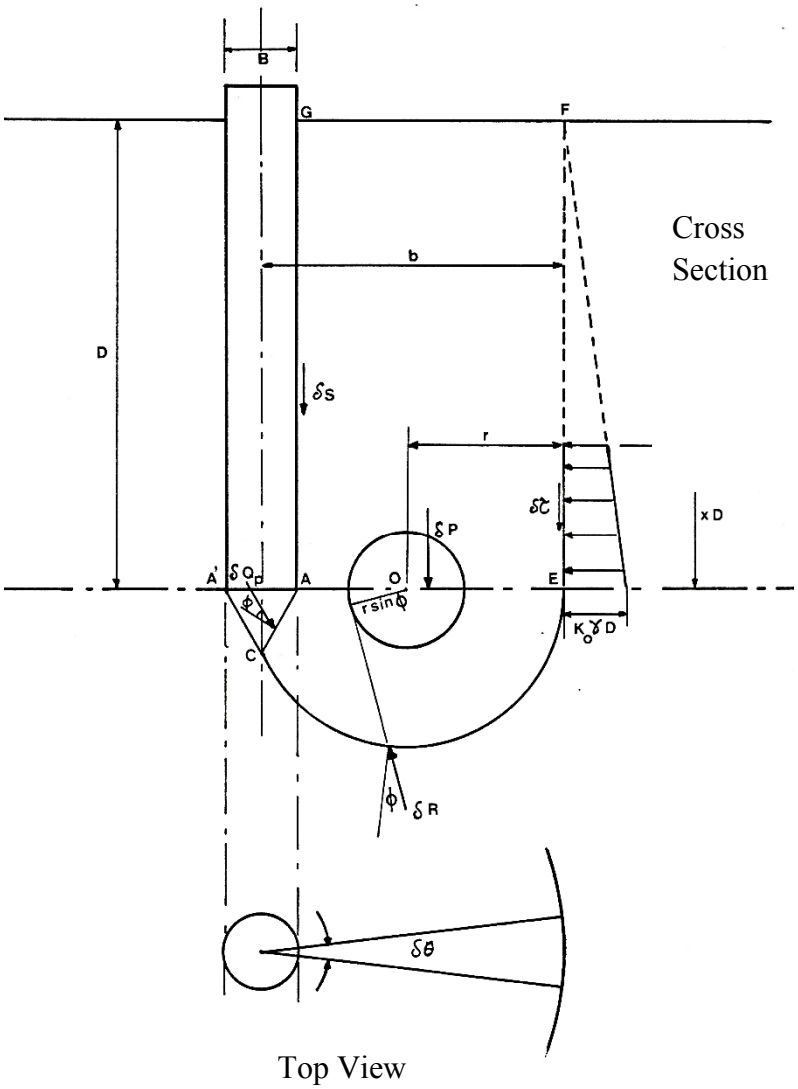

Figure 2.8 Skempton's assumed failure mechanism (adapted from Nguyen, 1991, after Skempton et al., 1953)

Berenzantzev et al. (1961) introduced a mechanism of failure similar to that assumed by Terzaghi in 1943. The direction of the shear force, T, in the assumed failure mechanism (Figure 2.9) opposes the downward movement of the soil annulus. The resulting surcharge, q_t, at the pile tip level is then the difference between the weight of the soil, W, and the shear force, T, acting on the outer surface of the failure mechanism and is expressed as follows:

$$q_t = \alpha_T \gamma D \tag{2.30}$$

where

α_T = coefficient dependent on the relative depth and friction angle

γ = unit weight of sand

D = pile embedment length

The ultimate point capacity is then given by the following expression:

$$q_u = A_k \gamma B + B_k q_t \tag{2.31}$$

where

A_k and B_k = capacity factors

B= pile diameter

It should be noted that the above mentioned mechanism does not account for shaft resistance.

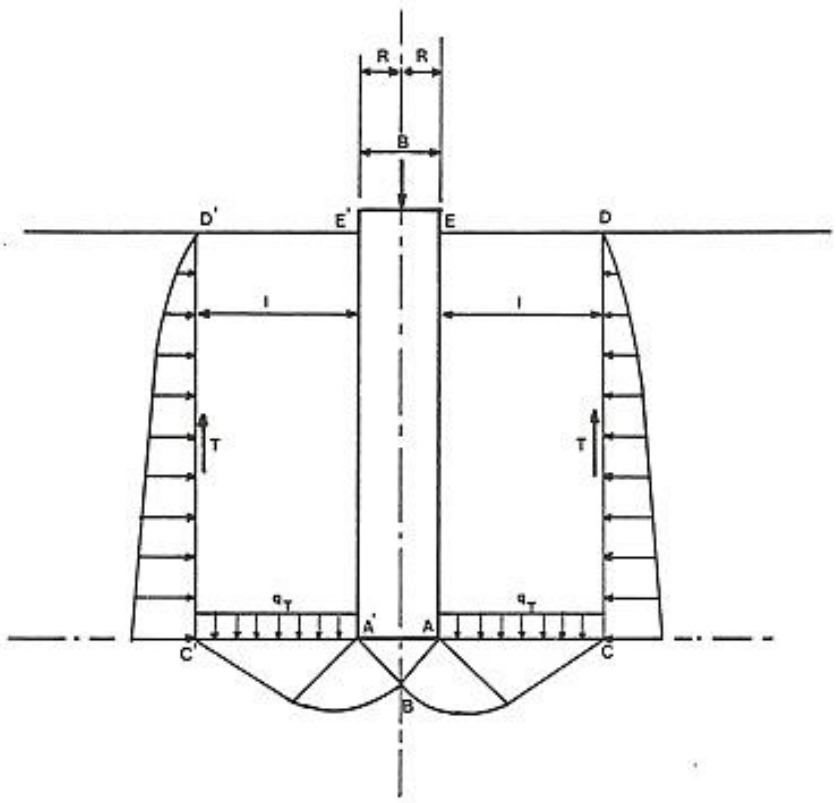

Figure 2.9 Berenzantzev's failure mechanism (adapted from Nguyen, 1991, after Berenzantzev et al., 1961)

Janbu and Senneset (1974) introduced a two dimensional variable failure mechanism in which the shear failure zones beneath the pile tip change geometry according to different failure conditions. The authors derived the following capacity factor:

$$N_q = \tan^2(45^o + \frac{\phi}{2}) e^{(\pi - 2\beta)(\tan\phi)} \tag{2.32}$$

where β is the angle the terminal failure surfaces AC and A'C' make with the horizontal at the pile tip level (Figure 2.10).

Janbu (1976) further developed Eq. 2.32 to account for partial shear strength mobilization along the failure surfaces and proposed the following:

$$N_q = \tan^2(45^o + \frac{\phi}{2})e^{(\pi - 2\beta)(F\tan\phi)} \tag{2.33}$$

Where F represents the degree of shear strength mobilization.

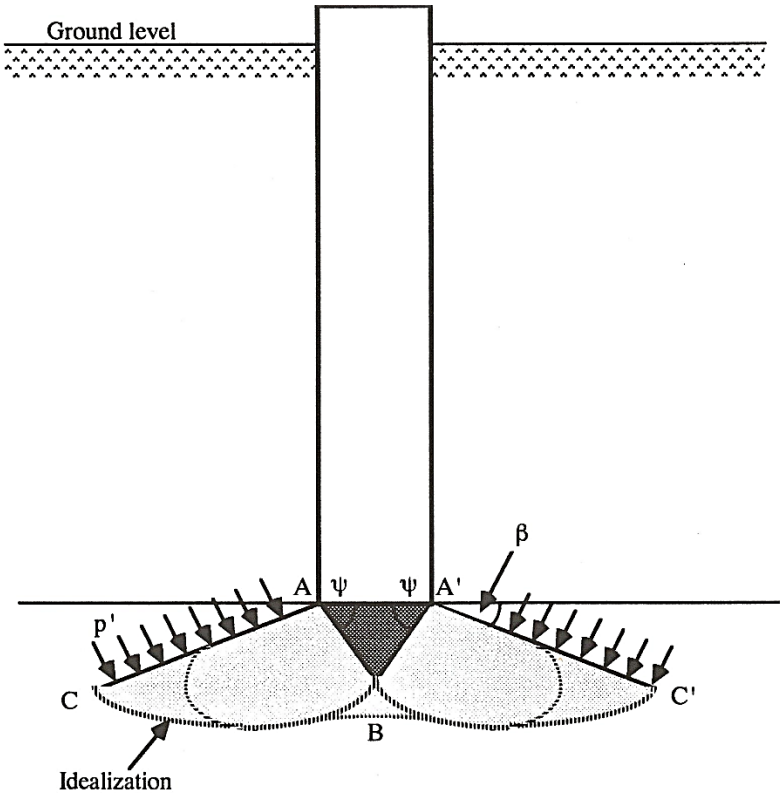

Figure 2.10 Janbu's failure mechanism (after Janbu and Senneset, 1974)

Once again it should be noted that the failure mechanism proposed by Janbu and Senneset excludes the effects of shaft resistance in pile capacity computations. Furthermore, with the exception of a few authors **(Terzaghi, 1943, Meyerhof, 1951, Durgunoglu and Michell, 1973)**, factors such as shaft resistance, f_s, and parameters such as K_o and K_s are precluded in bearing capacity theories.

In the literature, the work pertaining to skin friction developed on driven piles is predominately based on pile load tests both in the field and laboratory.

Broms and Silberman (1964) conducted compression, tension and torsion experimental tests on model piles with a length of 30 inches and outside diameters of 3/4 and 1-1/2 inches in order to evaluate the major factors affecting the shaft resistance of piles driven in uniform fine quartz sand. The factors considered were the dimensions of the piles, method of loading, the roughness of the pile surface and the relative density of the cohesionless soil surrounding the pile. The authors compared the experimental results for shaft resistance with those obtained from calculations using Eq. (2.27) with a value of $K_s = 1$ as proposed by Dorr (1922). The authors reported that for sand with low relative density $(D_r < 0.35)$ the average calculated values of the ratio $\frac{Q_{test}}{Q_{calc}}$ were 0.6, 0.23 and 0.02 for compression, tension and torsion tests, respectively. In the case of high relative density $(D_r > 0.70)$, the average ratios $\frac{Q_{test}}{Q_{calc}}$ were 9.84, 4.57 and 2.84 for compression, tension and torsion tests, respectively. Similar results were obtained by **Muller (1939)**. The authors concluded that the relative density of the sand surrounding the pile had a large effect on the measured skin friction of driven piles. The high relative density for the above mentioned test was achieved by way of a vibrating table. The possibility of an increase on the locked in stresses due to the sand preparation technique and stress history and hence, the potential effect on shaft resistance is not addressed by the authors.

Meyerhof (1976) stated that reliable values of K_s can only be obtained from load test on piles. The author analyzed available results of load tests on short piles above the critical

depth and presented the chart in Figure 2.2 for normally consolidated sands showing the variations of K_s with friction angle for various pile shapes and methods of installation. Figure 2.2 shows that the value of K_s for a given initial friction angle differs considerably from a lower limit of approximately K_o for bored piles to about four times that value for driven piles in dense sands.

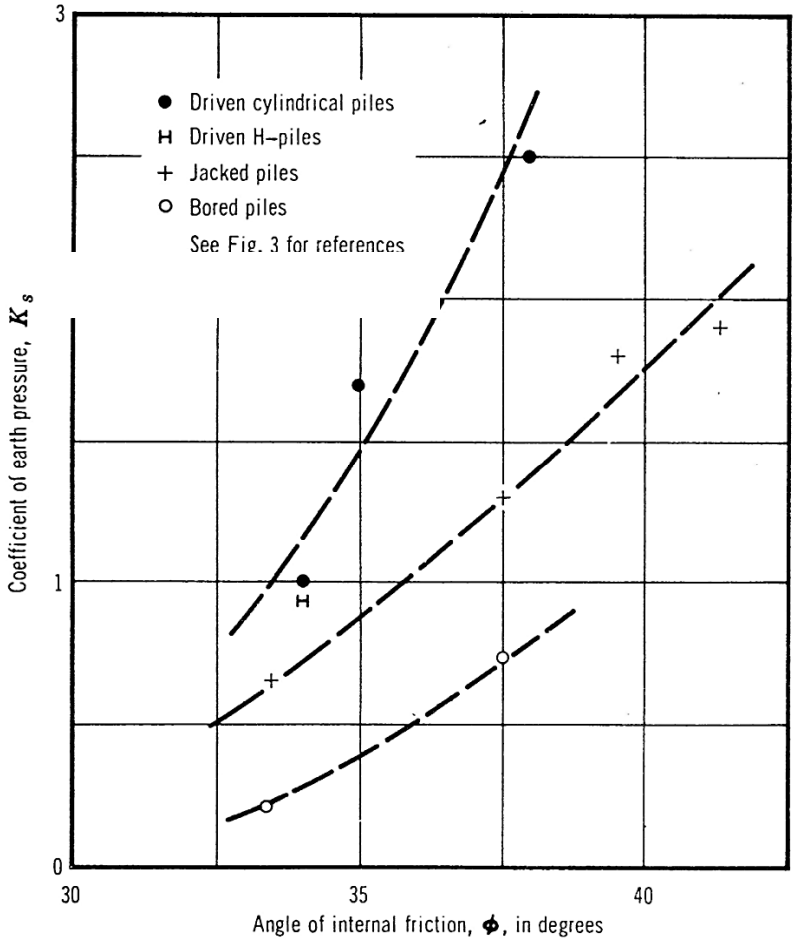

Figure 2.11 Coefficient of earth pressure on shaft of piles above critical depth in sand (adapted after Meyerhof, 1976)

Hanna and Afram (1986) conducted an experimental investigation in order to evaluate the pullout capacity of single vertical and batter piles in sand. The authors based their

investigation on the work of **Meyerhof (1973)** who proposed the following formulation for the pullout capacity of piles and anchors:

$$P_u = P_p \sin \delta \pi D + W_p \tag{2.34}$$

where

P_p = the passive earth pressure acting on the pile shaft

D = the pile diameter

W_p = the weight of the pile

δ = the friction angle between the pile and the sand mass

The authors proposed the following empirical formula to predict the uplift capacity of batter piles in sand:

$$P_{u\alpha} = P_u \cos(\frac{\alpha}{2}) \quad \text{for} \quad (0 \le \alpha \le 30^o) \tag{2.35}$$

where

α = angle of inclination of the pile with the with the vertical

and

$$P_u = \frac{1}{2} \gamma \pi D L^2 K_{u\alpha} + W_p \cos \alpha \tag{2.36}$$

where

γ = unit weight of sand

$K_{u\alpha}$ = uplift coefficient for batter piles

L = the length of the pile

The effects of the overconsolidation of the sand mass were not addressed in this investigation.

Hanna and Ghaly (1992) conducted an experimental and theoretical investigation on the effects of overconsolidation and the earth pressure at rest on the uplift capacity of screw anchors in sand. They determined that vibratory compaction represents a form of loading and unloading inducing high horizontal stresses in the sand mass which result in an increase of the coefficient of earth pressure at rest, and hence the overconsolidation of the sand deposit. They concluded that the uplift capacity of anchors increased significantly when installed in overconsolidated sand.

Hanna and Nguyen (2002) presented an axisymetric model to predict the capacity of a single, vertical pile in sand, subject to axial loading. The model proposed by the authors incorporates the interdependence of the shaft and point resistance, and punching shear as the unique mode of failure. The model also takes into account the sand density, the initial lateral earth pressure, the relative depth and the pile roughness. The formulations presented by the authors did not address the effects of stress history on the bearing capacity formulations. The model proposed by Hanna and Nguyen will be discussed in detail in Chapter 4 of this thesis for that it will serve as the basis for the proposed semi empirical model developed in this study.

2.4 Discussion

In Section 2.2 of this thesis, a historical development of earth pressure theories was presented showing a great deal of attention has been given to the role of overconsolidation on lateral stresses in a sand mass. However, these locked in stresses developed in the sand mass due to overconsolidation are excluded from the design theories to predict pile capacities. This is due to the complexity of the mechanism that governs the behavior of a sand mass around driven piles.

In this thesis, the effects of the initial state of stress of the sand mass prior to pile installation which is represented by the coefficient of lateral earth pressure of an overconsolidated sand mass, $K_{o(ocr)}$, the pile diameter and embedment length represented as the relative depth, L/D, as well as the friction angle between the pile and the sand on the shaft resistance and the average coefficient of earth pressure, K_s, developed around the pile shaft, will be examined.

Chapter 3

Experimental Investigation

3.1 General overview

The experimental setup used in this investigation was designed for compressive load tests on model piles driven in sand. A reaction frame was mounted on a steel tank where the sand mass was placed in compacted layers. The placement of sand was carried out by a sand placing mechanism where each layer was placed then compacted. The compaction induced stresses within the sand mass produced the desired OCR. The load was measured by pressure transducers and accordingly, the distribution of the coefficient of earth pressure was calculated.

Once the tank was filled with the predetermined overconsolidated sand, the model pile was driven into the sand mass by a strain-controlled actuator. Two different pile diameters were tested in order to examine the effect of pile diameter on the shaft's resistance. The model piles were instrumented in order to measure the pile's shaft and the tip resistance for a given soil condition.

3.2 Testing Setup

An overall view of the experimental set-up used in this investigation is depicted in Figure3.1. The main testing system consisted of a tank-reaction frame arrangement, the loading equipment, a data acquisition system, and the sand distribution arrangement.

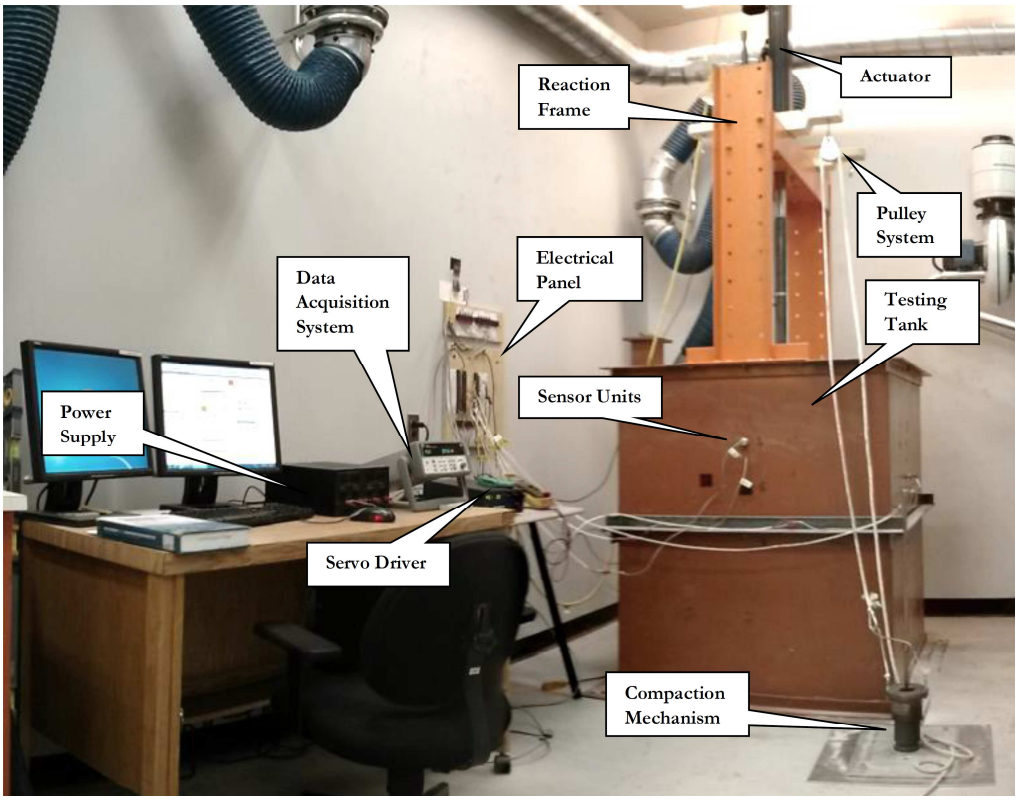

Figure 3.1 Overview of Experimental Setup

3.2.1 Testing Tank and Reaction Frame

A sketch of the tank-reaction frame and loading equipment configuration is given in Figure 3.2. The testing tank was made of steel plates with walls 6.5 mm thick, braced with angle iron to prevent lateral buckling. The dimensions of the tank are $1\times1\times1.25m$ in length, width and depth respectively.

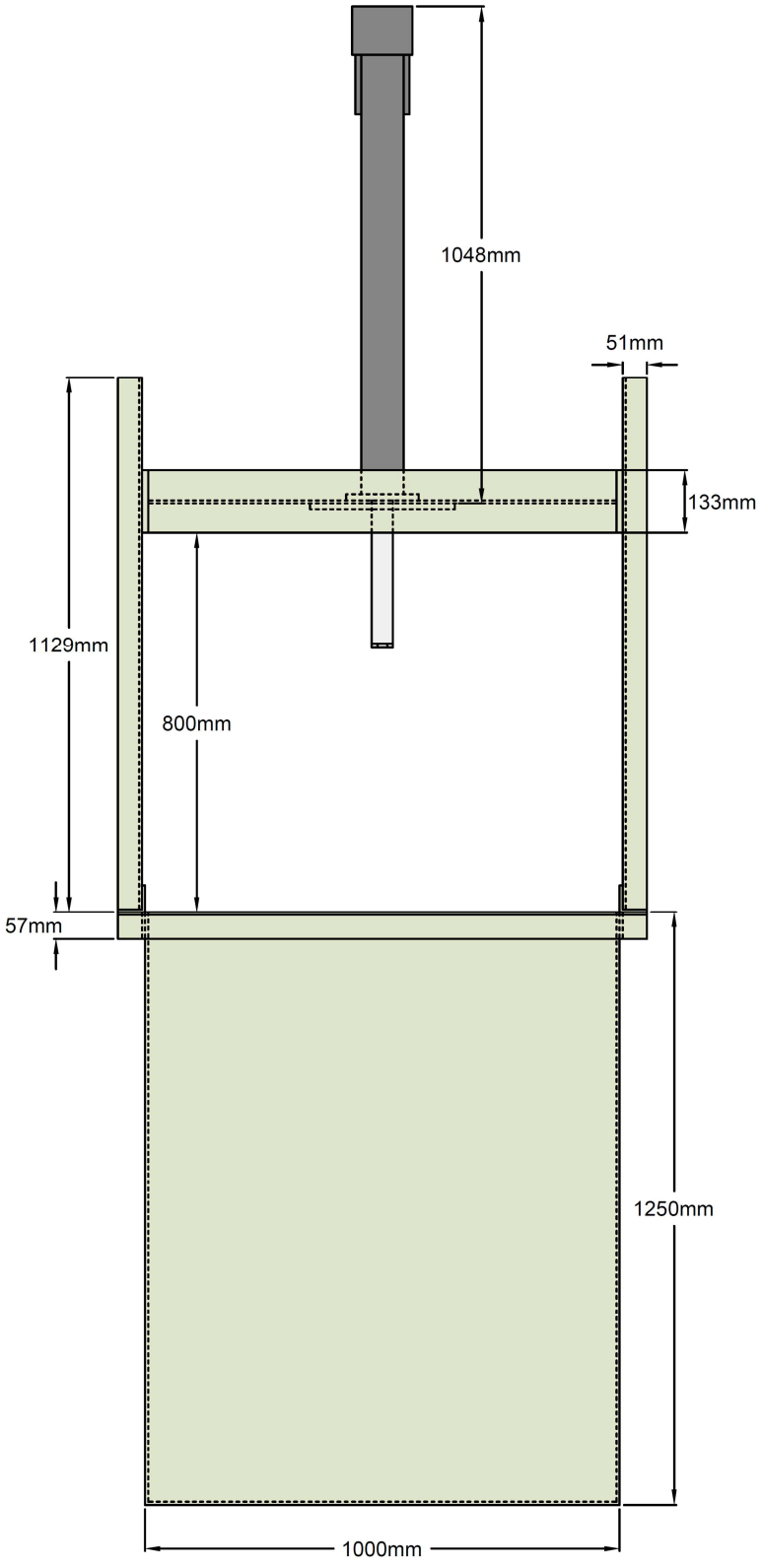

Figure 3.2 Overview of Experimental Setup

The tank was equipped with pressure transducer units designed to measure the vertical and horizontal stresses in the sand mass with depth. Figure 3.3 shows a view of the stress transducer units positioned in the tank. Figure 3.4 shows plan and elevation views of the transducer box placement. Further details on the stress transducer units are shown in Figures 3.4 and 3.5.

Figure 3.3 Stress Transducer Units

The reaction frame was constructed with a $W8\times5-1/4$ steel beam section and two $C8$ column sections and it is shown in Figure 3.1 and 3.2. The beam section was bolted to the column sections at a desired adjustable height. The beam-column assembly was then bolted to the tank. The beam section was reinforced at the middle of the span, where the loading system was attached, in order to prevent buckling.

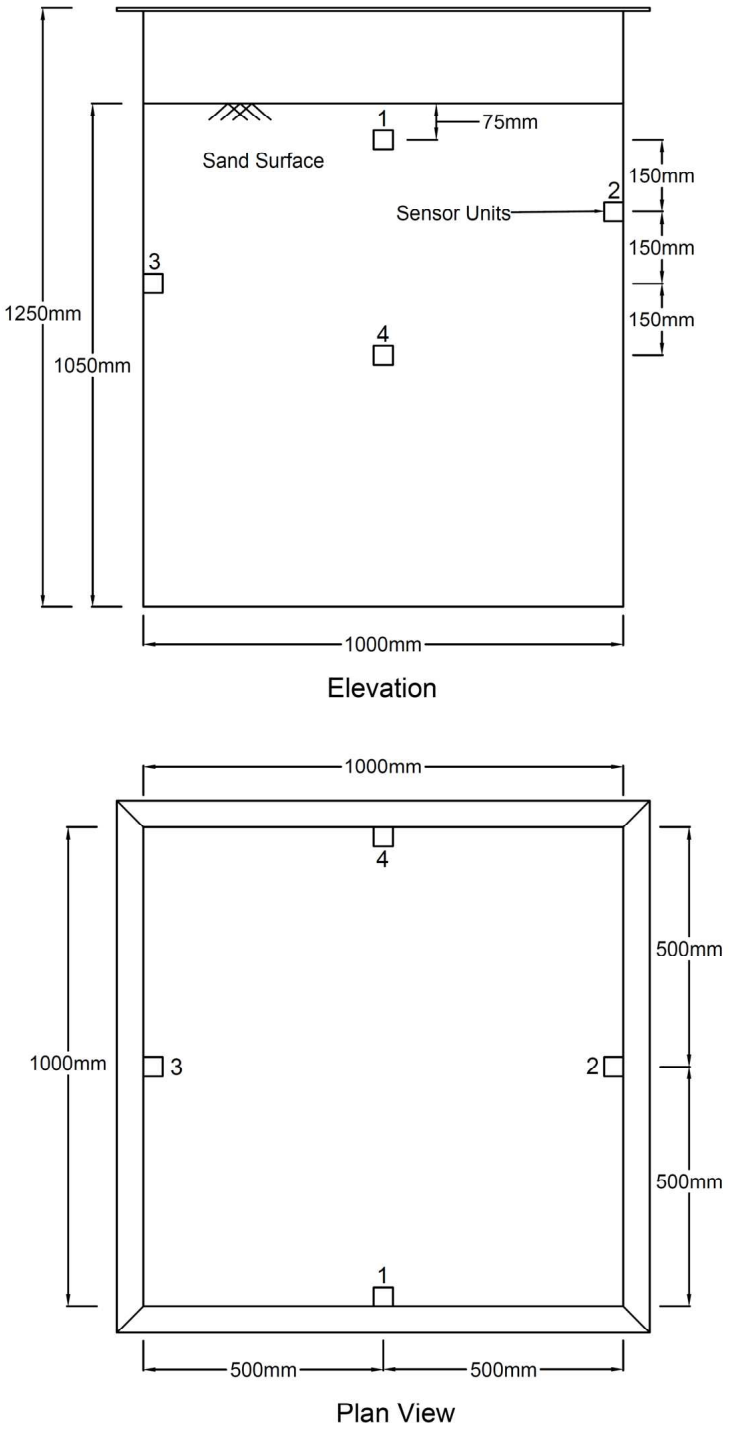

Figure 3.4 Placement plans of transducer units

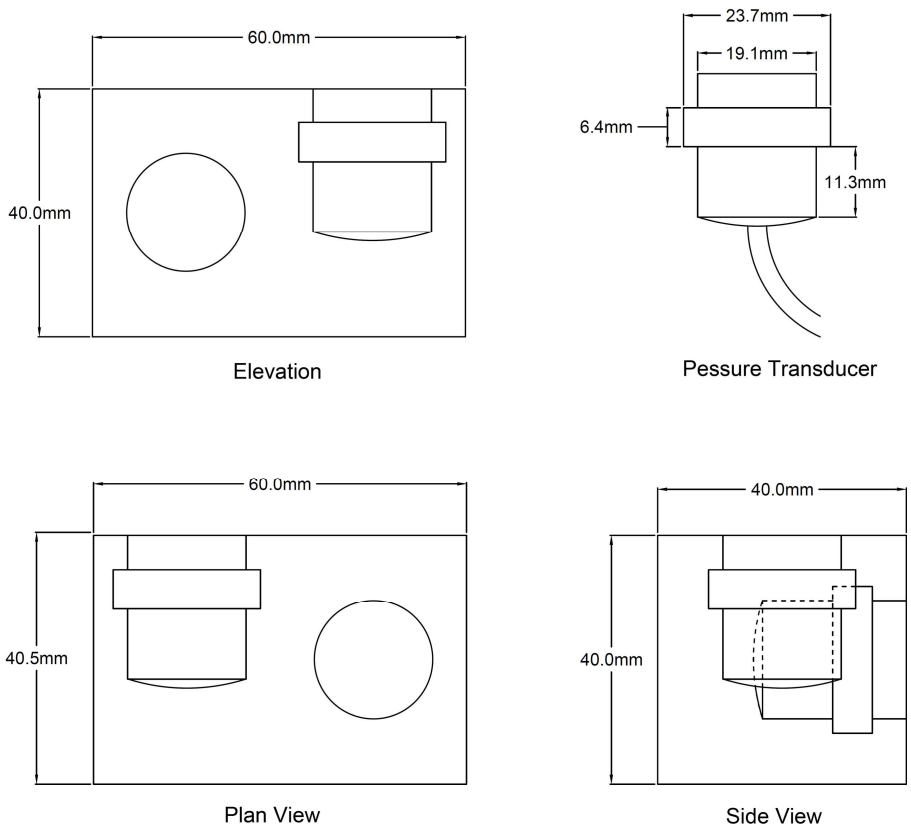

Figure 3.5 Transducer box unit used to measure earth pressures

Figure 3.6 Stress Transducer Unit Components

3.2.2 Loading System

The loading system was comprised of a TH4-Series Electric Cylinder Actuator, a Servo Drive and a power supply. The Actuator is capable of applying a maximum load of 10 kN at 5 amp and 60 V. The Servo Drive transmits the low energy signal from the controller, in this case being the Data Acquisition System, into a high energy signal to the motor. The driver was configured to operate in a voltage control mode which allowed for a strain controlled testing procedure.

3.2.3 Data Acquisition

The data produced during testing was recorded using a Data Acquisition System manufactured by Agilent Technologies. The system was used both for recording data as well as an output remote controller for the loading mechanism. Several computer programs using Visual Engineering Environment (VEE) were developed in order to collect the data received from pressure sensors, instrumented piles and LVDT's, as well as to dictate commands to the loading system.

3.2.4 Sand Placing Technique

Figure 3.7 shows a simple system design for the sand spreading operation. The objective of the mechanism is to minimize the height of fall of sand to eliminate the effect of fall distance on the relative density of the sand. This was achieved using a hose, industrial cargo bags and a hand crane-pulley system. The sand was placed in the test tank in layers 15 cm thick and compacted by a falling weight on to a compacting aluminum plate $50 \times 50 cm$ in length and width.

Figure 3.7 Sand Placing Technic

3.3 Sand Properties

The tests in this investigation where performed on Silica sand in the form of Quartz for which the sand particles were categorized as sub-rounded. The microscopic features of the sand particles can be seen in Figure 3.9. The laboratory tests performed on the sand included sieve analysis, specific gravity tests, and relative density as well a direct shear tests for the determination of the angle of friction of the sand at different relative densities.

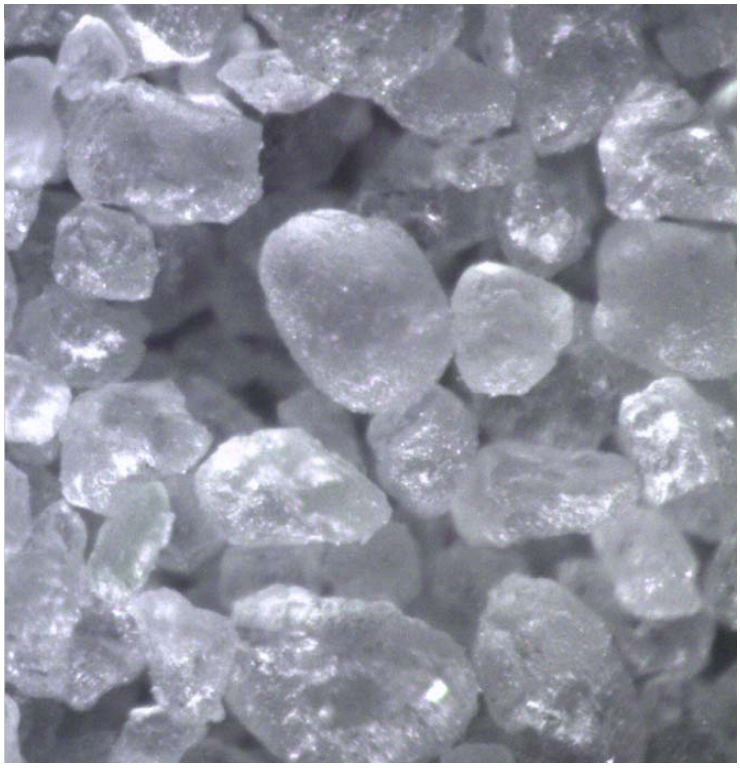

Figure 3.8 Microscope Image of Silica Sand

The grain size distribution curve presented in Figure 3.9 along with the microscopic image in Figure 3.8 indicate that the sand is uniform, of medium size and composed of sub angular quartz particles. The properties determined from the laboratory tests are summarized in Table 3.1.

Based on the relative density tests results, shear box tests were performed on sand samples subjected to different compaction energies in order to determine the variation of the friction angle at different void ratios. The results of the shear box tests are shown graphically in Figure 3.12 and summarized in Table 3.2.

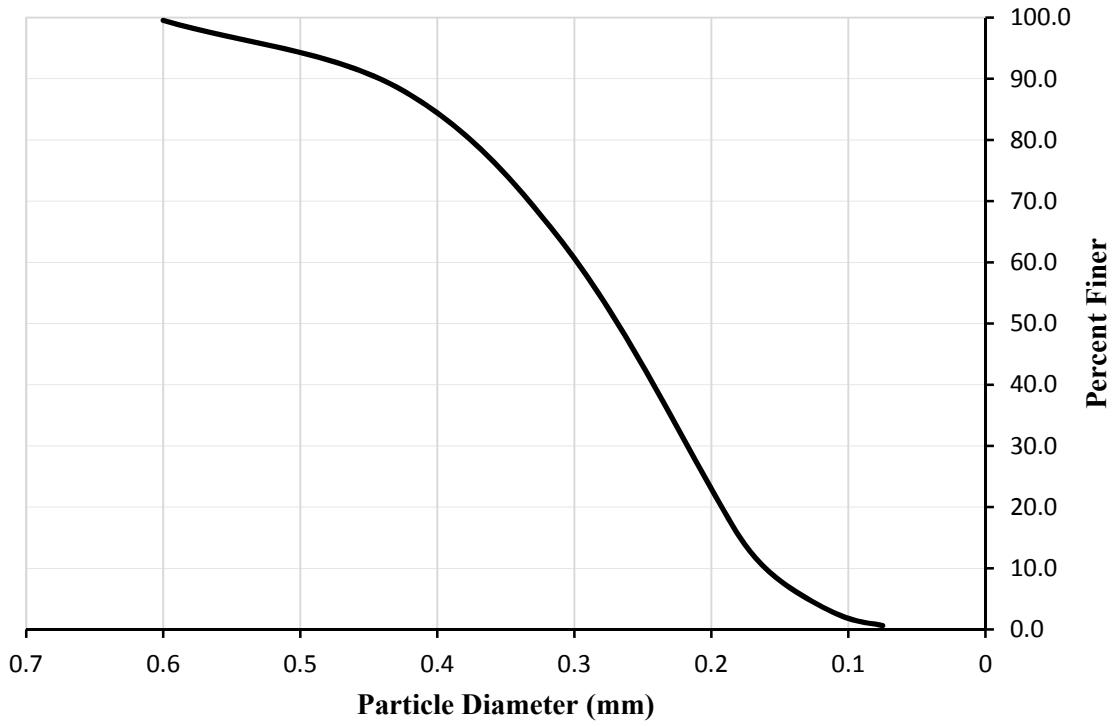

Figure 3.9 Particle Size Distribution

Table 3.1 Properties of Silica Sand

Soil Property	Silica sand 40-10
D_{10}(mm)	0.155
D_{30}(mm)	0.213
D_{50} (mm)	0.26
D_{60}(mm)	0.291
Coefficient of uniformity (C_u)	1.88
Coefficient of curvature (C_c)	1.01
Soil Classification (USCS)	SP
Maximum Dry Unit Weight (KN/m^3)	17.16
Minimum Dry Unit Weight (kN/m^3)	13.98
Minimum Void Ratio	0.4978
Maximum Void Ratio	0.8385
Specific Gravity (G_s)	2.62

Table 3.2 Friction Angle Variations with Relative Density

Relative Density	Void Ratio	Friction Angle
30.00	0.74	32.96
45.00	0.69	34.93
60.00	0.63	36.80
75.00	0.58	38.79

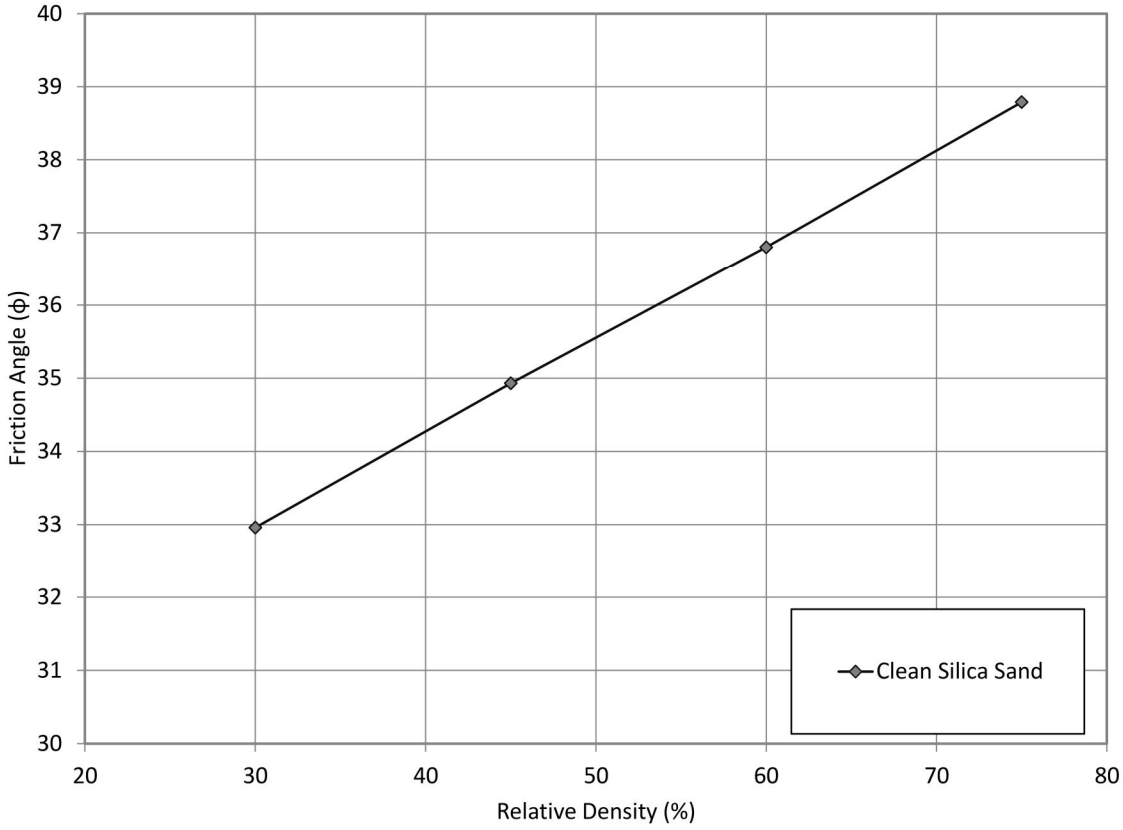

Figure 3.10 Friction angle versus relative density for clean Silica sand 4010

Since shaft resistance is dependent on the friction angle between the pile shaft and the soil, several tests were made to determine the proper grit of sand paper that could be

applied to the pile shaft in order to simulate the desired roughness. The ratio of the angle of friction of soil to the interface angle of friction, δ/ϕ for concrete piles is generally taken as unity **(Tomlinson, 2008).** Hence, direct shear test were made to find the proper sand paper grit that would offer an interface friction angle equal to the soil friction angle. Fig. 3.11 shows a set of wooden block cover with different grit sand paper made to fit in the shear box. The tests were once again conducted at different relative densities and the results are summarized in Figure 3.12 and Table 3.3 for the grit (150) used in this investigation. Details of the laboratory tests done on Silica sand can be found on Appendix A.

Figure 3.11 Direct shear blocks with different grit sand paper

Table 3.3 Interface friction angle of Silica Sand and sand paper (grit 150)

Relative Density (%)	□	**δ**	**δ/□**
30	32.96	33.17	1.01
45	34.93	36.29	1.04
60	36.80	39.11	1.06

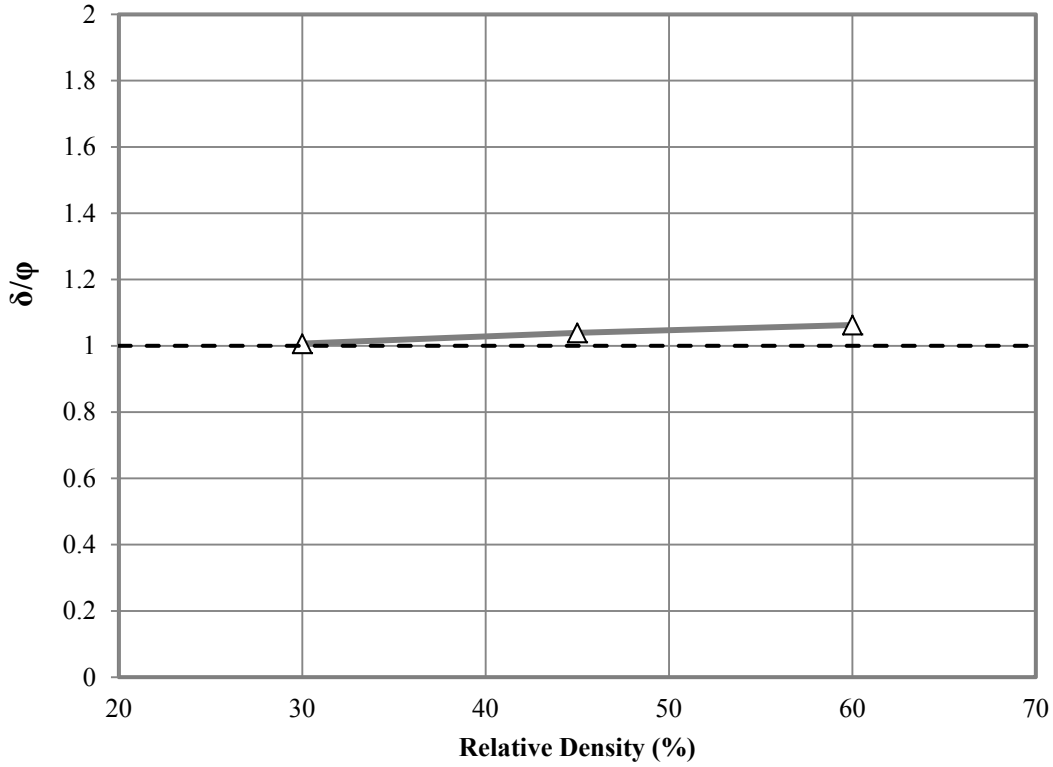

Figure 3.12 δ/φ for different relative densities of Silica sand

3.4 Model Piles

Two model piles were used in this investigation in order to determine the effect of increasing pile diameters when driven into overconsolidated sand. The piles were made of mechanical steel pipe, both 80 cm in length, with diameters of 2.86cm and 5.08 cm. Both piles were instrumented in order to measure their load carrying capacity. A piston-cylinder device was designed for each pile to be installed at the pile tip in order to house the available pressure transducers. The area of the piston was selected in such manner that the load could be transferred by the working fluid in the piston at a range that could be captured by the available pressure sensors. The piston-cylinder devices for the large

and small diameter piles installed at the pile tips are shown in Figure 3.13 and Figure 3.14, respectively. An additional mechanism was designed to measure the load at the pile head. This mechanism can be used for different pile diameters with the use of a reducing fitting. Again, a piston-cylinder device with oil as the working fluid was used in order to capture the load applied at the pile head. This mechanism is shown in Figure 3.16.

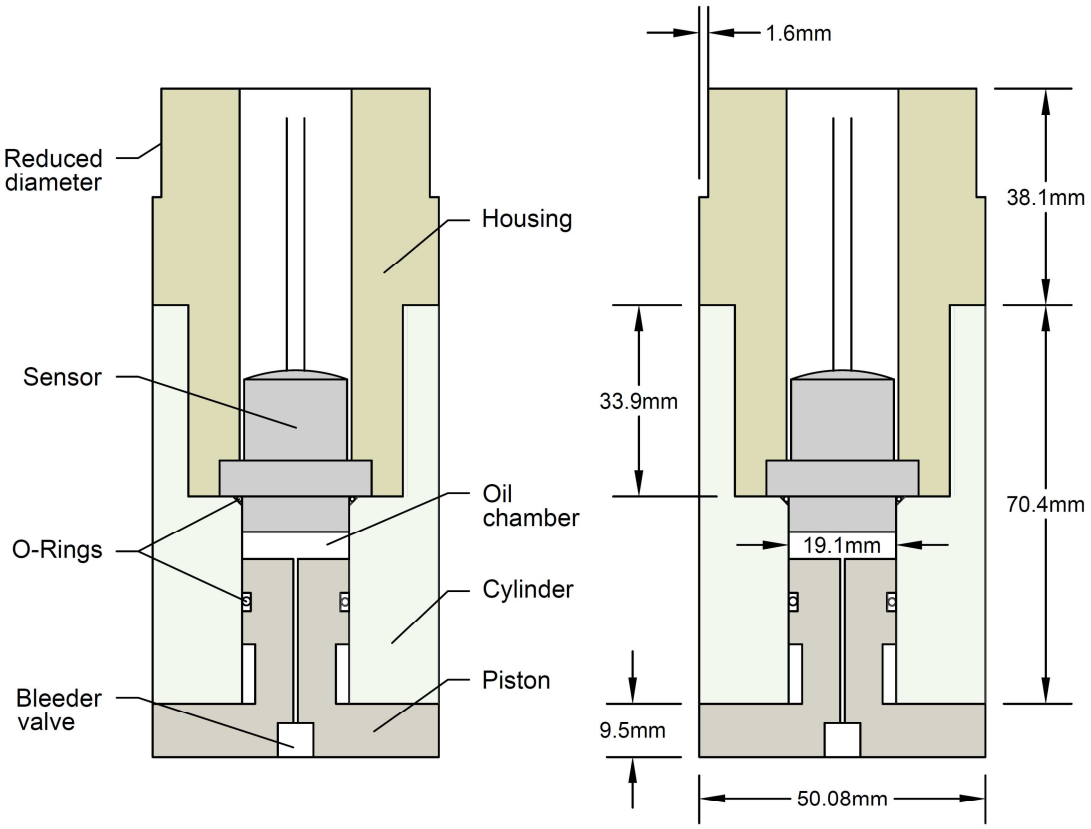

Figure 3.13 Piston-Cylinder device for large diameter pile

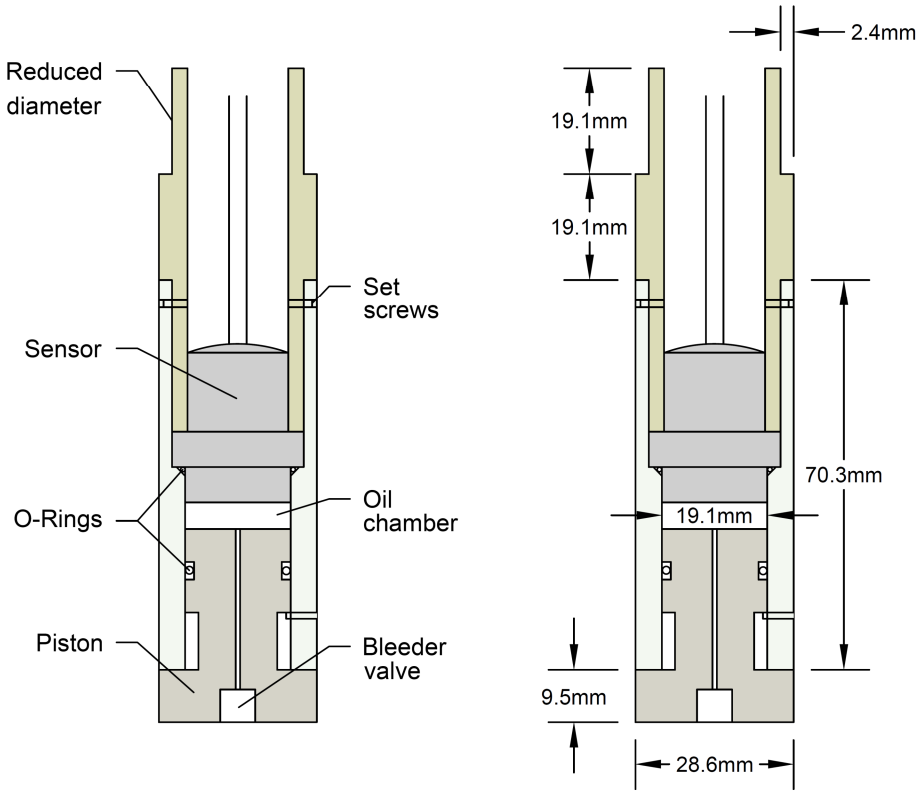

Figure 3.14 Piston-Cylinder device for small diameter pile

The assembly of the pile and piston-cylinder mechanisms for both pile diameters is depicted in Figure 3.17. The actual model piles are shown in in Fig. 3.15

Figure 3.15 Model piles

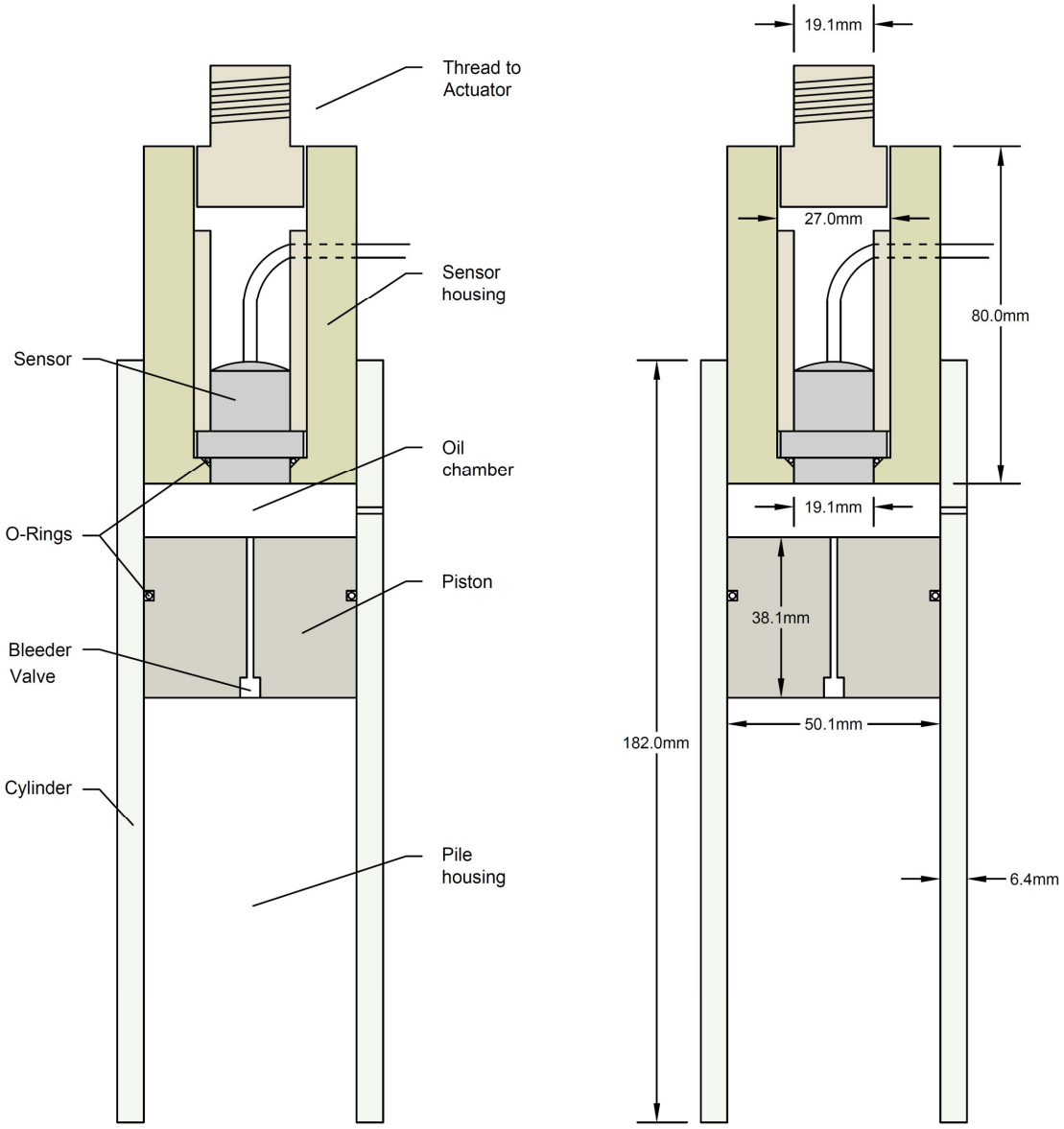

Figure 3.16 Pile head piston-cylinder device

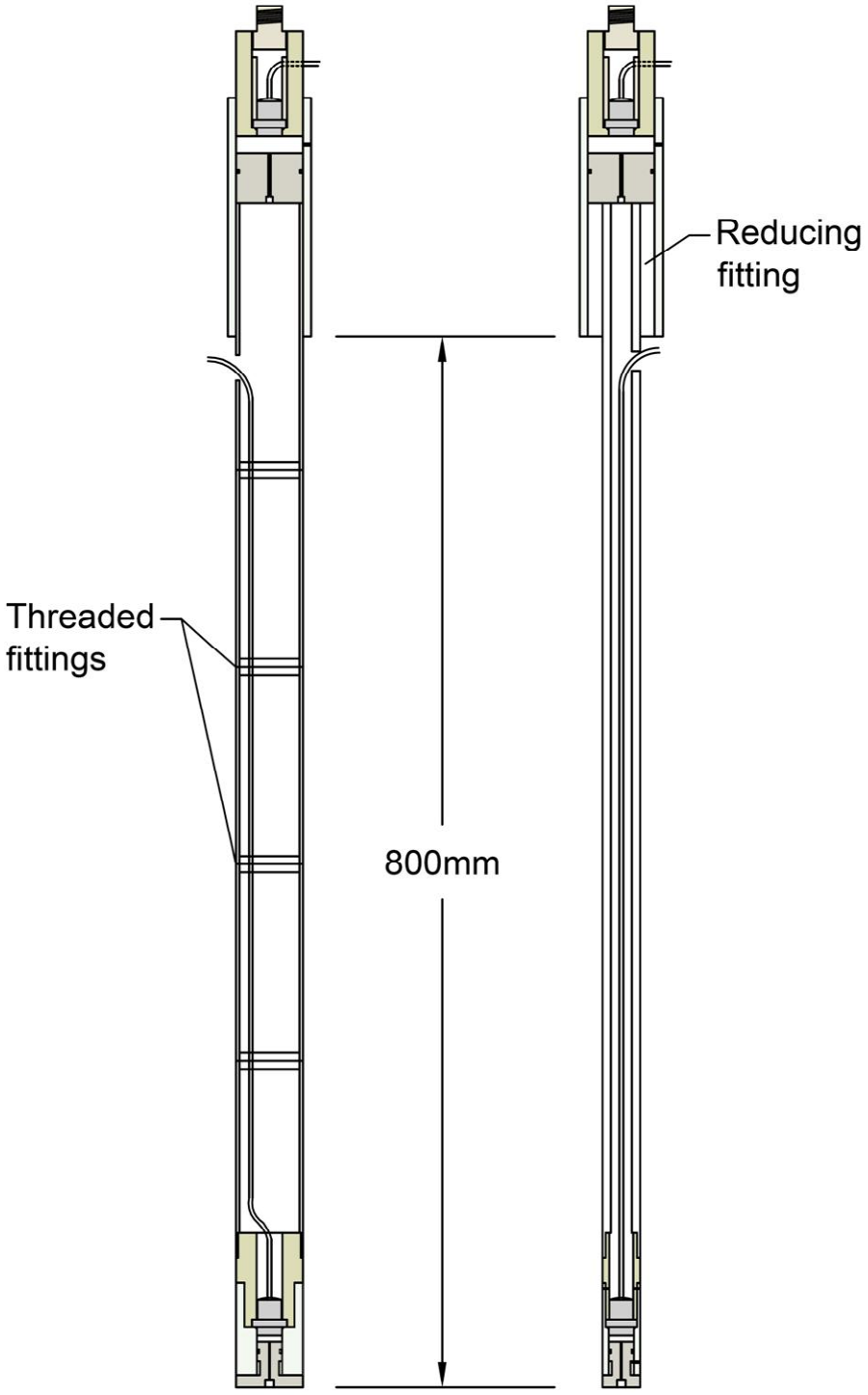

Figure 3.17 Instrumented piles

3.5 Test Procedure

The testing techniques adopted in this investigation are described in this section. The preparations and testing process were carried out with caution and consistency in order to assure repeatability of the testing conditions.

3.5.1 Sand Mass Preparation

For each test series, a sand deposit was first prepared in the testing tank using the sand distribution system mentioned in section 3.2.2. The sand was placed in layers 15 cm in height and compacted individually by dropping a 7.14 kg mass from 20 cm above the surface of the layer. The compaction effort was varied for each test series by increasing the number of drops. The area of the compacting plate was one fourth of the surface area of the deposit so the compacting procedure was repeated four times for each layer in order to compact the entire layer surface. The sketch in Figure 3.18 shows the layered profile of the sand mass in the tank and the position of the transducer units within the layers. Figure 3.20 shows the compaction device. Once the compaction was completed, the induced horizontal and vertical stresses were measured and registered by the Data Acquisition System. Hence, the state of overconsolidation with depth, prior to pile driving, can be estimated.

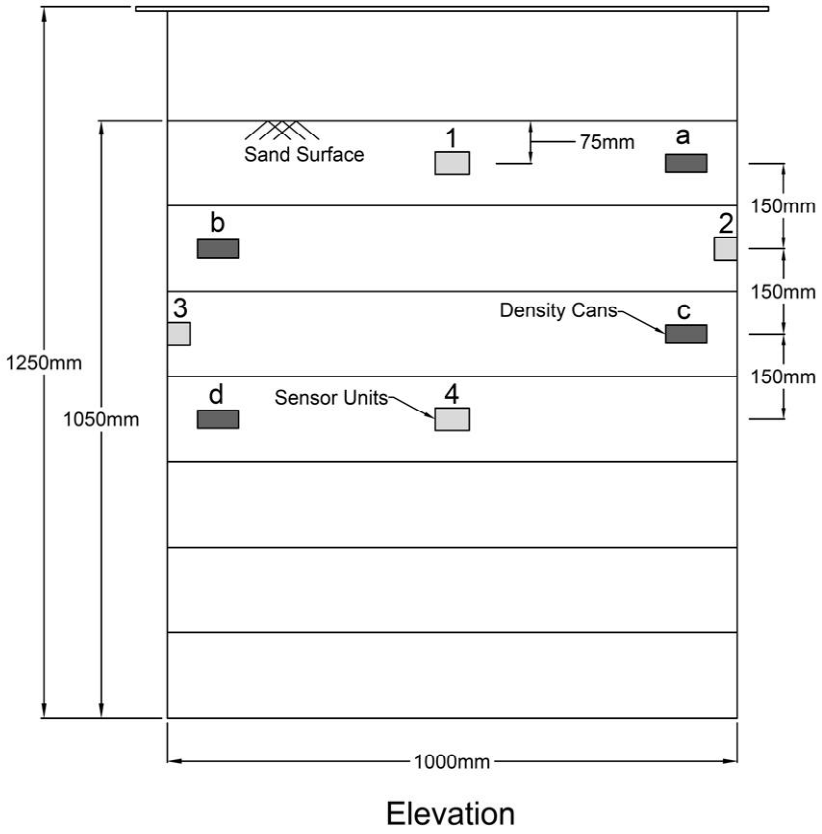

Figure 3.18 Density cans and sensor units in sand layers

The compaction energy applied to each layer is found by multiplying the potential energy stored by the compacting weight at 20 cm in height times the number of drops. Since the area of the compacting plate is one fourth of the layer area, the total energy applied to each layer is four times the above mentioned amount. Table 3.4 shows the energy applies per layer of each test series.

Table 3.4 Compaction energy

Series	Number of drops	Compaction plate areas per surface	Mass (kg)	Height of drop (m)	Gravity (m/s^2)	Energy applied per layer (kJ)
A-20	20	4	7.14	0.2	9.81	1.12
A-30	30	4	7.14	0.2	9.81	1.68
A-40	40	4	7.14	0.2	9.81	2.24
B-20	20	4	7.14	0.2	9.81	1.12
B-40	40	4	7.14	0.2	9.81	2.24

Figure 3.19 Compaction device

3.5.2 Unit Weight of the sand tested

The compaction energy applied in each test series was maintained constant for each layer. As a result, the lower layers received more compacting energy per unit volume. This approach caused the unit weight of the sand mass to increase with depth. In order to determine the unit weight distribution, density cans of known weights and volumes were placed within the layers of interest. After each test series was completed, the density cans were carefully retrieved and the unit weights were obtained. Hence, the relative densities and friction angles corresponding to each layer could be determined. The placement of the density cans in the tank is depicted in Figure 3.19

3.5.3 Pile Driving and Load Tests

Once the sand bed was prepared, the model pile was pushed vertically into the soil mass by the electric cylinder at a rate of 2 cm per minute to the selected depth. Verticality was assured by leveling the actuator cylinder to which the pile head mechanism was threaded prior to each test. The actuator was controlled by an LVDT mounted on the loading frame which sent a feedback signal to a loop in the VEE program. Once the desired displacement was reached, the pile was unloaded. The load test was then started at a constant penetration rate of 0.5 cm per minute. Each pile load test was continued until an axial displacement equal to 25mm was reached. At this point, the pile was unloaded and then pushed to the next depth level in order to carry out the next test. The axial displacement was continuously recorded as measured by the LVDT. The piston-cylinder device at the pile head recorded the applied axial load, whereas the tip resistance was recorded by the mechanism installed at the pile tip. The difference between these two readings provided the magnitude of the shaft resistance at failure.

3.5.3 Testing Program

Each test series consisted of multiple pile load tests. Table 3.5 presents the testing program followed in this investigation. Each test is labeled based on the diameter size of the pile, the number of drops used on each layer of the prepared sand mass and the test number. The letter A refers to the 50.8 mm diameter pile and the letter B corresponds to the 28.575 mm diameter pile. The two numbers following indicate the number of drops and the test number respectively. Four pile load tests for each A-Series and three pile load tests for each B-Series were performed with a total of 18 tests.

Table 3.5 Testing Program

Test Series	Test	Number of drops, N	Relative depth, L/D	Pile Diameter, D (mm)
A-20	A-20-1	20	5.4	50.8
	A-20-2	20	8.4	50.8
	A-20-3	20	11.4	50.8
	A-20-4	20	13	50.8
A-30	A-30-1	30	5.4	50.8
	A-30-2	30	8.4	50.8
	A-30-3	30	11.4	50.8
	A-30-4	30	13	50.8
A-40	A-40-1	40	5.4	50.8
	A-40-2	40	8.4	50.8
	A-40-3	40	11.4	50.8
	A-40-4	40	13	50.8
B-20	B-20-1	20	9.7	28.575
	B-20-2	20	14.9	28.575
	B-20-3	20	20.1	28.575
B-40	B-40-1	40	9.7	28.575
	B-40-2	40	14.9	28.575
	B-40-3	40	20.1	28.575

3.6 Experimental Results

A total of five series, three for the 5.01 cm pile and two for the 2.86 cm pile, were conducted in this investigation for which the results are presented herein. For each test series, multiple tests were performed at different relative depths. The results for the corresponding pile load tests were recorded from which the ultimate failure loads were determined. The distributions of overconsolidation, relative density and friction angle with depth were recorded for each series. The following sections will present the results of each test followed by the development of an analytical model that incorporates stress history of sand on the coefficient of earth pressure and shaft resistance.

3.7 Sand Mass Properties

Preliminary tests were conducted to determine the changes in unit weight and overconsolidation of the sand mass subjected to different compacting energies. Table 3.6 presents a summary of the measured unit weights obtained using density cans. Once the unit weigh distributions with depth were obtained, the friction angle and relative density variations with depth were determined from the results of direct shear and relative density tests. Figures 3.20, 3.21 and 3.22 show the distributions of unit weight, relative density and friction angle with depth, respectively. Table 3.7 shows the theoretical overburden stresses, the measured vertical stresses at the sensor's depth and the variations of the overconsolidation ratio with depth.

The degree of overconsolidation in the sand mass achieved by compaction was determined using Eq. 3.1 reintroduced by Hanna and Al Khoury, 2005.

$$OCR = \frac{\sigma_v}{\gamma h} \tag{3.1}$$

Where

σ_v = the measured vertical stresses at a given depth

γh = the theoretical overburden pressure

The graphs of the variation of OCR with depth for three different compaction energies are depicted in Figure 3.23.

Table 3.6 Experimental distributions of unit weight, relative density and friction angle with depth

Number of drops per plate area	Depth of density can (mm)	Measured unit weight (kN)	Corresponding relative density, R (%)	Corresponding friction angle, ϕ (degrees)
20	75	14.55	21.01	31.81
	225	14.68	25.71	32.41
	375	14.83	30.88	33.08
	525	14.79	35.81	33.72
30	75	14.70	26.58	32.53
	225	14.86	31.82	33.20
	375	14.94	34.78	33.58
	525	15.11	40.50	34.32
40	75	14.84	31.29	33.13
	225	14.89	36.09	33.75
	375	15.04	39.06	34.14
	525	15.23	44.31	34.82

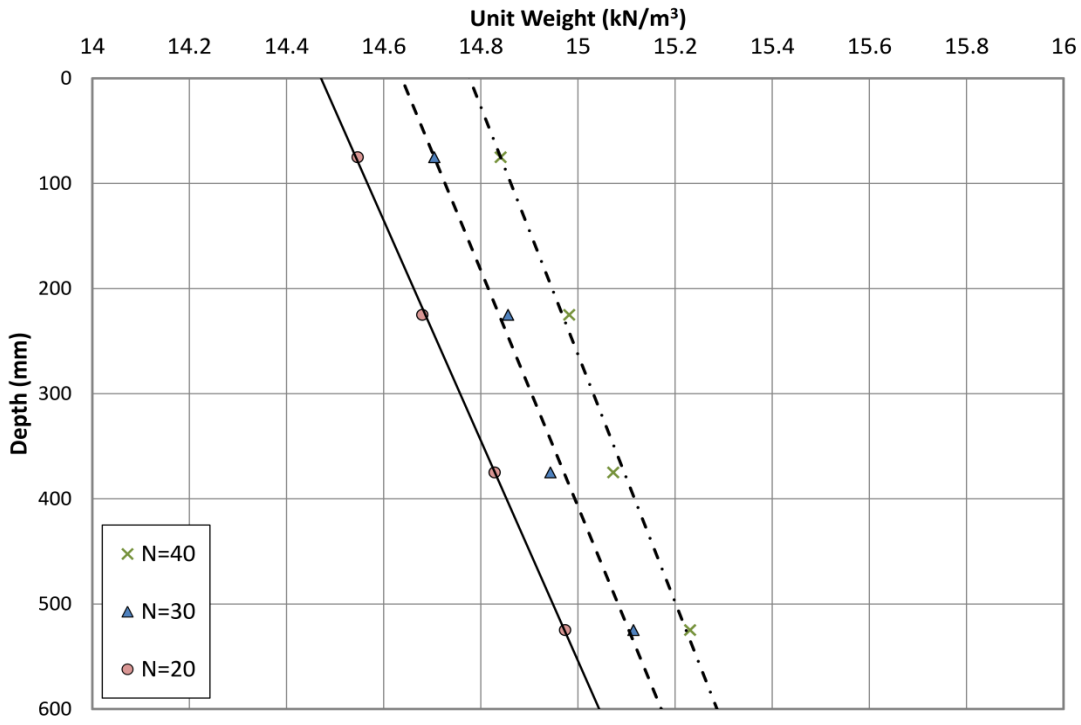

Figure 3.20 Unit weight distributions with depth for different compaction energies

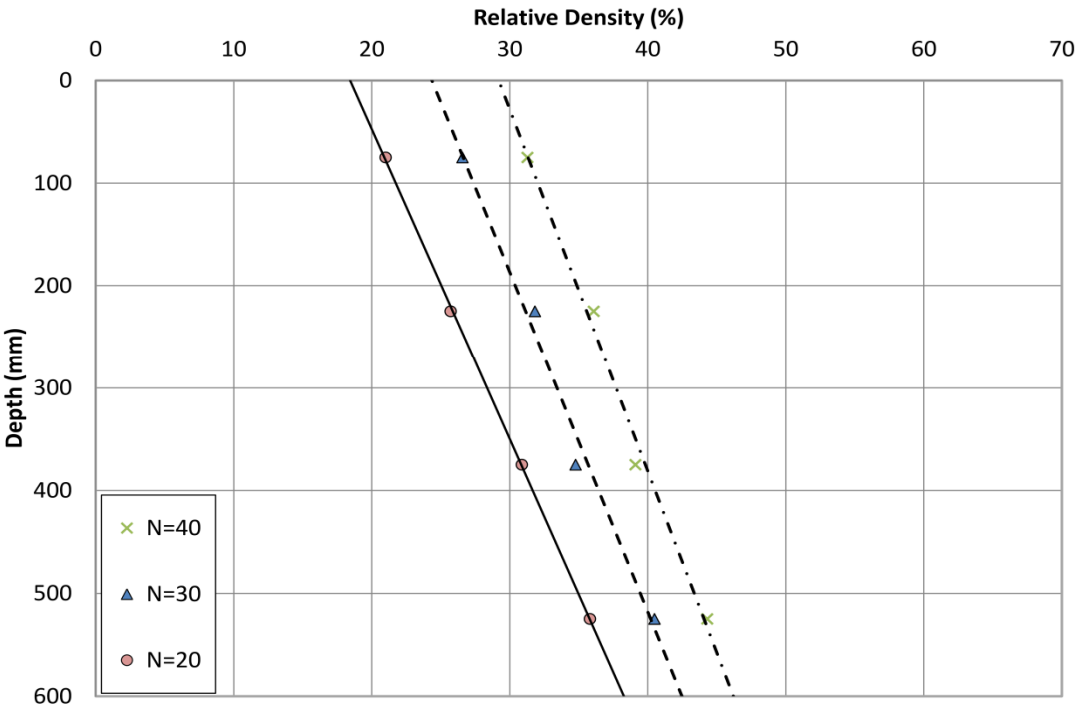

Figure 3.21 Experimental distributions of relative density with depth for different compaction energies

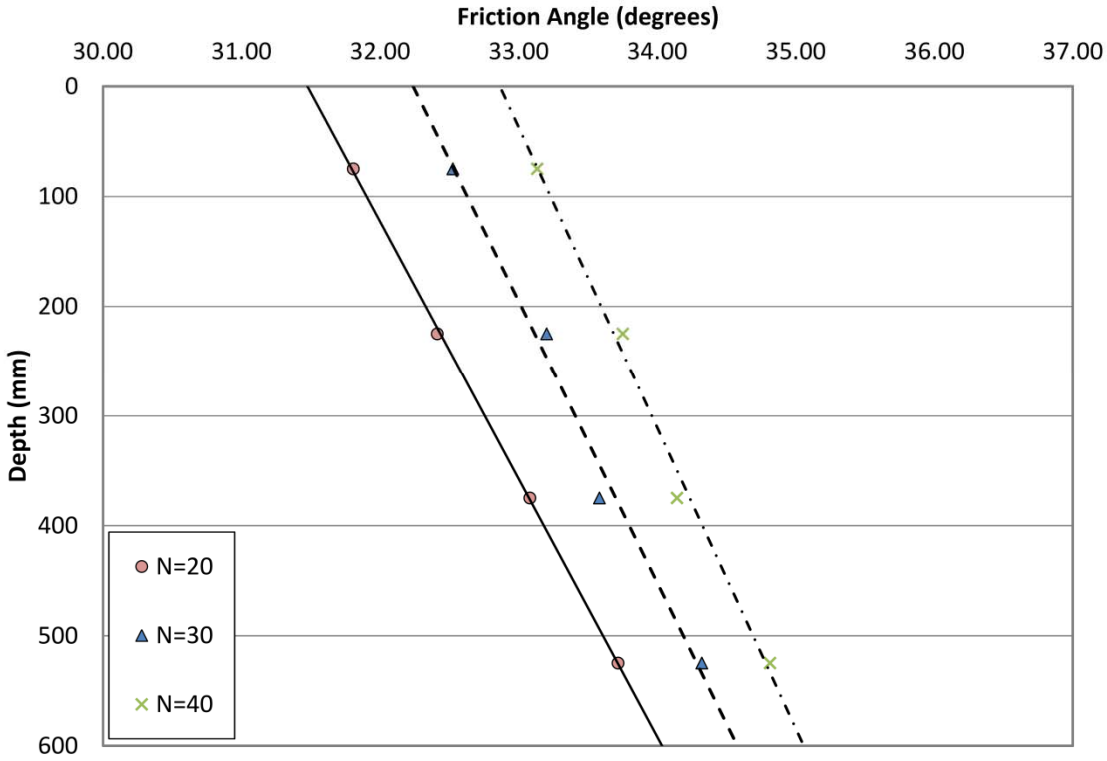

Figure 3.22 Friction angle with depth for different compaction energies

Table 3.7 Experimental distributions of OCR vs. depth for different compaction energies

Number of drops per plate area	Compaction energy per layer (kJ)	Depth of Sensor (mm)	Measured effective stress, σ_v' (kPa)	Theoretical effective stress, γh (kPa)	OCR, $\sigma_v'/\gamma h$
20	1.12	66	1.21	0.96	1.26
		218	8.04	3.19	2.53
		358	14.3	5.26	2.72
		507	23.41	7.47	3.13
30	1.68	64	1.79	0.94	1.91
		214	8.53	3.16	2.70
		356	18.53	5.28	3.50
		513	28.27	7.64	3.70
40	2.24	66	2.01	0.98	2.05
		218	11.01	3.22	3.42
		358	20.90	5.36	3.90
		507	34.41	7.62	4.51

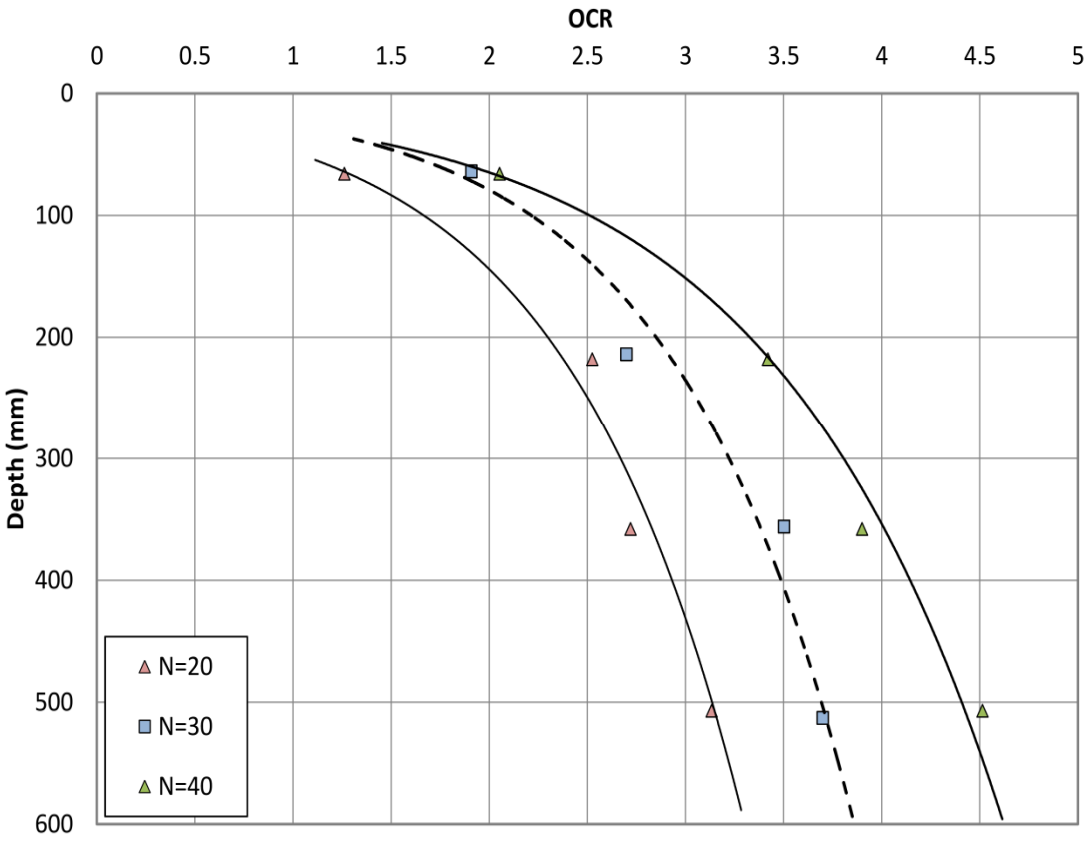

Figure 3.23 OCR distributions with depth for different compaction energies

3.7 Pile load tests

A total of eighteen pile load tests were performed in this investigation as described in the testing program on chapter three. The ultimate loads Q_u and the point resistance Q_p were determined using the tangent intersection method mentioned in the previous chapter. The shaft resistance Q_s was taken to be equivalent shaft capacity as the difference between the ultimate and point resistance determined from the ultimate displacement in their corresponding load settlement curves. The variations of the load on the pile head, pile tip and shaft resistance with axial pile displacement are shown in

Figures 3.26 to 3.43. An example of the application of the tangent intersection method is depicted in Figure 3.44. The results of the pile load tests are summarized in Table 3.8. Figures 3.24 and 3.25 show the pile installation method.

Figure 3.24 Method of pile installation for large diameter pile

Figure 3.25 Installation of small diameter pile

Table 3.8 Results of pile load tests on model piles

Model Pile	Pile Test	Nominal Depth, L (mm)	Relative depth, L/D	Ultimate Pile Capacity, Q_u (kgf)	Point Resistance, Q_t (kgf)	Shaft Resistance, Q_s (kgf)
50.8 mm. Diameter	A-20-1	275.98	5.4	185	179.6	5.4
	A-20-2	426.29	8.4	313.5	297	16.5
	A-20-3	576.8	11.4	442	402	40
	A-20-4	660.56	13	531	467	64
	A-30-1	275.51	5.4	226.7	219.3	7.4
	A-30-2	427.01	8.4	397.5	374.5	23
	A-30-3	574.9	11.4	580	527	53
	A-30-4	659.07	13	680	597	83
	A-40-1	275.97	5.4	244.5	235	9.5
	A-40-2	426.36	8.4	398	369	29
	A-40-3	575.9	11.4	600.5	533.5	67
	A-40-4	660.33	13	698	585.7	112
28.575 mm. Diameter	B-20-1	276.2	9.7	77.5	74.1	3.4
	B-20-2	426.23	14.9	134.2	122.5	11.9
	B-20-3	577.25	20.1	230	203	27
	B-40-1	276.33	9.7	98.5	92.4	6.1
	B-40-2	426.59	14.9	211.3	192	19.3
	B-40-3	575.41	20.1	302	256	46

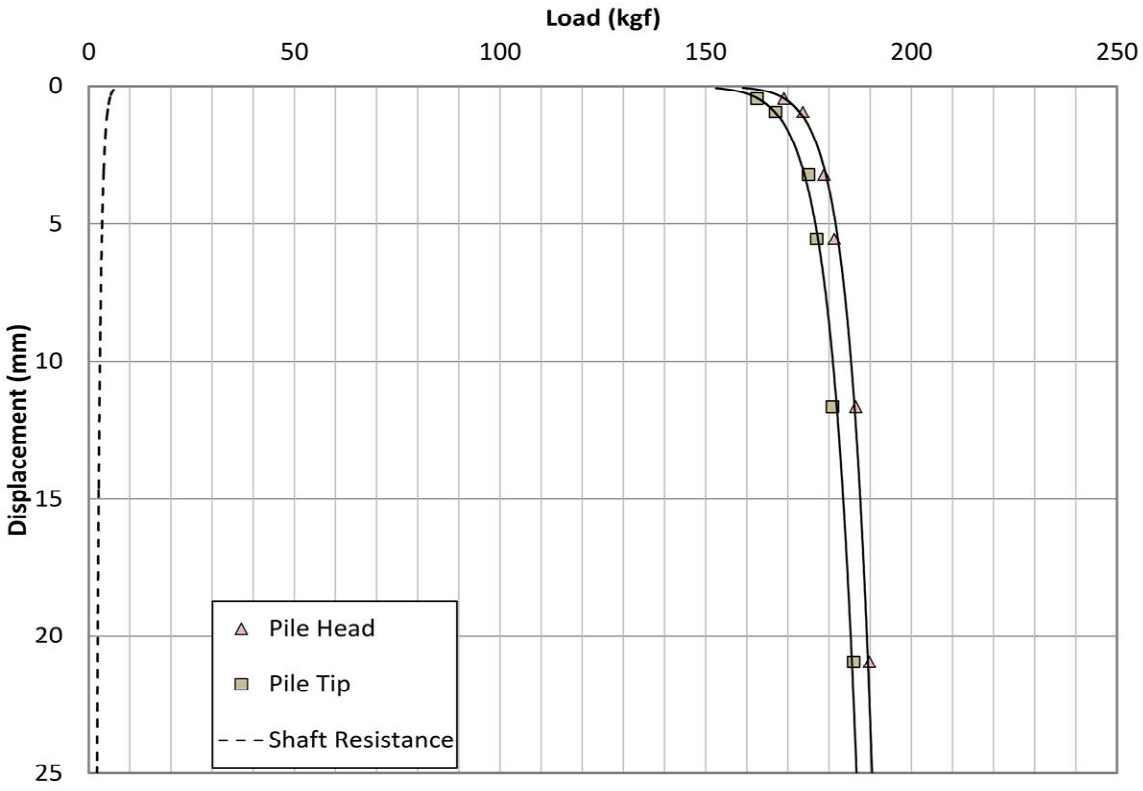

Figure 3.26 Load-Displacement curve for test A-20-1 (L/D=5.4)

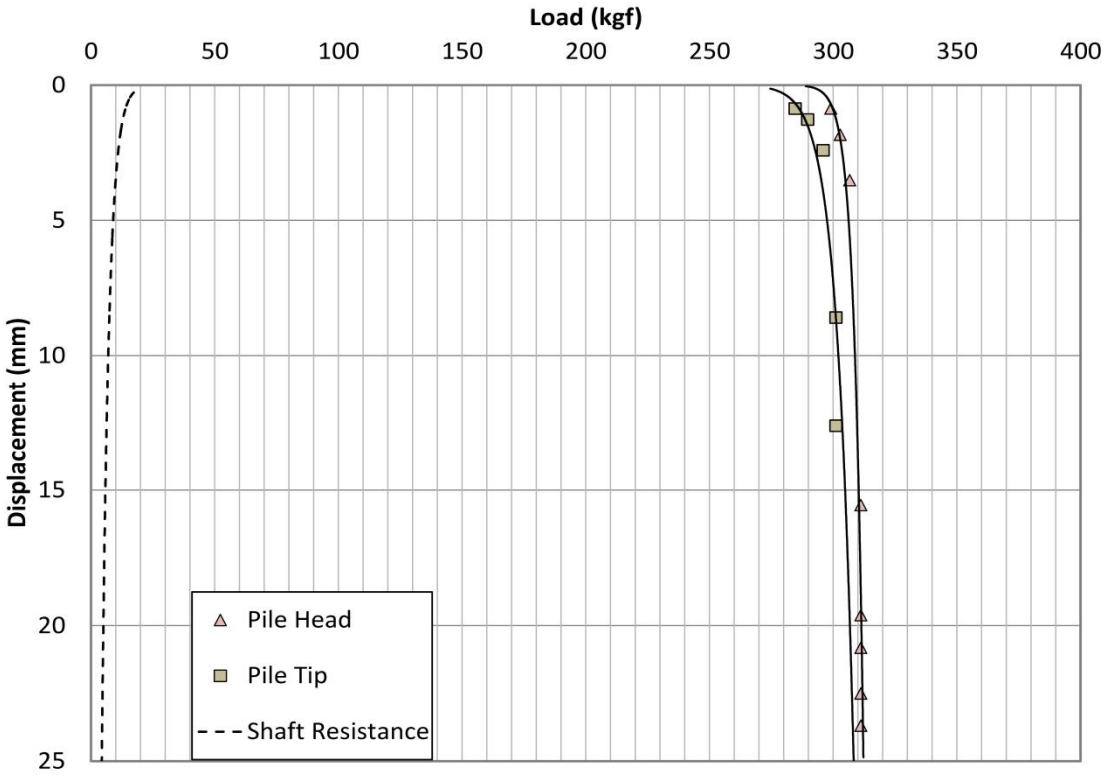

Figure 3.27 Load-Displacement curve for test A-20-2 (L/D=8.4)

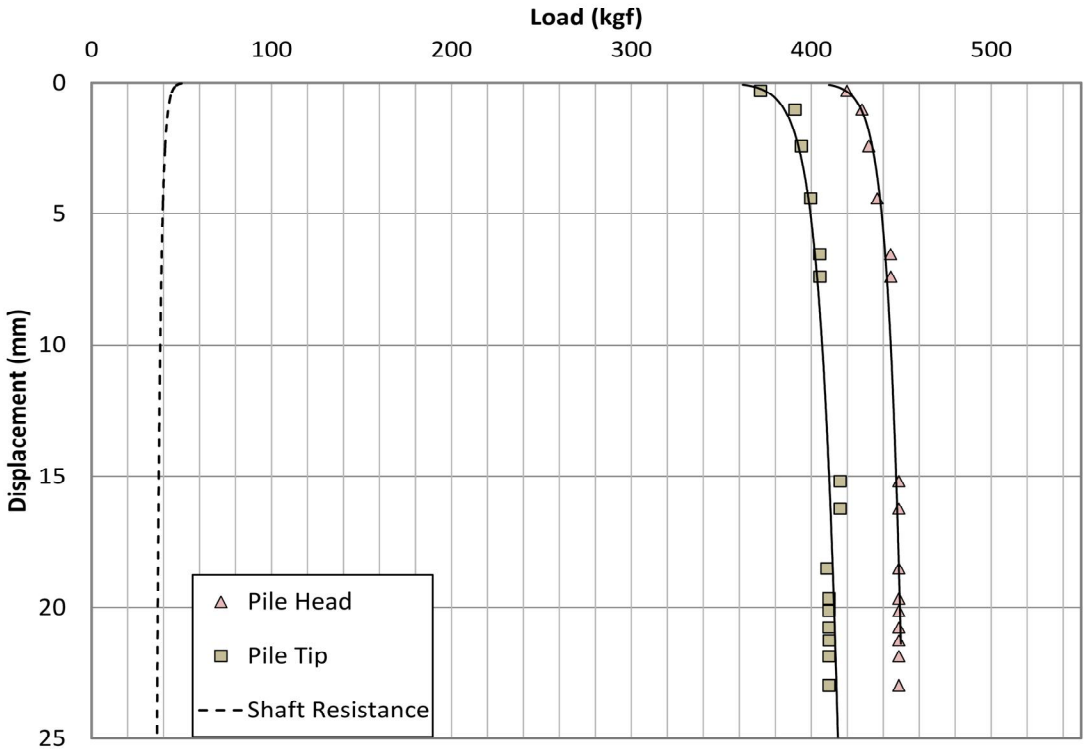

Figure 3.28 Load-Displacement curve for test A-20-3 (L/D=11.4)

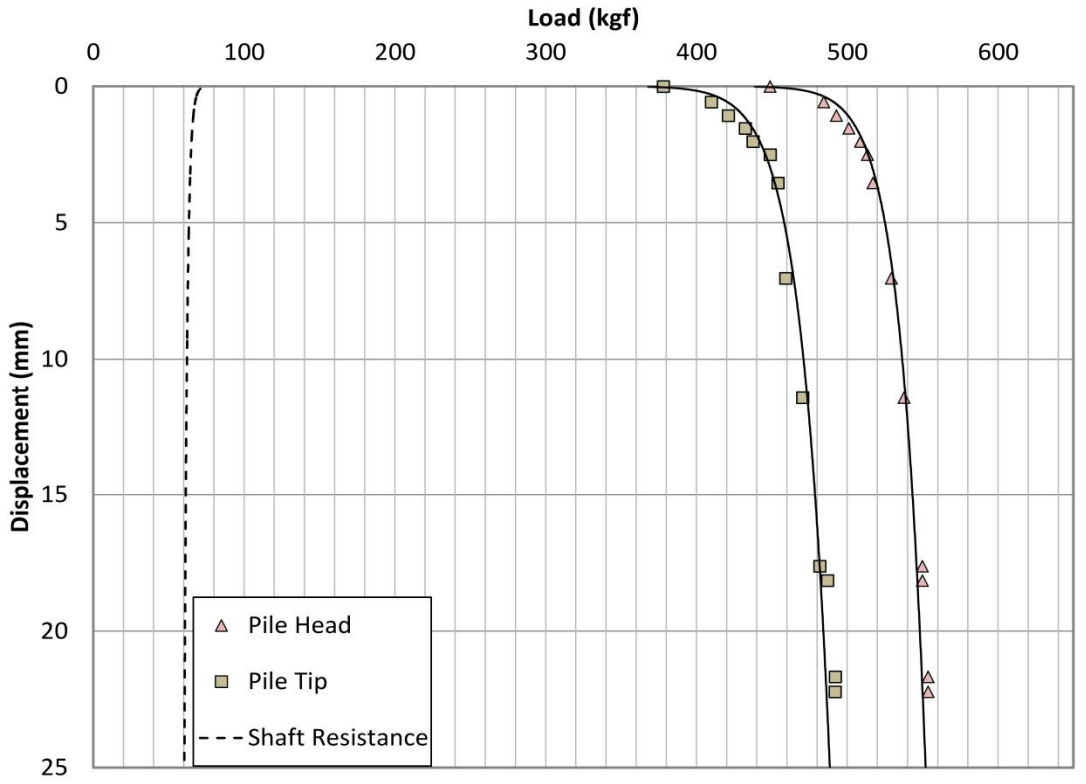

Figure 3.29 Load-Displacement curve for test A-20-4 (L/D=13)

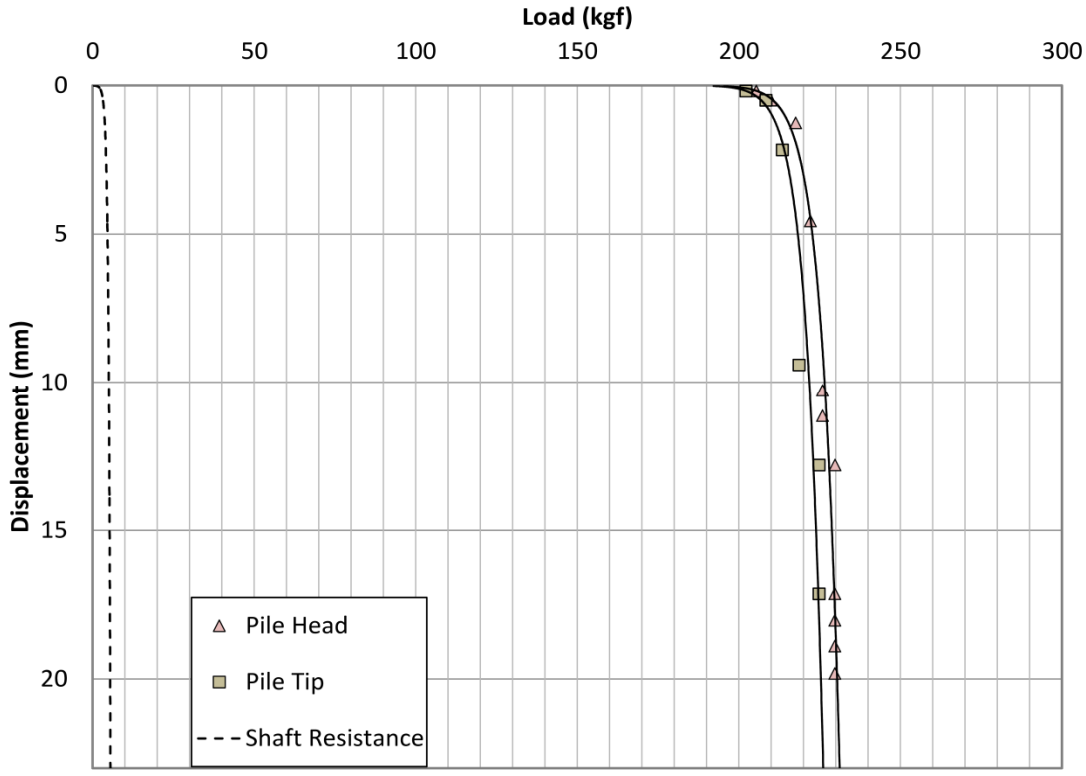

Figure 3.30 Load-Displacement curve for test A-30-1 (L/D=5.4)

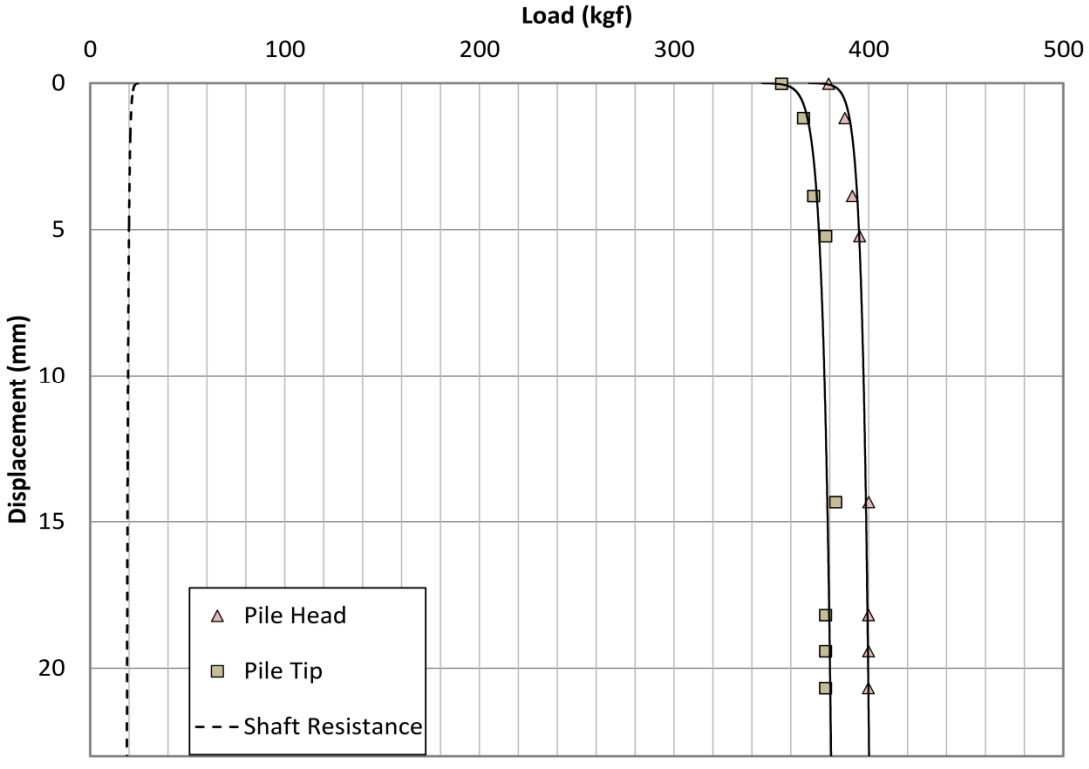

Figure 3.31 Load-Displacement curve for test A-30-2 (L/D=8.4)

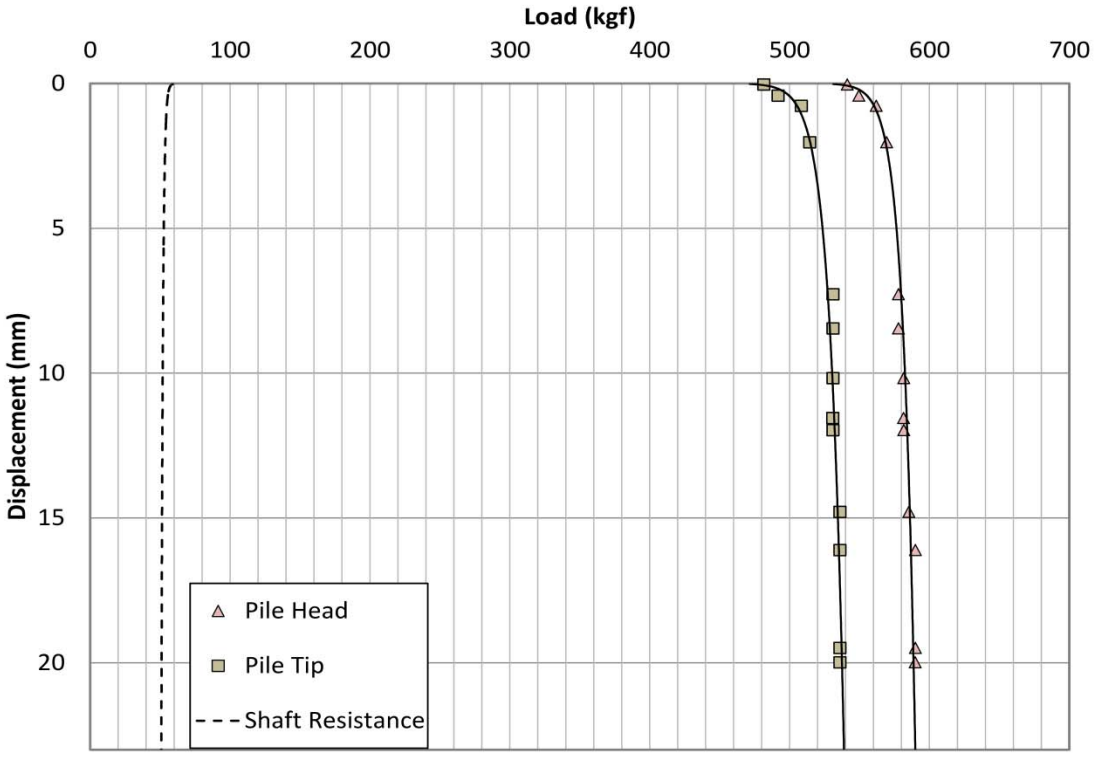

Figure 3.32 Load-Displacement curve for test A-30-3 (L/D=11.4)

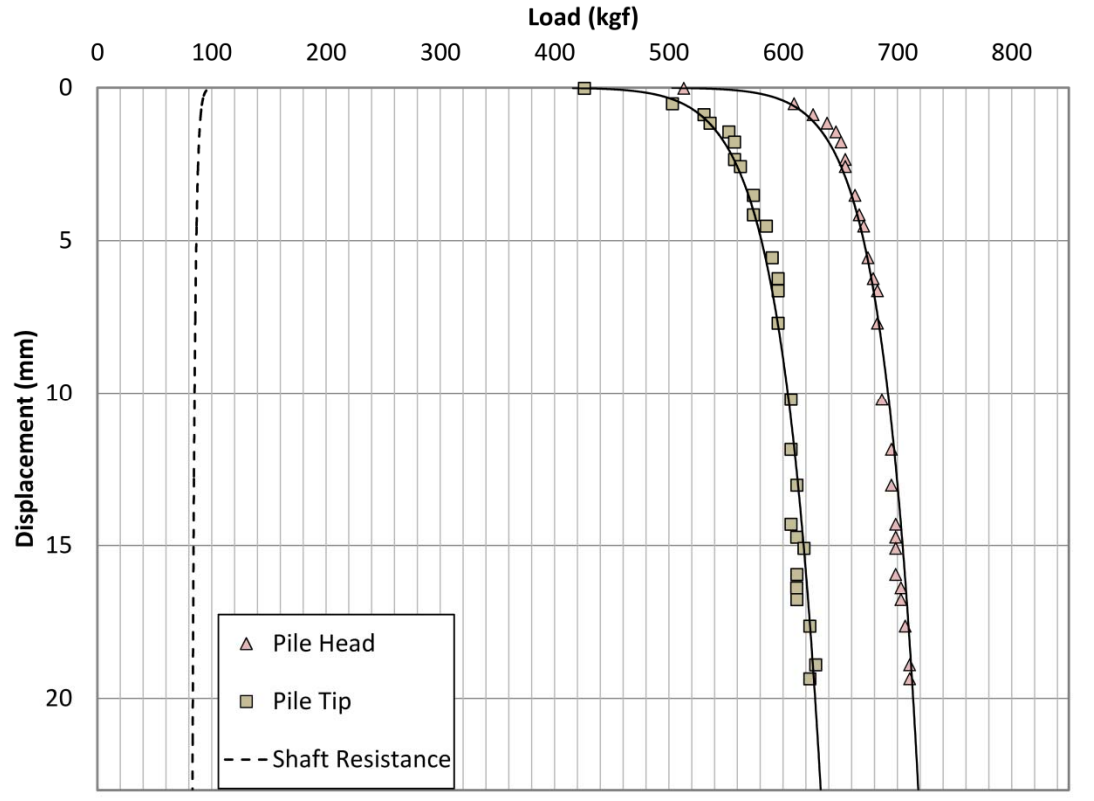

Figure 3.33 Load-Displacement curve for test A-30-4 (L/D=13)

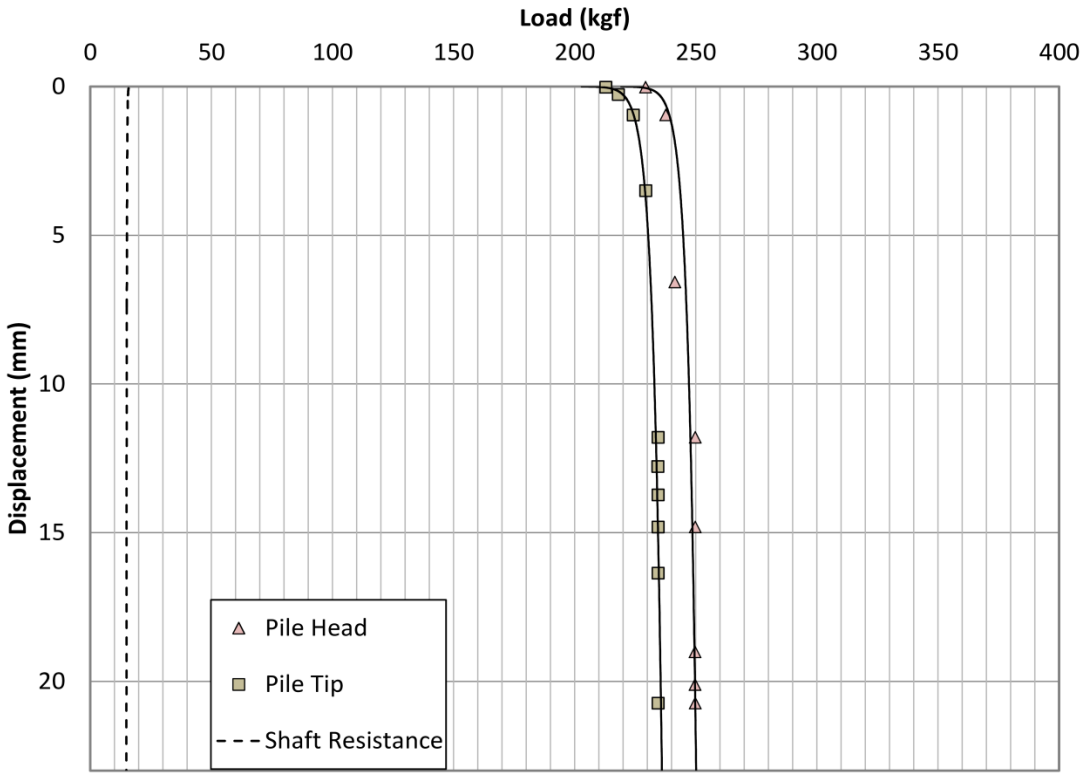

Figure 3.34 Load-Displacement curve for test A-40-1 (L/D=5.4)

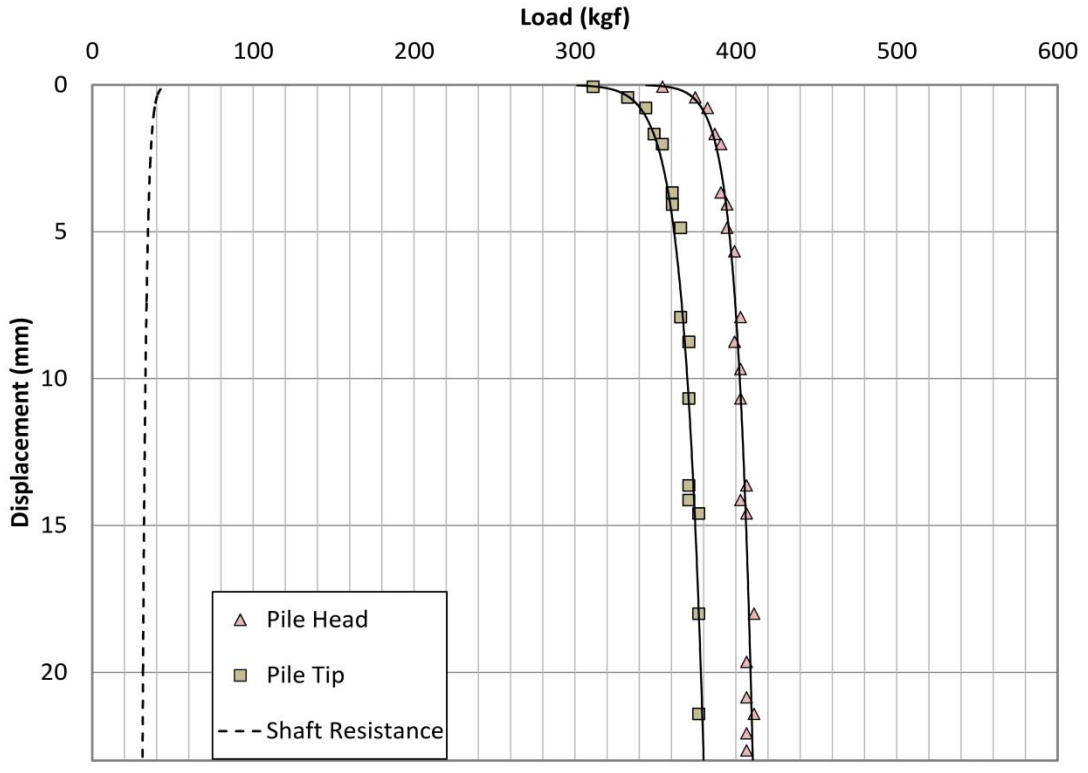

Figure 3.35 Load-Displacement curve for test A-40-2 (L/D=8.4)

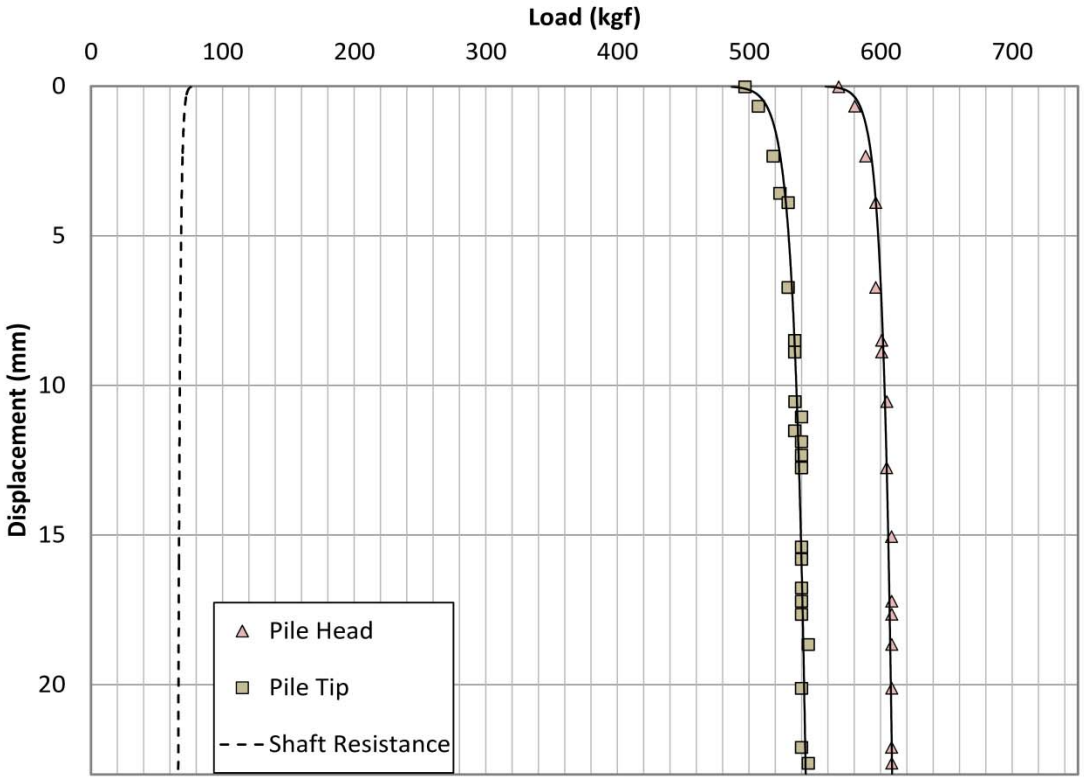

Figure 3.36 Load-Displacement curve for test A-40-3 (L/D=11.4)

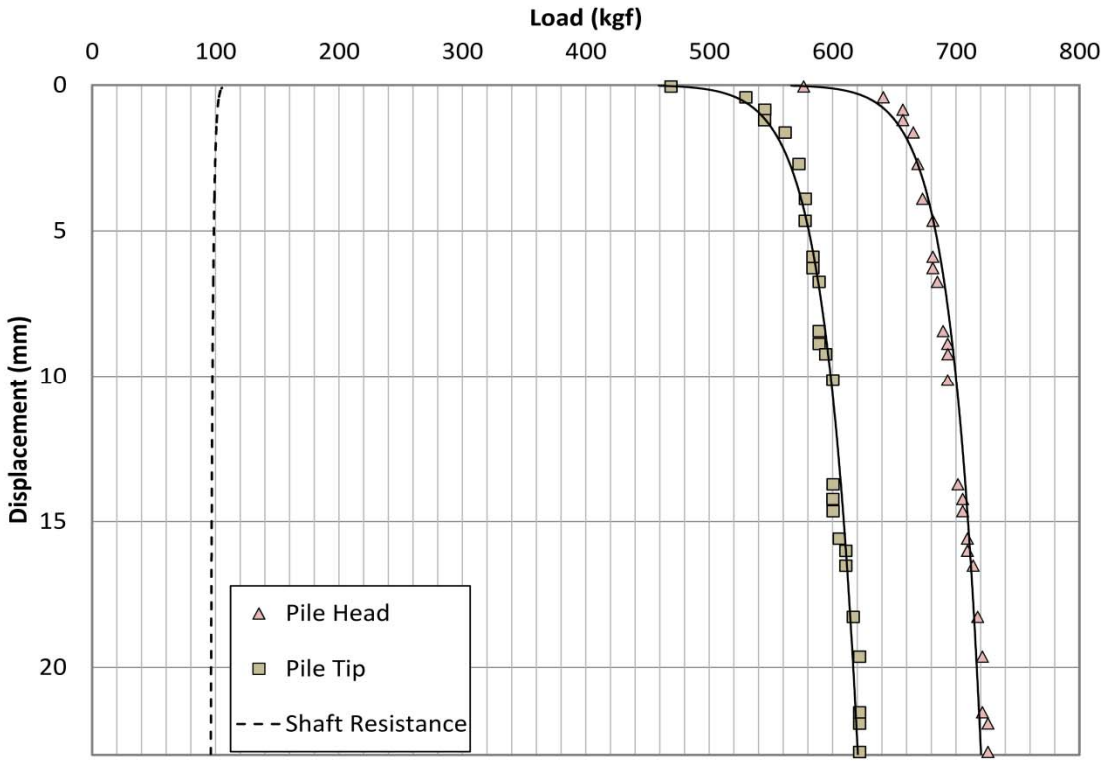

Figure 3.37 Load-Displacement curve for test A-40-4 (L/D=13)

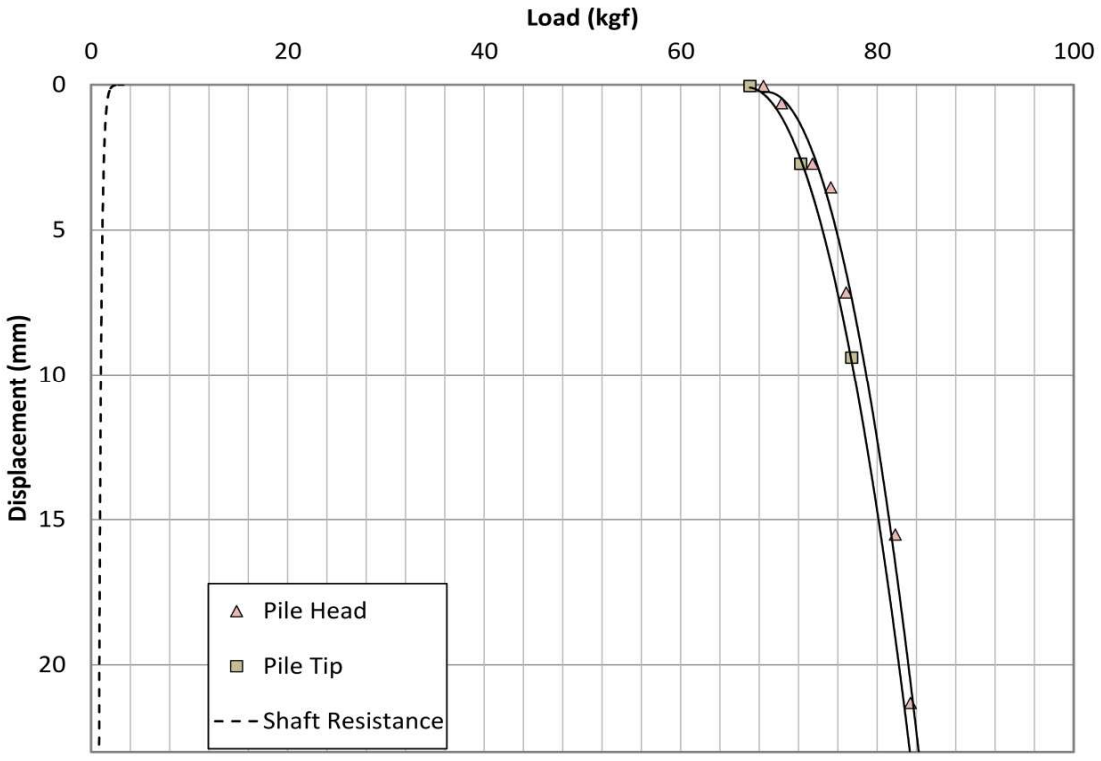

Figure 3.38 Load-Displacement curve for test B-20-1 (L/D=9.7)

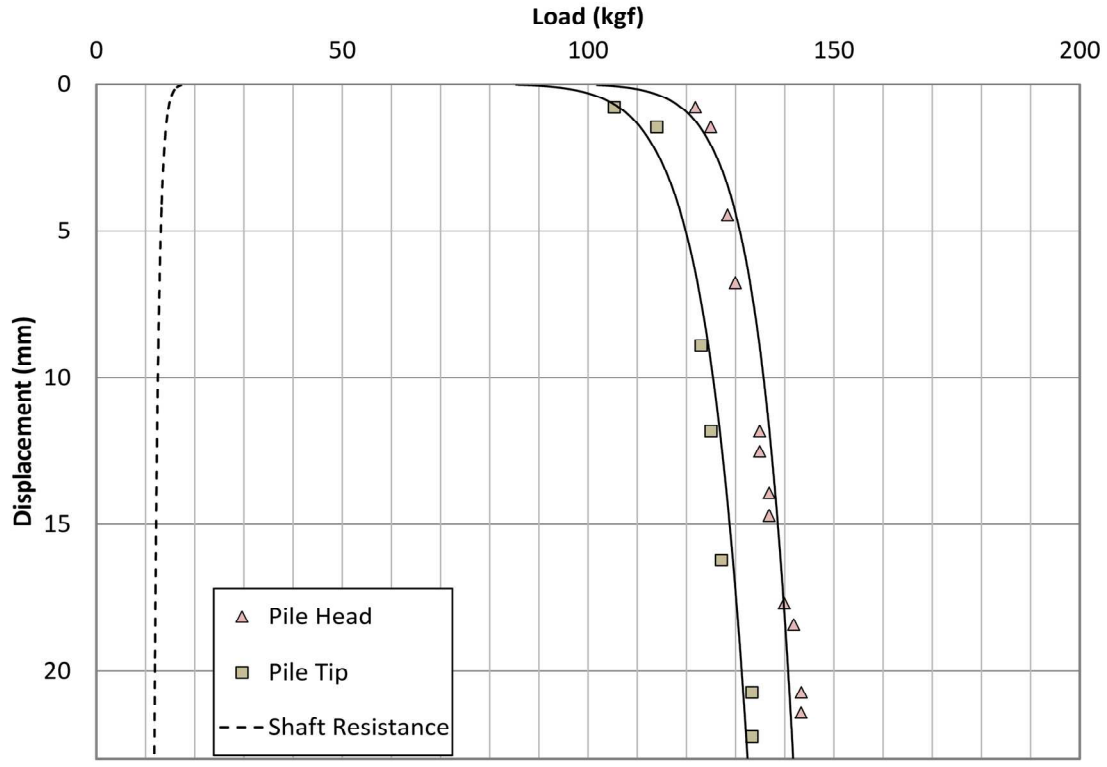

Figure 3.39 Load-Displacement curve for test B-20-2 (L/D=14.9)

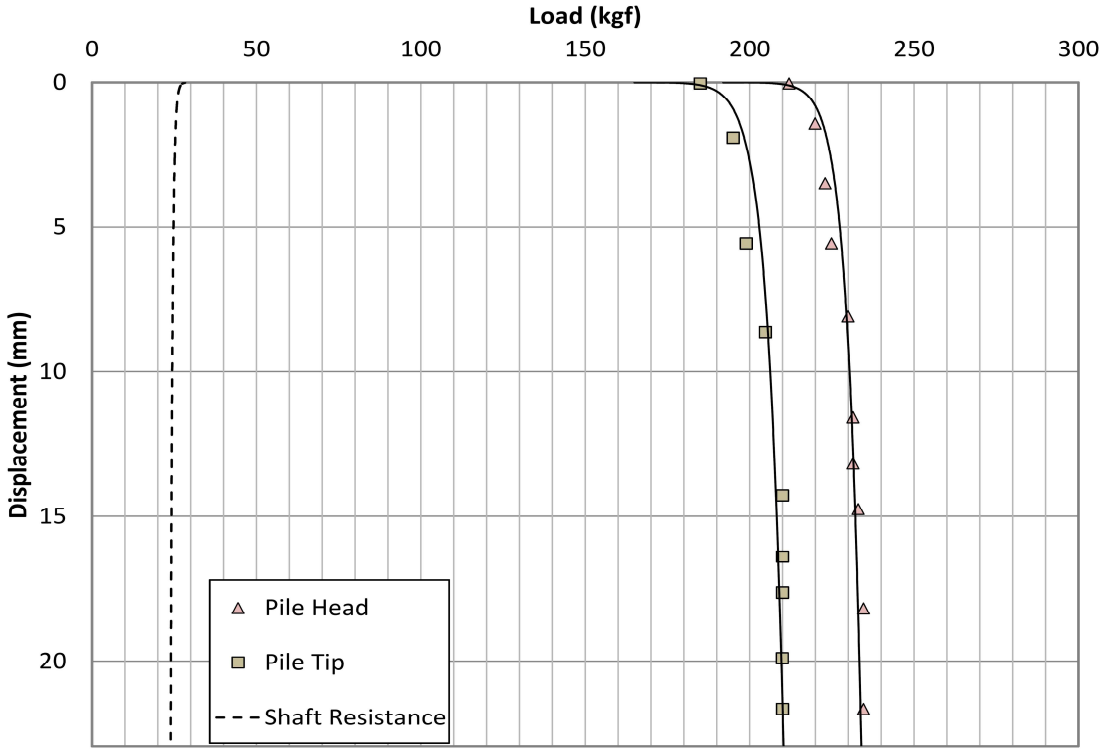

Figure 3.40 Load-Displacement curve for test B-20-3 (L/D=20.1)

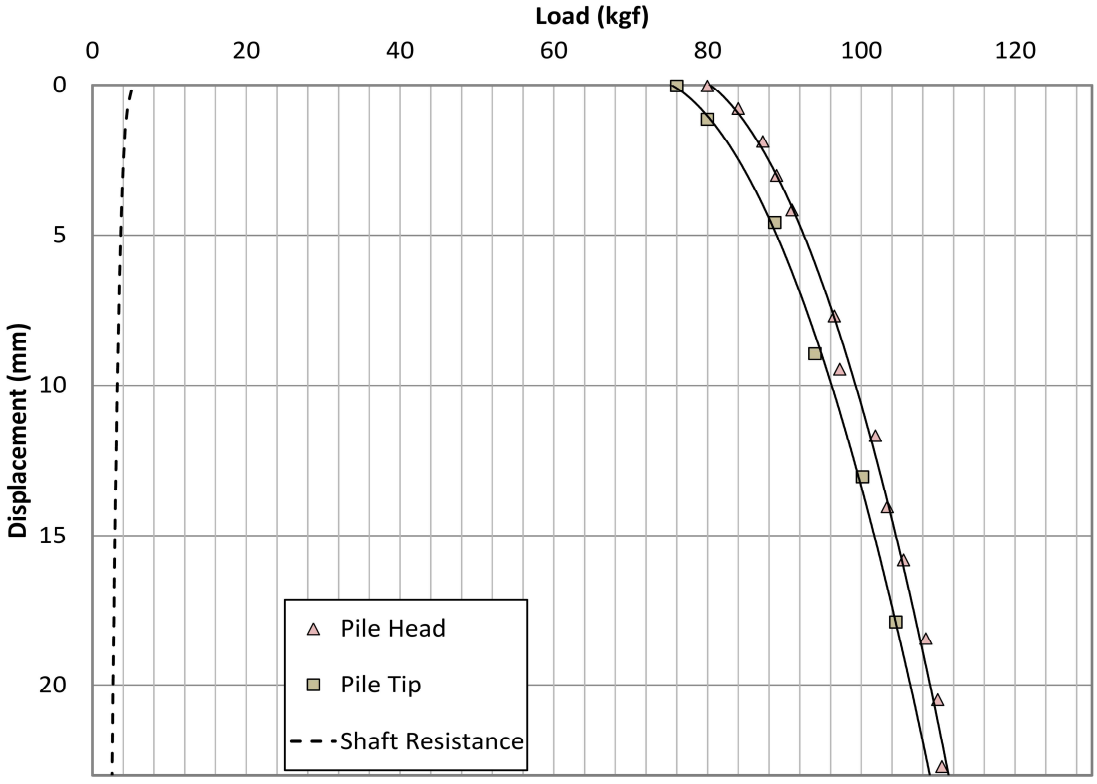

Figure 3.41 Load-Displacement curve for test B-40-1 (L/D=9.7)

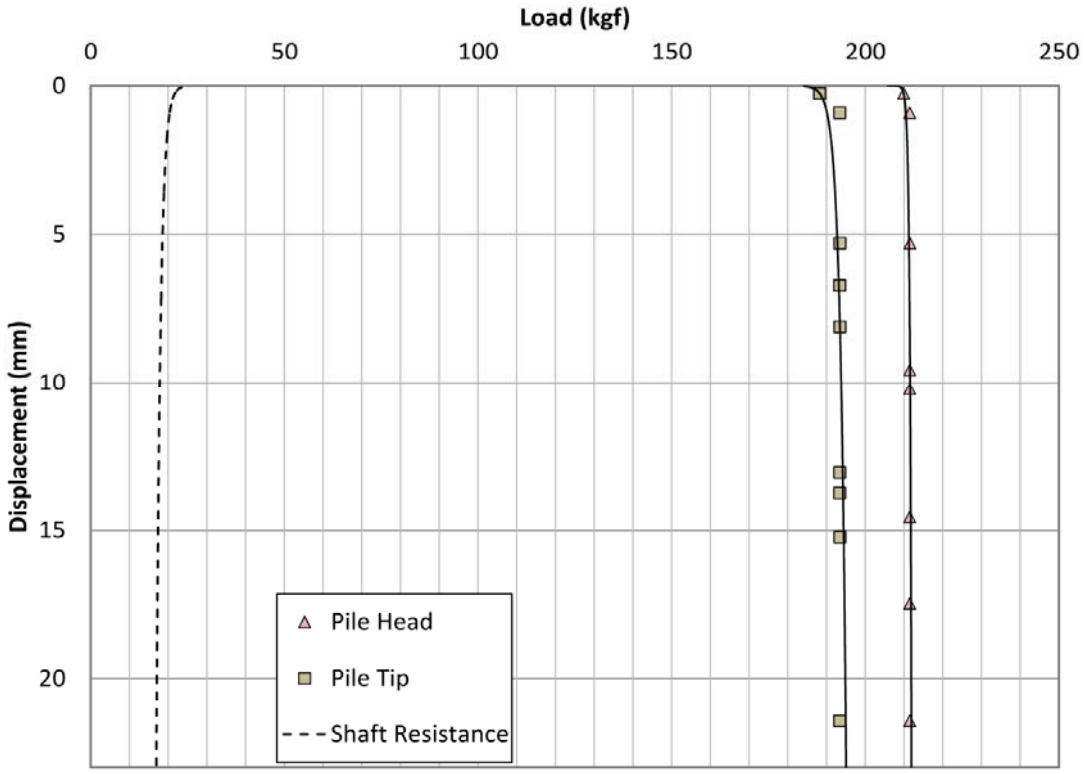

Figure 3.42 Load-Displacement curve for test B-40-2 (L/D=14.9)

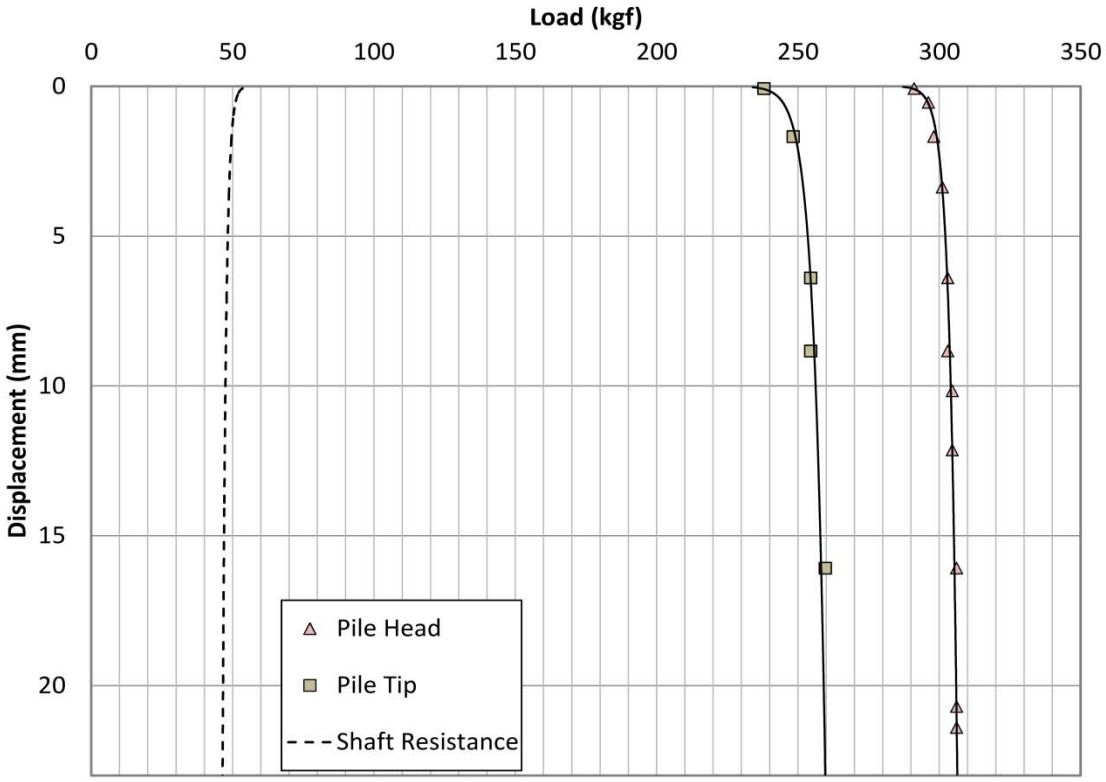

Figure 3.43 Load-Displacement curve for test B-40-3 (L/D=20.1)

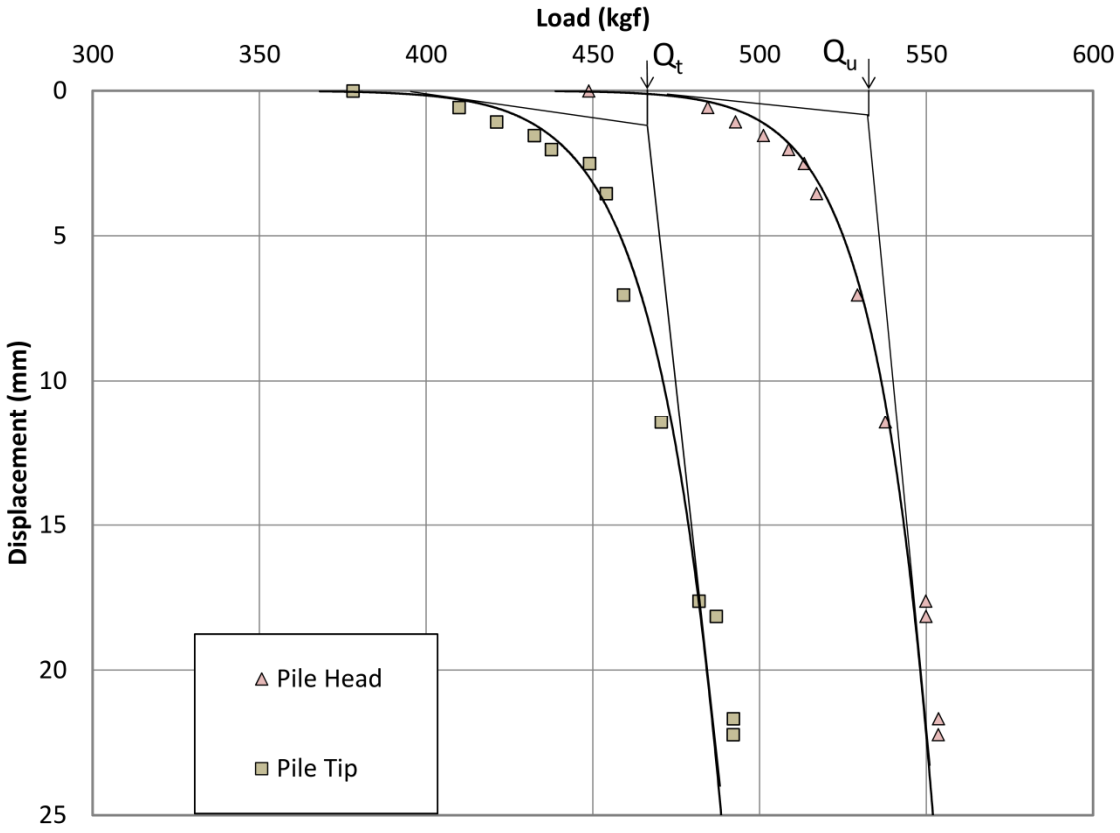

Figure 3.44 Tangent intersection method; Test A-20-4

The total shaft resistance versus depth plots with trend lines for all series are presented in the figures to follow. Figure 3.45 shows the variations of shaft resistance, $Q_{s,}$ with depth of embedment for the A-Series. The variations of Qs with depth for the B-Series are shown in Figure 3.46. The variation of average unit shaft resistance, $f_{s,}$ versus relative depth for all series is presented in Figure 3.47.

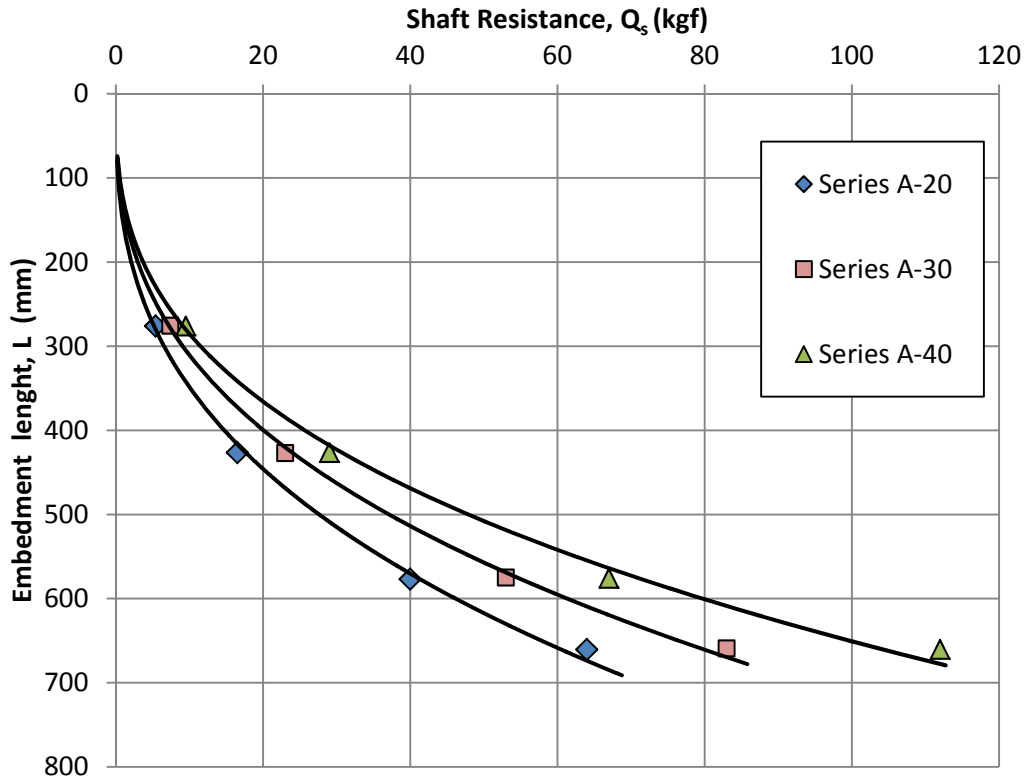

Figure 3.45 Shaft resistance versus depth for the 5.08 cm. diameter pile

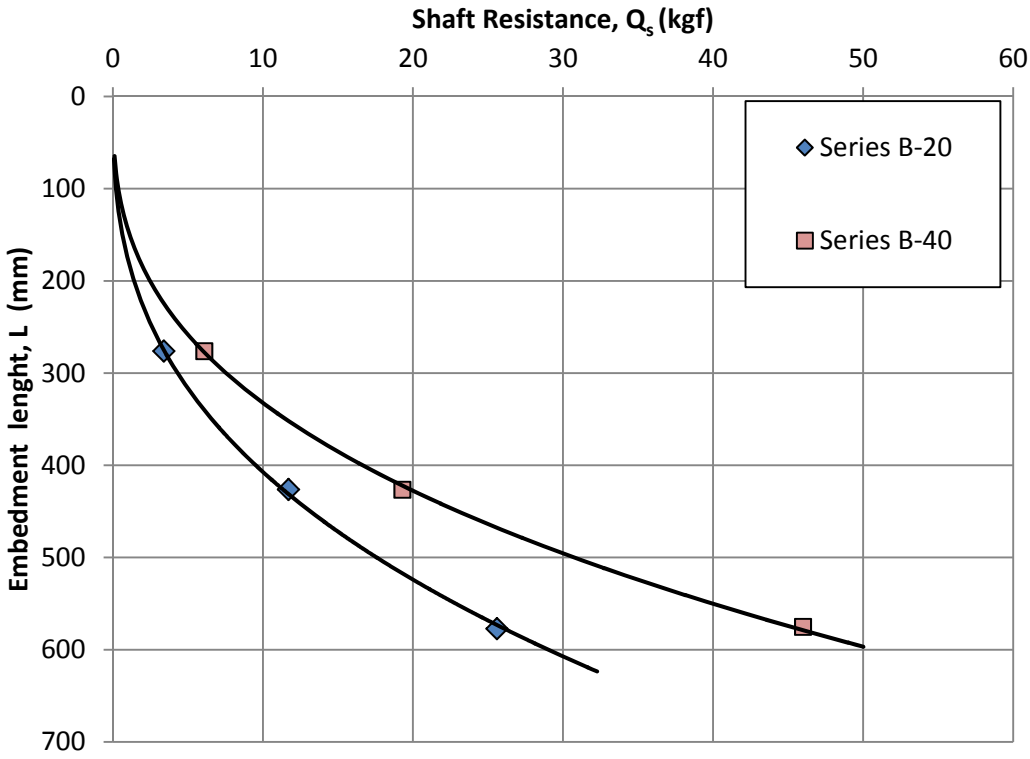

Figure 3.46 Shaft resistance versus depth for the 2.86 cm. diameter pile

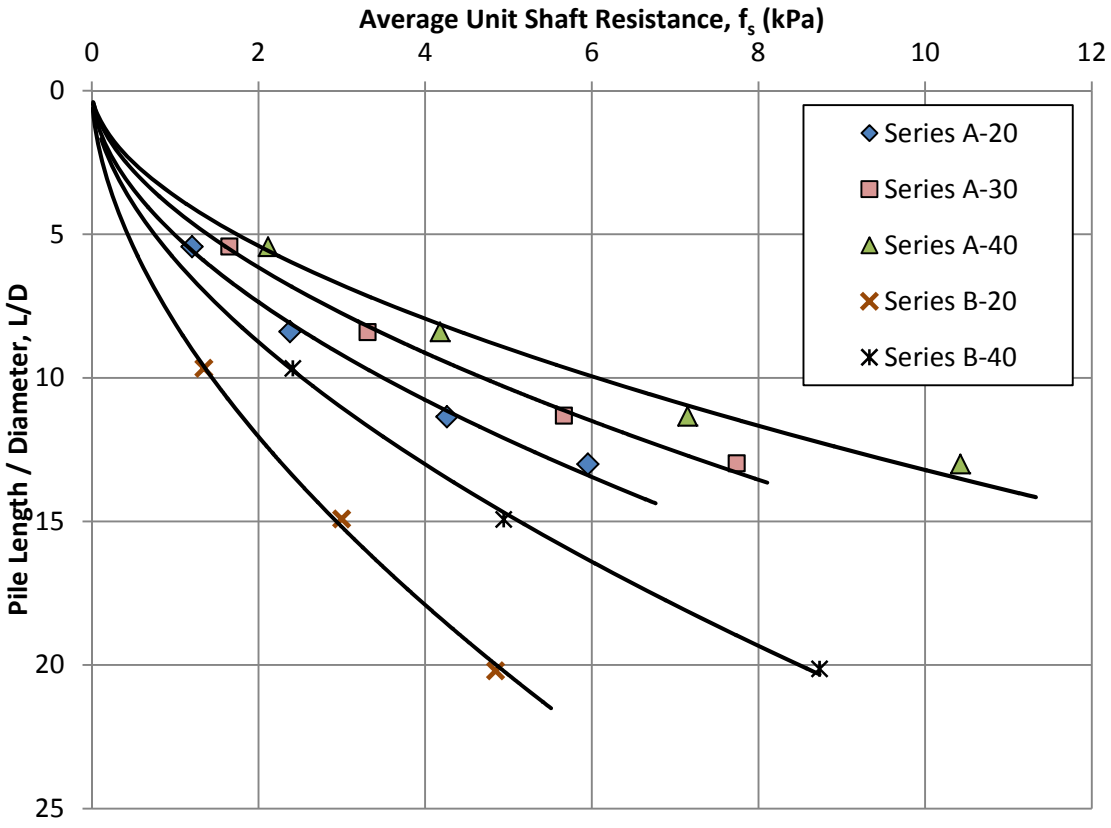

Figure 3.47 Average unit shat resistance versus depth for all series

Chapter 4

Analytical Model

4.1 General

Theoretical models of failure mechanisms around pile foundations are generally developed from an assumed geometry of the soil deposit around the pile shaft referred to as the influence zone and a system of forces acting on it. In chapter two, an account of various failure mechanisms assumed by different authors was given. Except for a few authors, **(Tezaghi, 1943, Skempton et al., 1953, Hanna and Nguyen, 2002)**, the determination of shaft resistance has been omitted from analytical models of bearing capacity of piles. Furthermore, the effect of overconsolidation on piles driven in sand has been ignored in the development of rational bearing capacity theories present in the literature. In this section, a modification of the failure mechanism introduced by **Hanna and Nguyen (2002)** is presented to incorporate the effects of stress history of sand on the shaft resistance of driven piles.

When a closed ended circular pile is driven into a sand deposit, a cone-shaped region develops beneath the advancing pile tip moving downward pushing the surrounding soil in a radial and upward direction **(Vesic, 1967)**. The extent of this disturbance defines the zone of influence, that is, the volume of soil that is disturbed by the advancing pile exerting a reaction which amounts to the pile's capacity. The horizontal extent of the zone of influence is denoted as the radius of influence. Outside the radius of influence, the sand deposit is assumed undisturbed and the stresses acting on the outer surface of the influence zone are according to the at rest condition of the surrounding soil. A depiction of the soil-pile system is shown in Figure 4.1.

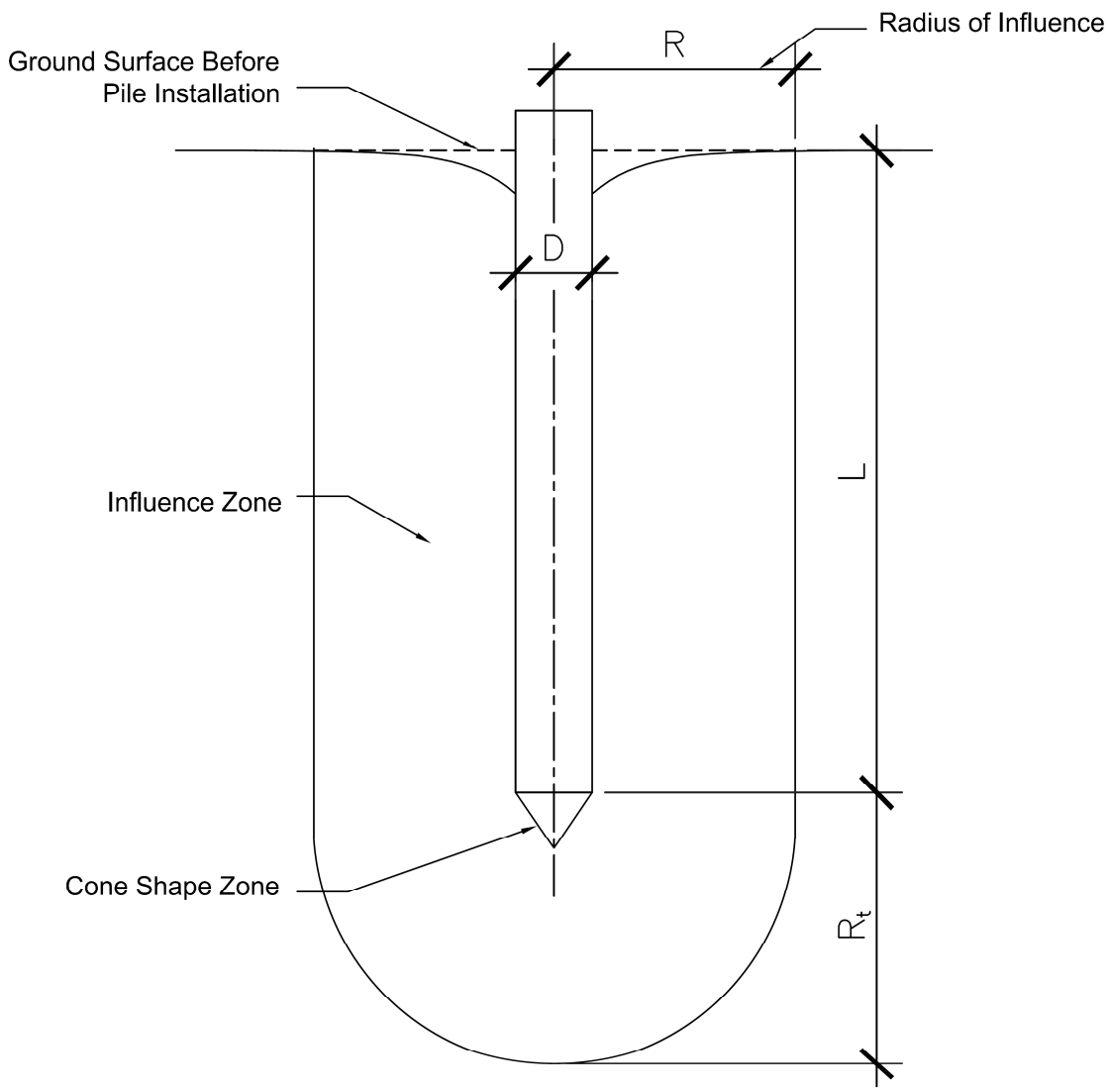

Figure 4.1 Influence Zone

4.2 Failure Mechanism

Analogous to the critical shear failure surfaces proposed by **Hanna and Nguyen (2002)**, Figure 4.2 shows the failure mechanism to be considered herein. The section is divided into three zones:

Zone I: Consists of two Trapezoidal zones acde and a'c'd'e' bounded horizontally by the pile shaft and the outer boundary of the influence zone, and vertically by the ground surface and segment ac and a'c' making an angle beta from the horizontal at the pile tip.

Zone II: Consists of two radial shear zones Bac and Ba'c' bounded below by log spirals Bc and Bc' passing throw the apex at B and terminating at c and c' a horizontal distance equal to the radius of influence.

Zone III: Consists of a wedge zone aBa' beneath the pile tip.

In this thesis, only zone I will be considered in the analysis for that it is the interest of the author to evaluate the shaft resistance related to stress history and the volume of soil displaced by the pile, that is, the pile geometry.

The following assumptions are made regarding the critical shear surfaces of zone I:

i. No shear resistance is mobilized along the boundary cd and c'd' of the influence zone.
ii. The shear resistance along ac and a'c' is locally mobilized with maximum values at a and a' equal to ϕ and decreasing linearly to zero at c and c'. In effect, the angle of shear resistance ϕ_β along ac and a'c' is taken to be equal to $\phi/2$.

The volume of sand within the influence zone is considered to be axisymmetric for a single vertical pile under axial loading. Hence, it is sufficient to analyze only a sector of the volume of zone I, namely the volume generated by zone deac of the cross section shown in Figure 4.2 as it revolves through an angle $\Delta\varsigma$ around the pile axis.

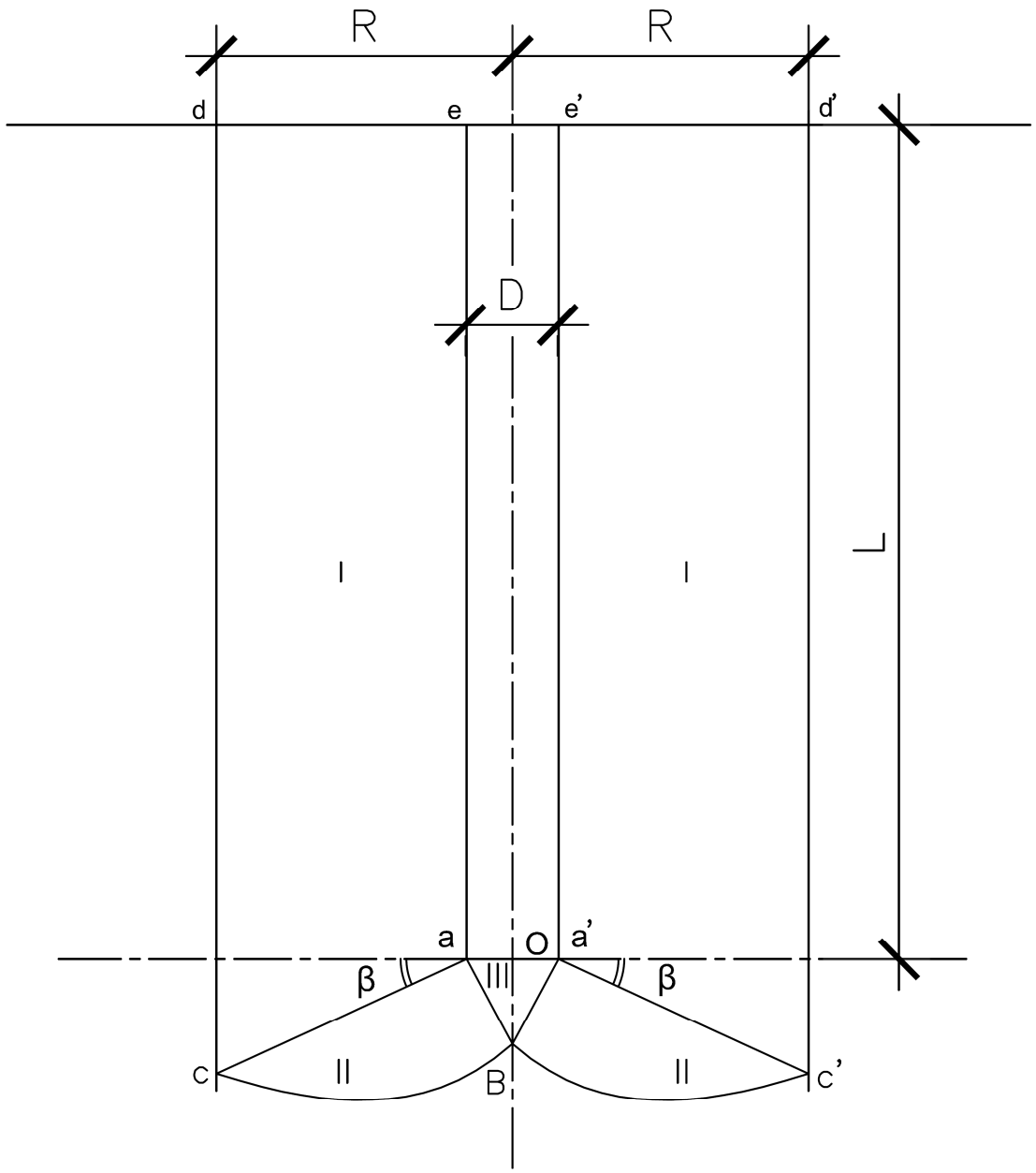

Figure 4.2 Assumed failure mechanism (after Hanna and Nguyen, 2002)

The volume generated by this rotation as well as the system of forces acting on it is shown in Figure 4.3.

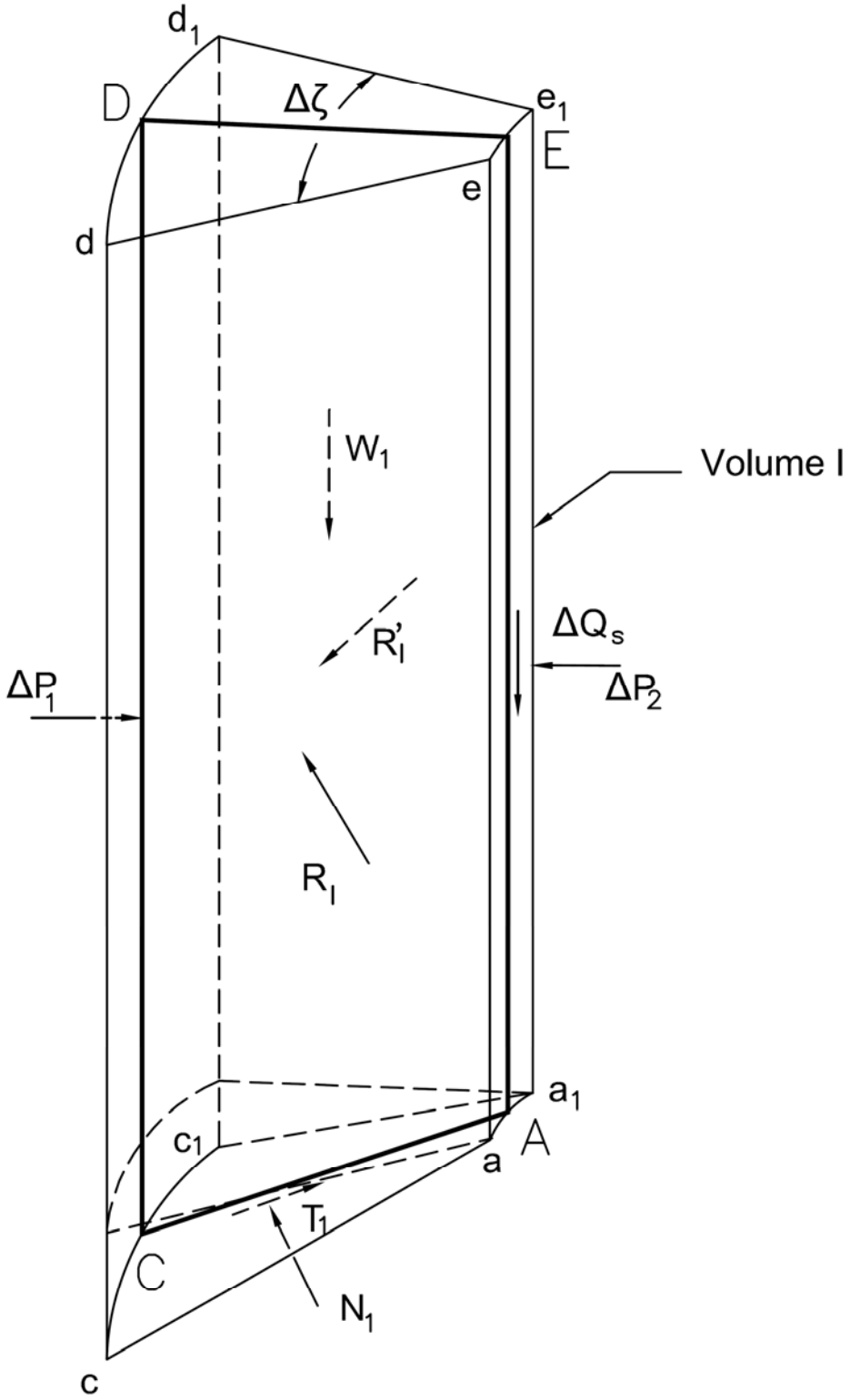

Figure 4.3 Volume generated by a rotation of the plane section acde through an angle Δζ around the pile axis (after Hanna and Nguyen, 2002)

4.2.1 Determination of Shaft Resistance Q_s

The system of forces acting on volume I are shown in Figure 4.3 and include the weight of the soil wedge $W_{I,}$ the tangential and normal forces N_1 and T_1 of the earth pressure acting on the surface acc_1a_1, the normal earth pressure force ΔP_1 acting on the surface $cdd_1c_{1,}$ the resultant forces R_1 and R'_1 of earth pressure acting on surfaces acde and $a_1c_1d_1e_{1,}$ respectively, and the tangential and normal forces ΔP_2 and ΔQ_s acting on the surface aee_1a_1. Examination of Figure 4.3 shows that the problem can be transformed into a two dimensional one by applying the forces on the plane of symmetry. The resulting system is shown in Figure 4.4. Once the forces acting on the volume I are identified, a method of solution for shaft resistance can be developed. Each of the forces introduced can be evaluated as follows:

i. The soil weight W_I of volume I is calculated as the product of the area of the trapezoid ACDE and the distance travelled by its centroid over an angle of rotation $\Delta\zeta$ around the pile axis times the unit weight and is given by Eq. 4.2 (Pappus-Guldinus' Theorem).

$$W_1 = Area(ACDE) * (\bar{x} + \frac{D}{2}) * \Delta\zeta * \gamma \tag{4.2}$$

where the *x* coordinate of the centroid $\bar{x}$ of trapezoid ACDE is found as follows:

$$\bar{x} = \frac{R'(L + 2(L + R'\tan\beta)}{3(L + (L + R'\tan\beta)} \tag{4.3}$$

and

$$R' = R - \frac{D}{2} \tag{4.4}$$

where

R= radius of influence

D= pile diameter

L= embedment length

Note: The unit weight distributions on the experiments conducted herein are linear with depth so the unit weights considered in the analysis will be those at the centroid.

ii. The tangential and normal forces N_1 and T_1 of the earth pressure acting on the surface acc_1a_1 can be related by the following expression:

$$T_1 = N_1 \tan \phi_\beta \tag{4.5}$$

where ϕ_β is the average mobilized friction angle along AC.

iii. The resultant ΔP_1 of the earth pressure of an overconsolidated sand deposit is given by :

$$\Delta P_1 = \frac{1}{2}(K_o^{oc} \gamma D_1^2) \times R \times \Delta\zeta \tag{4.6}$$

where

$$K_o^{oc} = (1 - \sin\phi)(OCR)^{\sin\phi - 0.18} \tag{4.7}$$

after **Hanna and Al-Romhein (2008)**

D_1 = length of segment CD

R = radius of influence as proposed by **Berezantzev (1961)** and is obtained from the following expression:

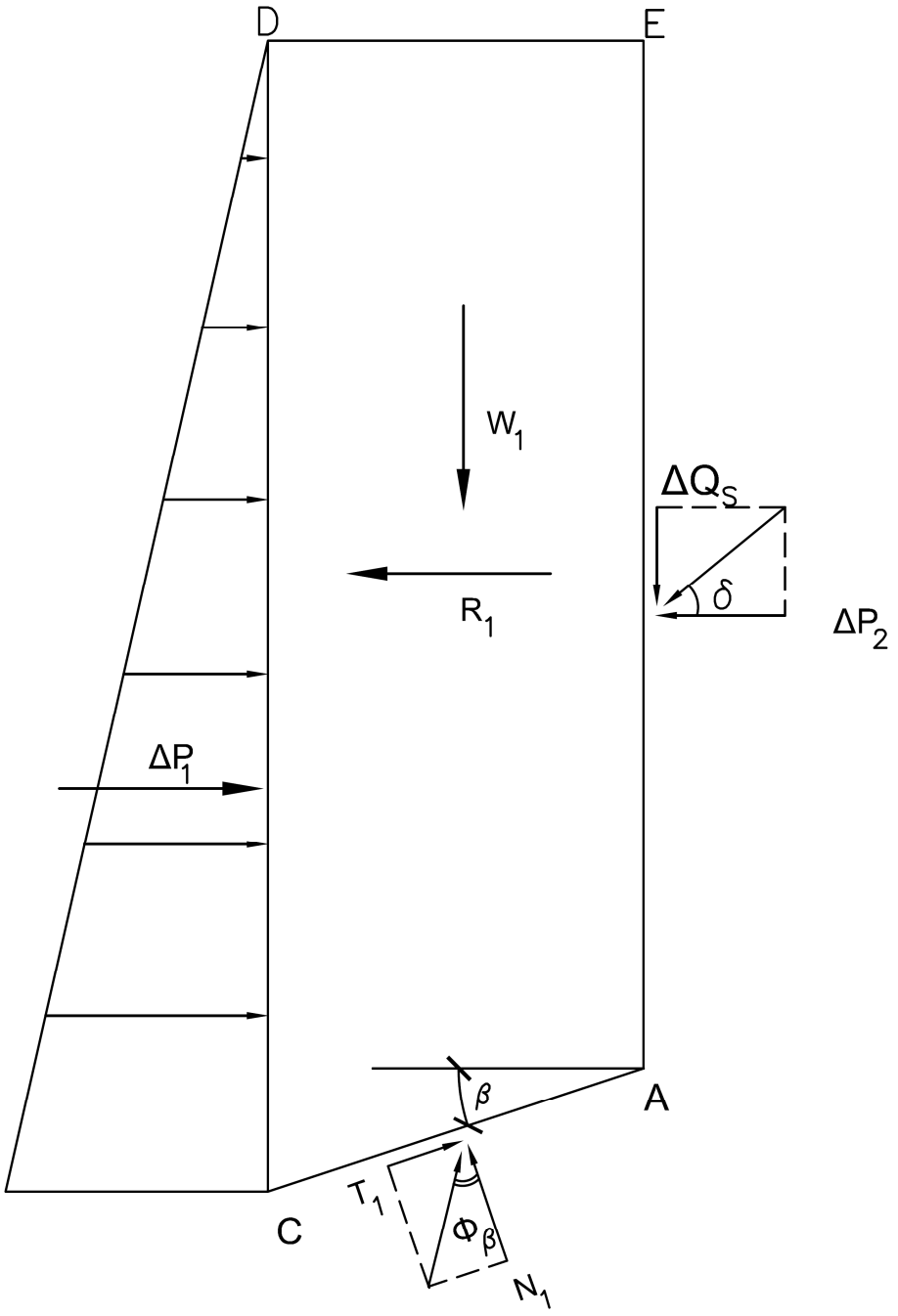

Figure 4.4 Two dimensional system of forces acting on the plane of symmetry of Volume I (After Hanna and Nguyen, 2002)

$$\frac{R}{D}=\frac{1}{2}\left(1+\frac{\sqrt{2}e^{(\frac{\pi}{2}-\frac{\phi}{2})\tan\frac{\phi}{2}}}{\sin(\frac{\pi}{4}-\frac{\phi}{2})}\right) \tag{4.8}$$

where

D = is the pile diameter

$\Delta\zeta$ = angle of rotation in radian

iv. The resultant R_1 is found by examination of Figure 4.5 where the normal components of R_I and R'_I to the plane of symmetry cancel one another.

Hence,

$$R_1=R_{I(x)}+R'_{I(x)} \tag{4.9}$$

$$R_1 = R_I \sin(\frac{\Delta\zeta}{2}) + R'_I \sin(\frac{\Delta\zeta}{2}) \tag{4.10}$$

Since $R_I=R'_I$

$$R_1 = 2R_I \sin(\frac{\Delta\zeta}{2}) = 2R'_I \sin(\frac{\Delta\zeta}{2}) \tag{4.11}$$

where

$R_{I(x)} = R'_{I(x)}$ = the components of R_1 parallel to the plane of symmetry.

In order to determine the forces R_I or R'_I, an assumption on the distribution of the coefficient of earth pressure inside volume I must be made for that the actual distribution is unknown due to the chances on the stress distribution around the pile induced by the pile installation.

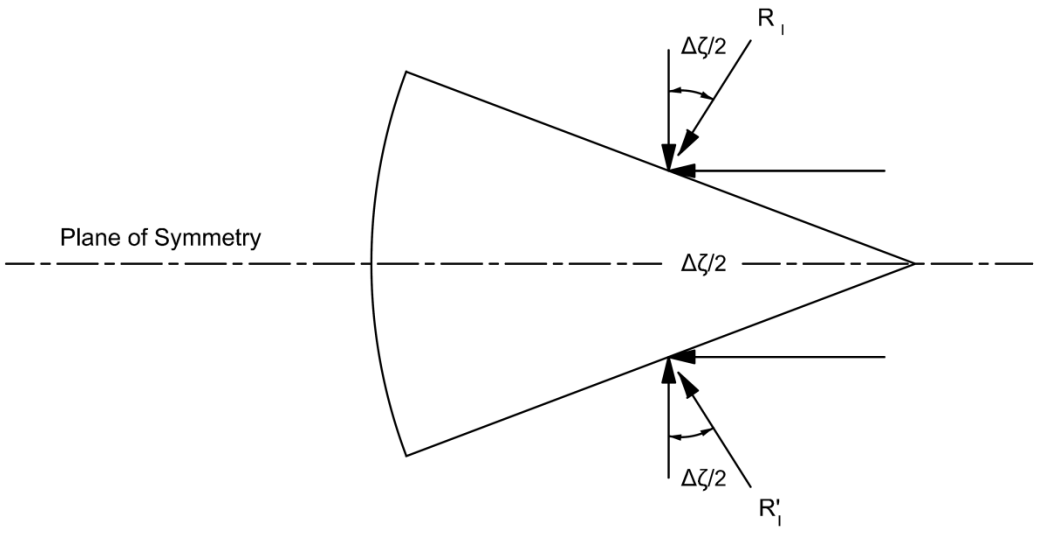

Figure 4.5 Top view of volume I and components of RI and R'I

An equivalent coefficient K_E equal to the coefficient of earth pressure at rest given by **Jaky (1948)** will be consider in the analysis. Then, the force RI = R'I can be calculated as a hydrostatic force acting on the trapezoid acde submerged in a fluid with unit weight equal to $K_E \gamma$. The hydrostatic force is equal to the product of the area of the trapezoid and the hydrostatic pressure at its centroid. It is convenient to express R_I and R'_I as follows:

$$R_I = R'_I = F_1 + F_2 \tag{4.12}$$

where

$F_1 =$ resultant earth pressure force acting on the rectangle ahde

$F_2 =$ resultant earth pressure force acting on the triangle ahc

Forces F_1 and F_2 are found by inspection of Figure 4.6 as follows:

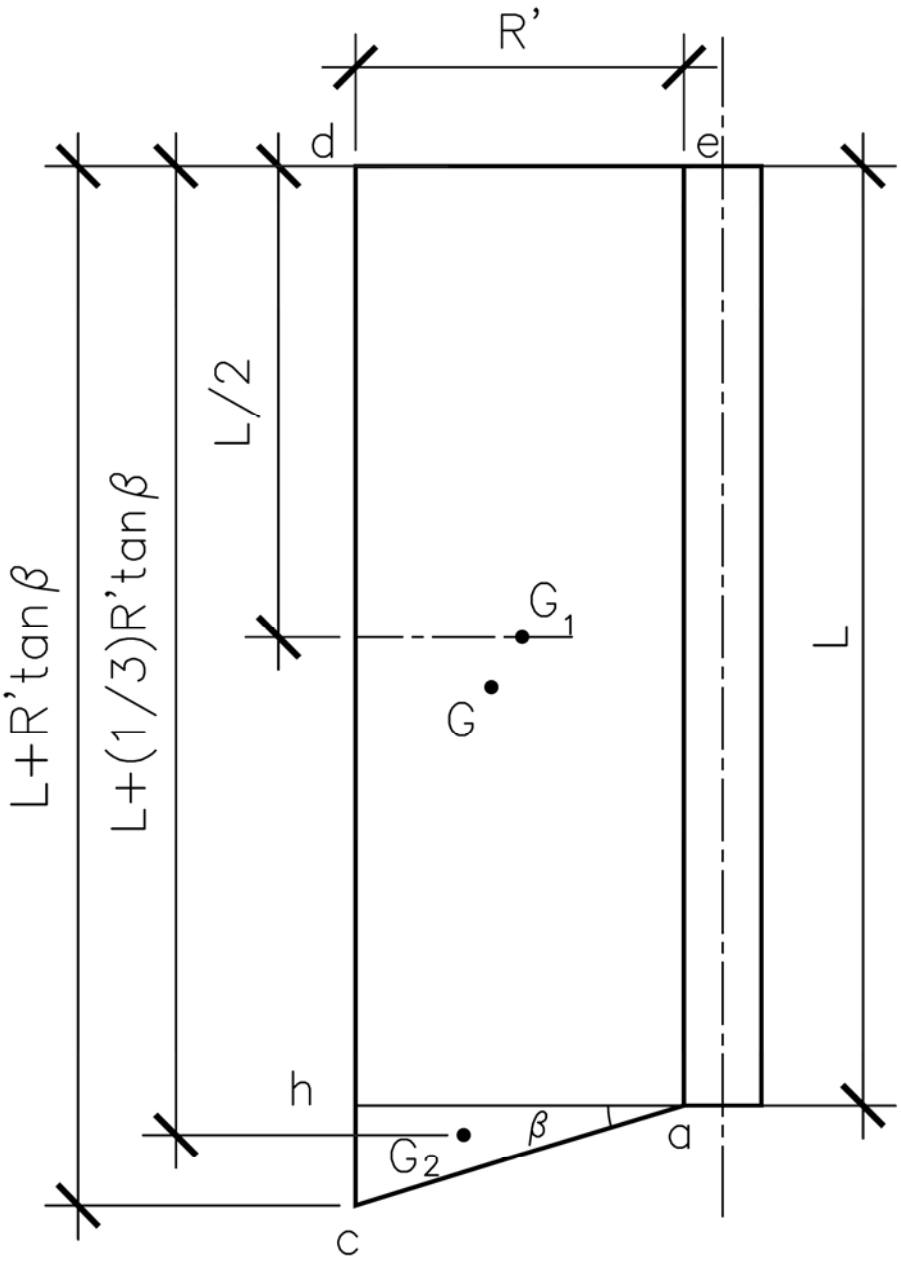

Figure 4.6 Diagram of plane acde and centroids used for calculations of earth pressure inside the influence zone in volume I (After Hanna and Nguyen, 2002)

$$F_1 = (\underbrace{\frac{1}{2}K_E\gamma L}_{hydrostatic\_pressure})(\underbrace{L * R'}_{area}) = \frac{1}{2}K_E\gamma L^2 R' \tag{4.13}$$

$$F_2 = \left[\underbrace{\left(L + \frac{1}{3}R'\tan\beta\right)K_E\gamma}_{hydrostatic\_pressure}\right]\left[\underbrace{\frac{1}{2}(R'\tan\beta)R'}_{area}\right] = \frac{1}{2}K_E\gamma R'\left[R'\tan\beta(L + \frac{1}{3}R'\tan\beta\right] \tag{4.14}$$

Hence,

$$R_I = R'_I = \frac{1}{2}K_E\gamma R'\left[L^2 + LR'\tan\beta + \frac{1}{3}(R'\tan\beta)^2\right] \tag{4.15}$$

Where

R'=R-D/2

R = radius of influence

L = embedment length

D = pile diameter

β = angle segment AC makes with the horizontal at pile tip measured positive in the downward direction.

v. The normal force ΔP_2 can be found by the application of a generalized method of slices introduced by **Sarma (1979)**. In this method, a soil mass enclosed in a plane slip surface is divided into an arbitrary number of slices of any size for which its sides can take any orientation. Sarma derived the following recurrence relation relating the normal forces E_i and E_{i+1} acting on the left and right sides of the slice, respectively:

$$E_{i+1} = \frac{\cos(\phi_{Bi} - \alpha_i + \phi_{Si} - \omega_i)\cos(\phi_{Si+1})}{\cos(\phi_{Bi} - \alpha_i + \phi_{Si+1} - \omega_{i+1})\cos(\phi_{Si})}E_i$$

$$+\frac{(W_i + FV_i)(\cos\phi_{Si+1})\sin(\phi_{Bi} - \alpha_i)}{\cos(\phi_{Bi} - \alpha_i + \phi_{Si+1} - \omega_{i+1})}$$

$$+\frac{FH_i(\cos\phi_{Si+1})\cos(\phi_{Bi} - \alpha_i)}{\cos(\phi_{Bi} - \alpha_i + \phi_{Si+1} - \omega_{i+1})} \tag{4.16}$$

where

E_{i+1} and E_i = normal forces acting on slice i

α_i = base slope of slice i

ω_{i+1} and ω_i = tilt of the sides of slice i

ϕ_{Bi} = mobilized angle of friction at mid-point of the base of slice i

ϕ_{Si+1} and ϕ_{Si} = average mobilized friction angle along the sides of slice i

W_i = weight of slice i

F_i = Resultant of other external forces acting on slice i

FH_i and FV_i = horizontal and vertical components of F_i

The notation and sign convention are given in Figure 4.7

If the plane of symmetry ACDE is considered as a single slice with vertical sides and $\delta = \phi$, Eq. 4.16 can be applied using the notation in Figure 4.4 to obtain an expression for ΔP_2 for as follows:

$$\Delta P_2 = \frac{\Delta E_1 \cos\phi\cos(\phi_\beta - \beta) + W_1 \cos\phi\sin(\phi_\beta - \beta) - R_1 \cos\phi\cos(\phi_\beta - \beta)}{\cos(\phi_\beta - \beta + \phi)} \tag{4.17}$$

The shear force acting on the surface aee_1a_1 through a rotation angle $\Delta\zeta$ is given by:

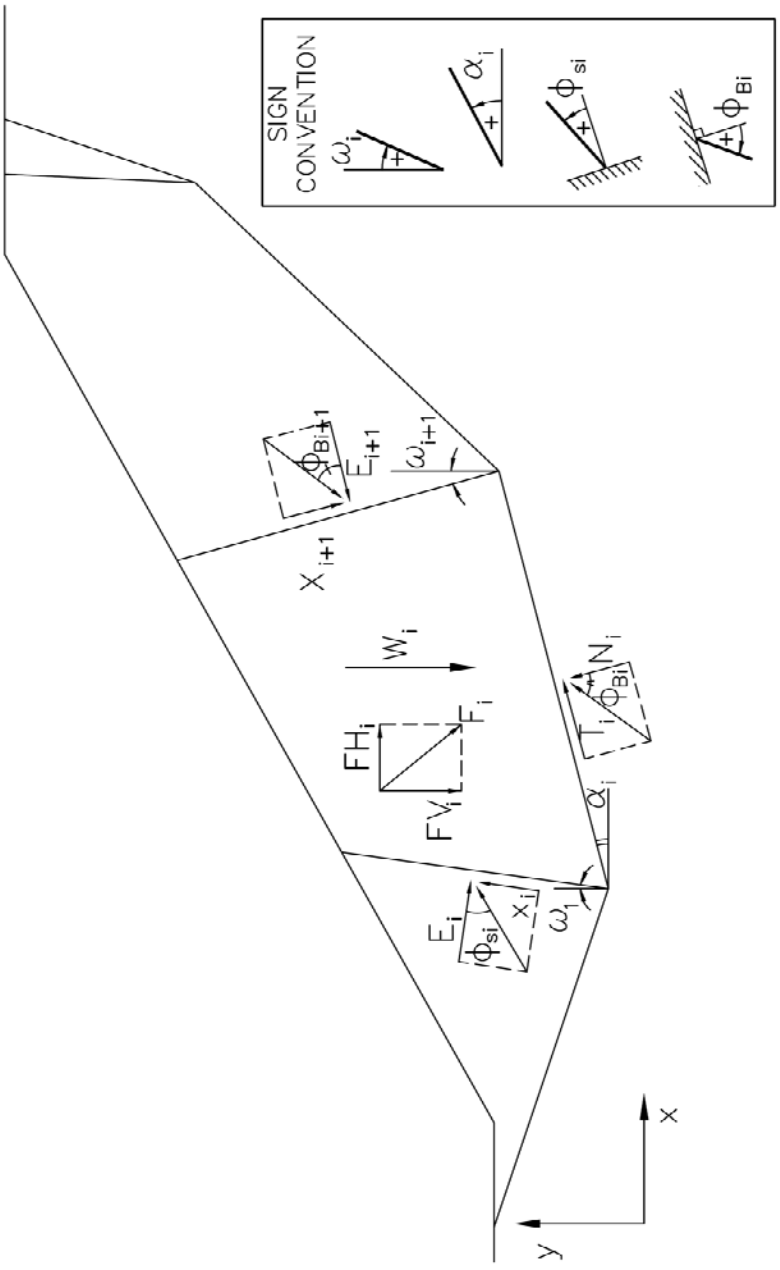

Figure 4.7 Configuration and sign convention for Sarma's method of slices

$$\Delta Q_s = \Delta P_2 \tan\phi \tag{4.18}$$

Hence the total shaft resistance Q_s is given by the following relation:

$$Q_s = \Delta Q_s (\frac{2\pi}{\Delta\zeta}) = \Delta P_2 \tan\phi (\frac{2\pi}{\Delta\zeta}) \tag{4.19}$$

It should be noted here that the tangential and normal components acting on the base of the slice i are eliminated in the derivation of Eq. 4.15.

The model presented in this section to study the shaft resistance of a single pile in overconsolidated sand involves the following variables: $L, D, \phi, \delta, K_o^{oc}, K_E, R$ and β . The last three are considered to be the model parameters where K_E and R are fixed by the model assumptions. The angle beta, however, is difficult to predict from theory without knowledge of the point resistance on overconsolidated sand. **Hanna and Nguyen (2002)** presented their work on the interdependence of point and shaft resistance in normally consolidated sands. The interdependence is explained by the influence of the angle beta on shaft resistance. That is, for a given soil friction angle and pile relative depth the bearing capacity factor proposed by **Berezantev (1961)** is used in a computer program by trial and error varying the angle beta until Berezantev's factor is matched. Then, a model analogous to the one presented herein (different assumed earth pressures) is used with the angle beta to calculate the shaft resistance of the given pile. However, the difficulty in utilizing the approach followed by **Hanna and Nguyen (2002)** rises with the lack of theoretical formulations which incorporate OCR in the derivation of bearing capacity factors.

4.2.2 Determination of the Angle Beta

An empirical approach for the determination of the angle beta as a function of relative depth, *L/D* and overconsolidation ratio, *OCR* is implemented in this section. The results of test series A-20, A-30 and A-40 will be used exclusively in order to develop a chart that relates the angle Beta to $OCR_{(ave)}$ and the aspect ratio *L/D*. Recall from chapter three that for the A-series, the compaction energy was changed resulting on different distributions of *OCR* and relative densities with depth. Also, four tests in each series were conducted at four different relative depths. The embedment length *L* was repeated across the three series. As a result, for the same relative depth, three tests were obtained with different average overconsolidation ratios. Hence, four sets of tests, each set at a different relative depth and all at different average overconsolidation ratios were obtained.

The aspect ratio for the A-series varied from 5.4 to a maximum of 13. In order to develop a chart, a database was generated using the trend lines of the variation of Q_s, unit weight, friction angle, *OCR*, *L/D*, and the corresponding earth pressures with depth for the three different A-series. The database was used to extrapolate the results up to a relative depth of 20. The analytical model introduced in the previous section was coded in excel and the properties for each test were entered. The value of beta was changed until agreement between the experimental results and the model prediction for Qs was reached. The plots of the angle beta vs. *OCR* showed a linear relationship for a given L/D. The generated chart is presented in Figure 4.8. The analytical model formulations were then coded in to a C++ program, S-PILE, which in conjunction with the chart presented in Figure 4.36 can be used to estimate the shaft resistance of a driven pile in

overconsolidated sand, and hence, the average coefficient of earth pressure, Ks, surrounding the pile shaft. The program S-Pile is presented in Appendix B.

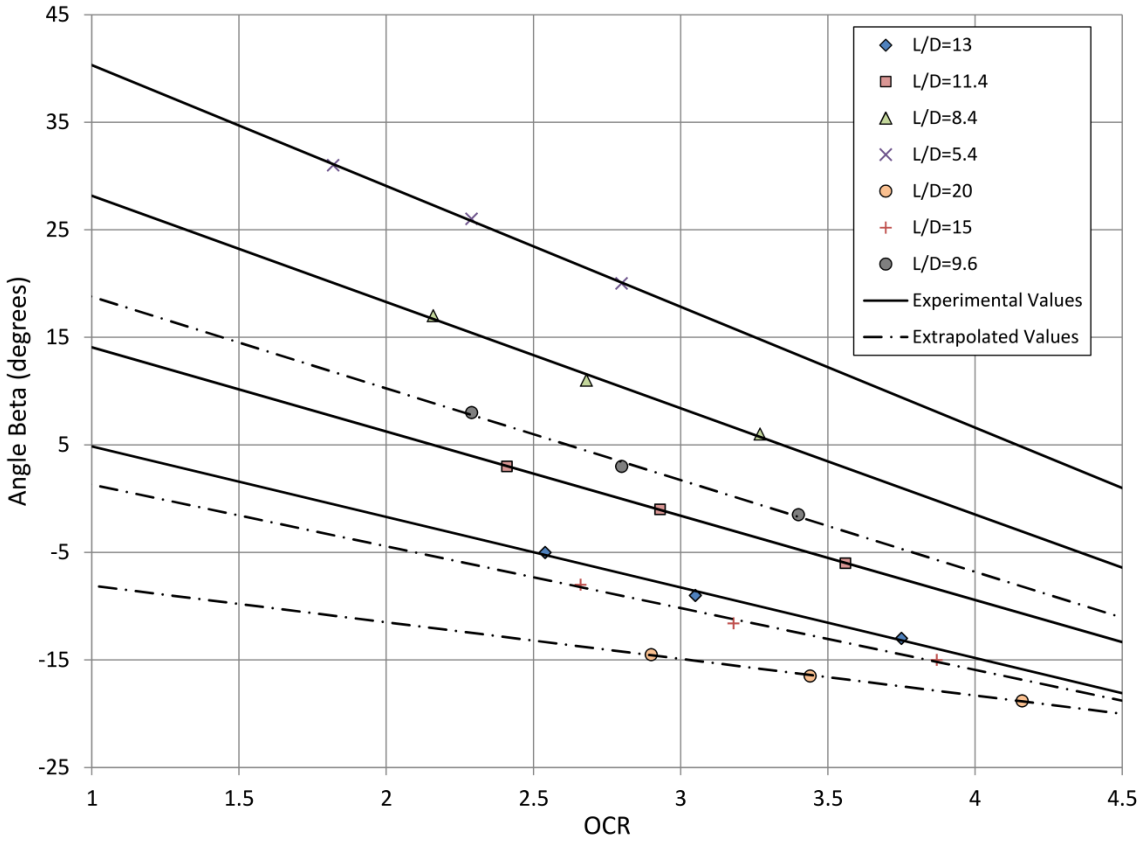

Figure 4.8 Angle Beta as a function of OCR and L/D

With knowledge of the insitu stresses, soil properties and the pile geometry, the computation of Q_s can be done with the application of the model presented in this section. The corresponding coefficient of earth pressure at the pile shaft in overconsolidated sand K_s^{oc} can be determined from the predicted values of Q_s as follows:

$$K_s^{oc} = \frac{2Q_s}{\gamma' L(\tan\delta) A_s} \tag{4.20}$$

where

L= embedment length

δ = angle of friction between pile shaft and sand

A_s = area of embedded shaft

γ' = effective unit weight of the sand

4.3 Model Validation

Recall from section 4.2 that only the results from series A-20, A-30 and A-40 were used in order to establish a relationship between the angle beta, the aspect ratio, and *OCR*. In this section the results of the experimental test obtained in series B-20 and B-40 will be used to assess the predictive value of the proposed model.

For a given pile load test, the verification process consists of the following steps:

1. Determine the experimental value of the average overconsolidation ratio down to nominal depth from the database generated during analysis.
2. For the given value of relative depth and the value of OCR from step one, determine the angle Beta from Figure 4.8
3. Input the averaged soil properties generated by the data base along with the angle beta into the program S-PILE containing the mathematical computations of the model and obtain a value for Q_s
4. Compare the model results with the experimental values of Q_s

5. Repeat the above mentioned steps for the next pile load test

The model results used for validation as well as the experimental results are presented in Table 4.1.

Table 4.1 Model validation

Pile Test	Depth (mm)	Relative depth, L/D	Average OCR down to nominal depth	Angle Beta, β (degrees) (figure 4.8)	Model Shaft Resistance, Q_s (kgf)	Measured Shaft Resistance, Q_s (kgf)	Percent difference %
B-20-1	276.2	9.6	1.82	11.8	3.61	3.4	5.8
B-20-2	426.23	14.9	2.16	-5.3	12.6	11.9	5.6
B-20-3	577.25	20.1	2.43	-13	30.1	27	10.3
B-40-1	276.33	9.6	2.81	3.6	6.24	6.1	2.2
B-40-2	426.59	14.9	3.24	-11.2	21.4	19.3	9.8
B-40-3	575.41	20.1	3.56	-17	49.25	46	6.6

The results in Table 4.1 are depicted graphically in Figures 4.9 and 4.10 for the B-20 test series and B-40 test series, respectively. It should be noted that the predictions of the proposed method are in good agreement with the experimental results. The deviation of the predicted results from the experimental data, as the aspect ratio becomes greater than fifteen, can be seen as evidence of the presence of a critical depth in overconsolidated sand. Furthermore, Figure 4.9 shows that values generated by the proposed method at higher average overconsolidation ratios (B-40 Series) come closer to the experimental results for aspect ratios greater than 15. However, the effects of overconsolidation on the critical depth are beyond the scope of this thesis.

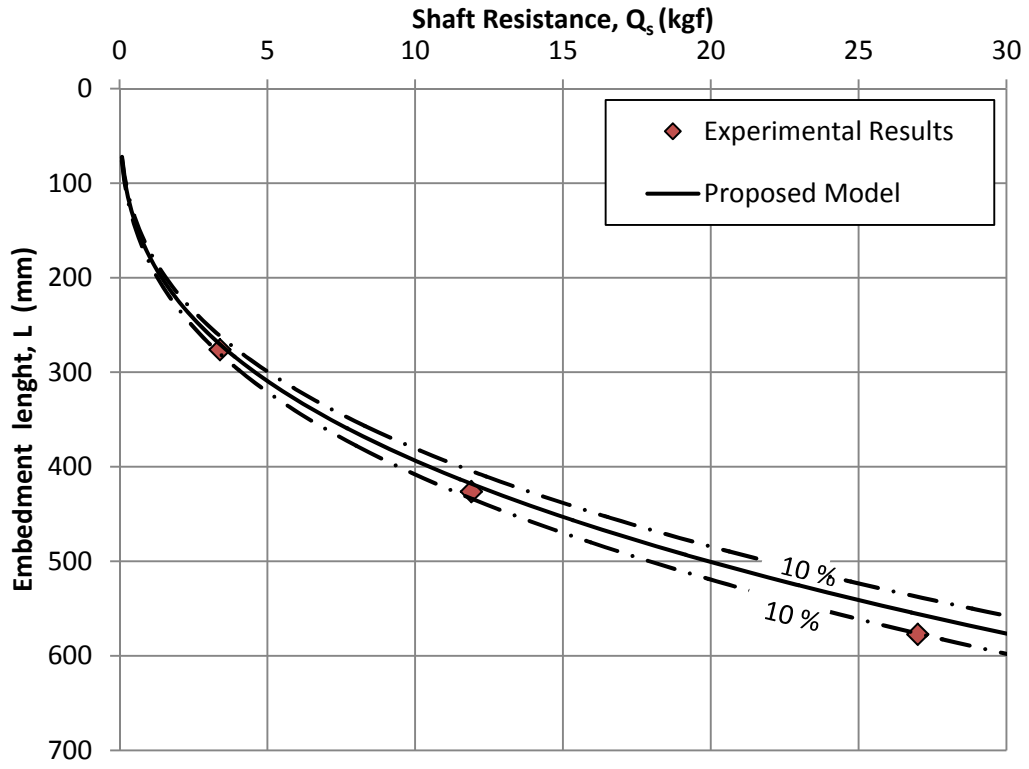

Figure 4.9 Model validation with series B-20

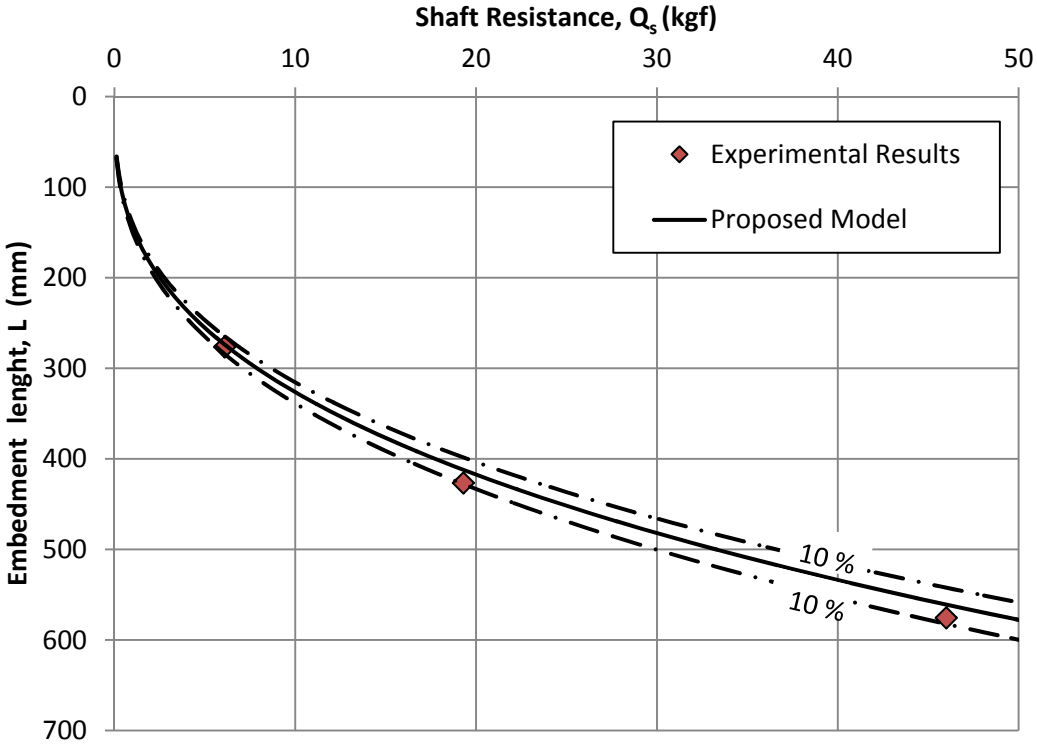

Figure 4.10 Model validation with series B-40

The model can now be used to generate a generalized design chart to aid with the determination of the angle Beta as a function of OCR for L/D values ranging from 10 to 20 at 2.5 intervals (Figure 4.39). Figure 4.11 was developed by interpolation, using the experimental results with trend lines of load versus depth of embedment. Furthermore, the variations of the coefficient of earth pressure, K_s^{oc}, for a given OCR, L/D and friction angle for loose to medium dense sands can now be determined from back calculations using Eq. 4.19. These variations are presented in Figure 4.12 to 4.15 for friction angles ranging from 30^o to 36^o. The plots on these figures were develop using the semi empirical model developed herein.

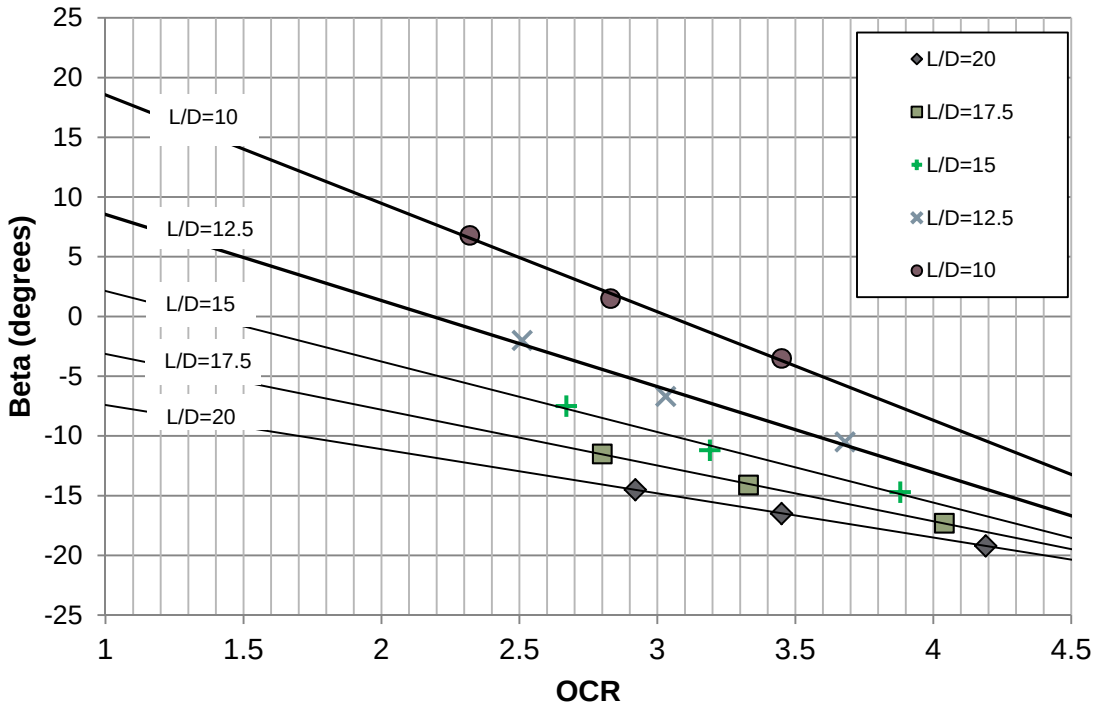

Figure 4.11 Angle Beta versus OCR for various L/D values

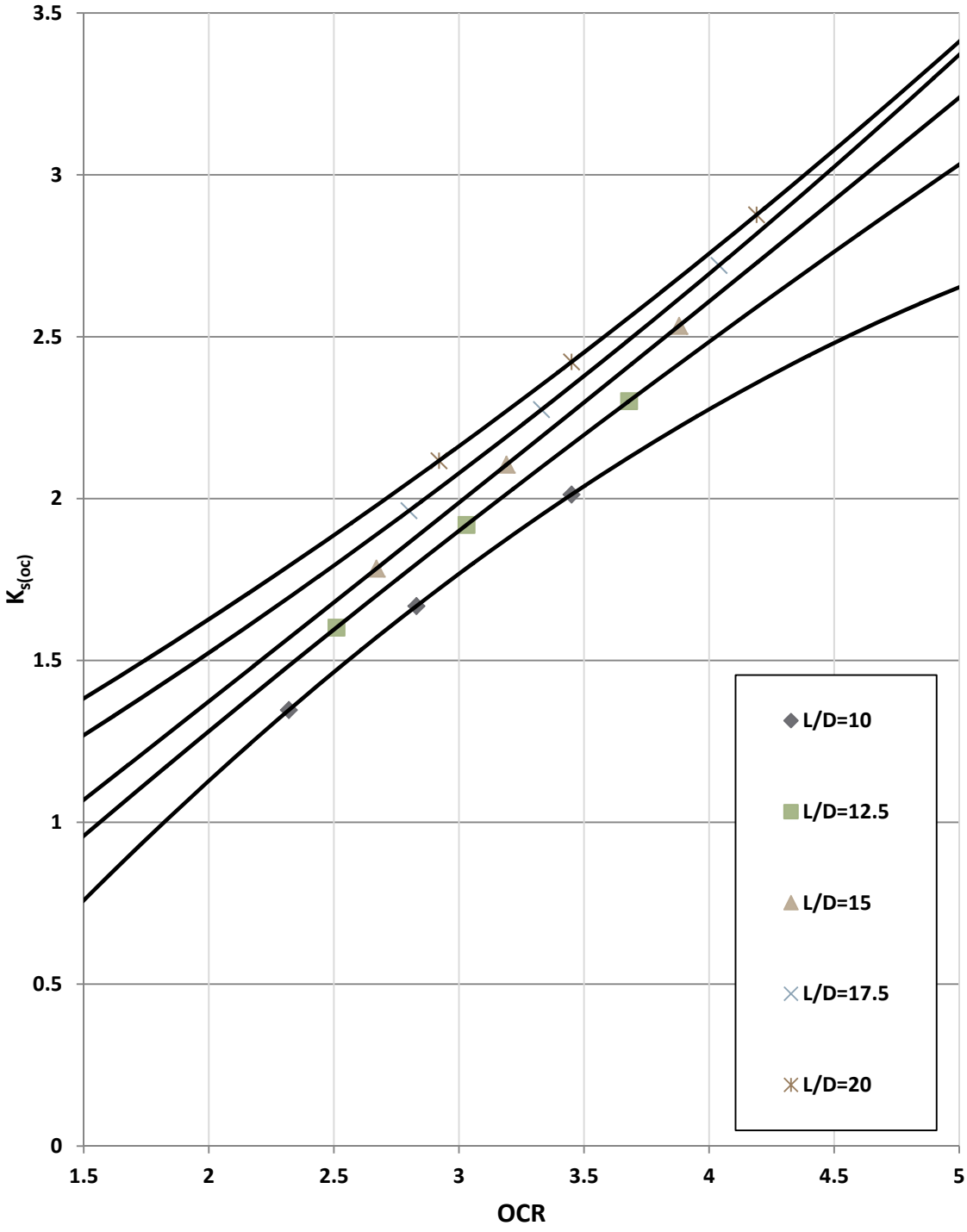

Figure 4.12 Ks(oc) versus OCR for various L/D values ($\phi = 30^o$)

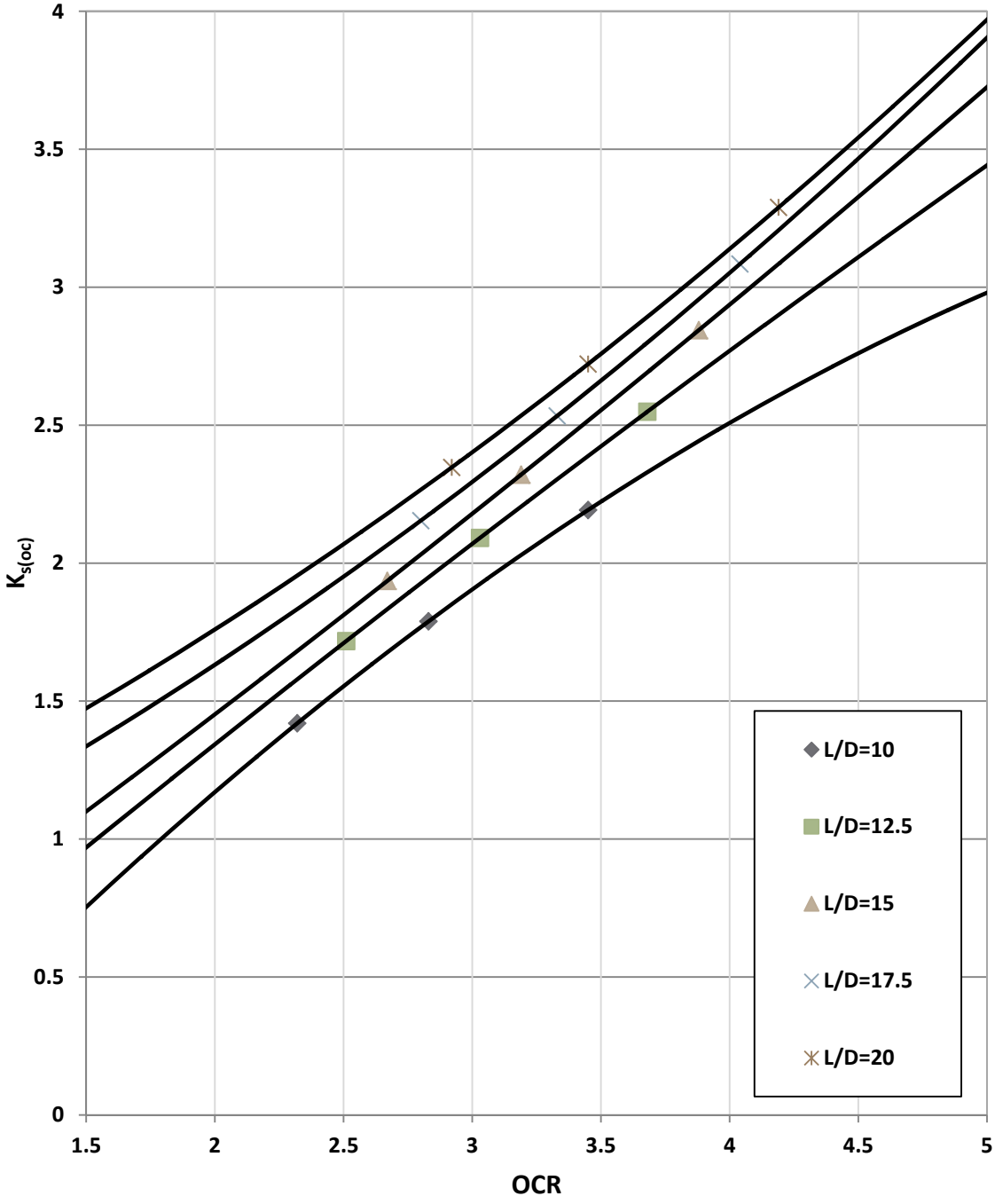

Figure 4.13 Ks(oc) versus OCR for various L/D values ($\phi = 32^o$)

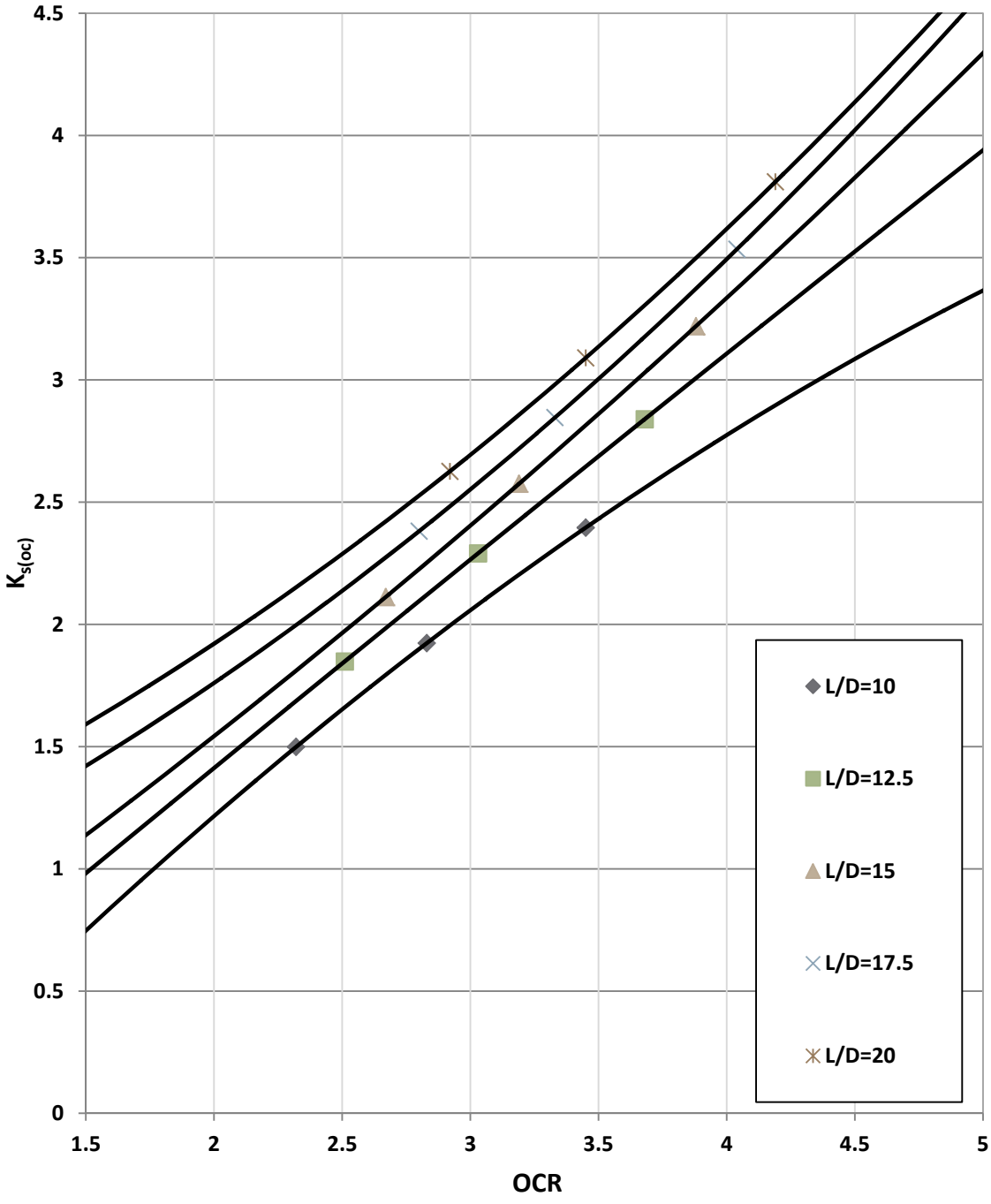

Figure 4.14 Ks(oc) versus OCR for various L/D values ($\phi = 34^o$)

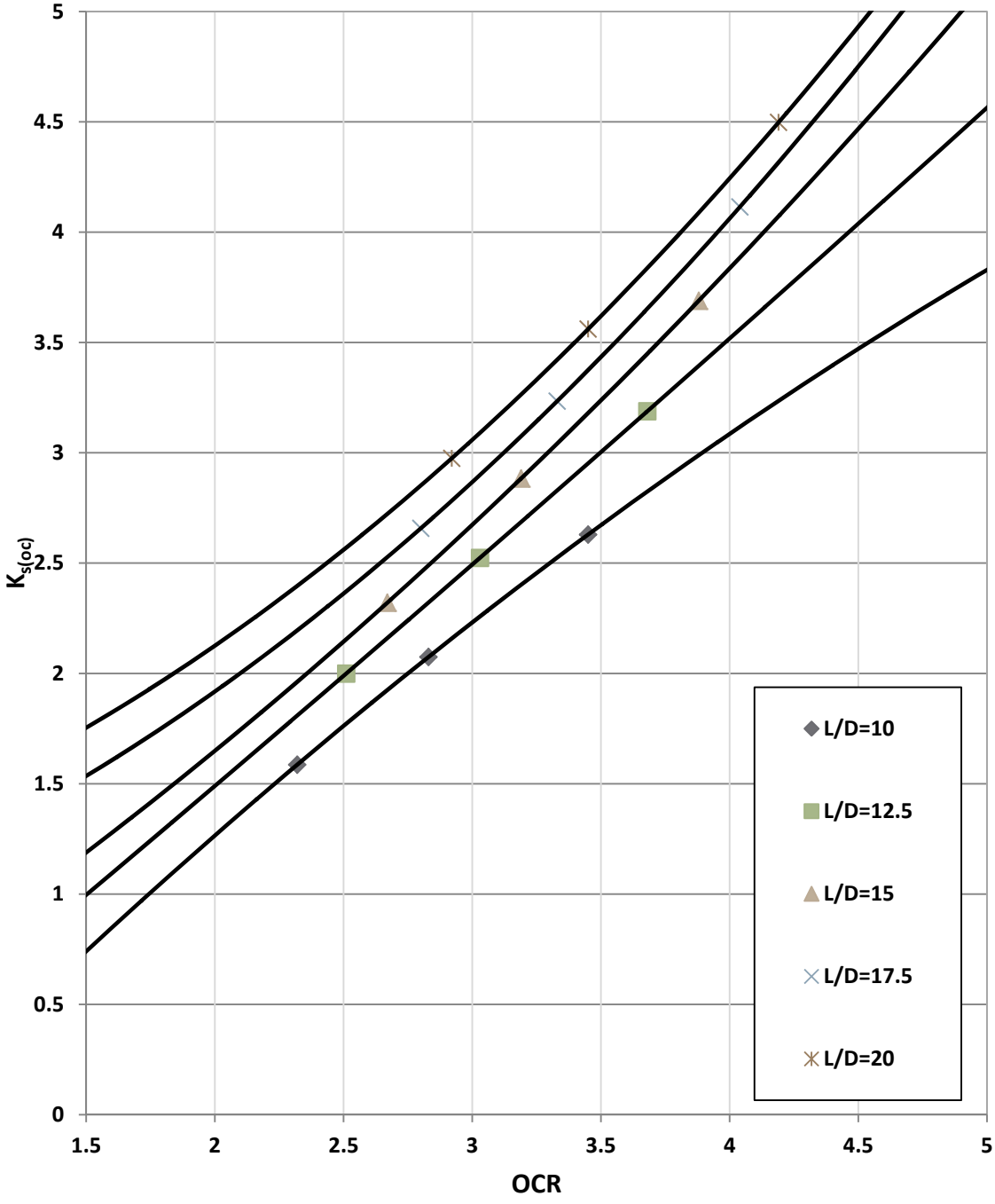

Figure 4.15 Ks(oc) versus OCR for various L/D values ($\phi = 36^o$)

4.4 Design Procedure

The proposed model for the estimation of shaft resistance of driven piles in overconsolidated sand can be implemented by taking the following steps:

1. Determine the length of embedment (L) and diameter (D) of the pile to be used
2. Estimate the average friction angle of the sand deposit down to the nominal depth (L) by direct shear tests or correlations for CPT or SPT tests
3. Determine the friction angle of the sand deposit at the pile tip elevation as in step 2
4. Determine the average unit weight of the sand deposit down to the nominal depth (laboratory tests)
5. Determine the average overconsolidation ratio of the deposit down to the nominal depth by iteration of the following equations:

$$K_{o(oc)} = (1-\sin\phi)OCR^{(1-\sin\phi)} \qquad \text{Mayne and Kulhawy (1982)}$$

$$K_{o(oc)} = 0.192(q_c / p_a)^{0.22}(\sigma'_{vo} / p_a)^{-0.31}OCR^{(0.27)} \qquad \text{Mayne (1995)}$$

   For a given friction angle, q_c, σ'_{vo}, and p_a, vary OCR until the values of $K_{o(oc)}$ are in close agreement; repeat this steps with depth and average the OCR values
6. Based on the values of $OCR_{(ave)}$ and the relative depth (L/D), determine the angle Beta from Figure 4.11.
7. Run the program S_PILE presented in Appendix B and enter the parameters obtained in steps 1 through 6 when prompt.
8. Read the output value for Q_s

Alternatively, Qs may be determined using the charts presented in Figures 4.12 to 4.15 by the following procedure:

1. For a given average friction angle, overconsolidation ratio and L/D enter the appropriate chart and read the value of $K_{s(oc)}$
2. Once the value of Ks is known, the beta method can be implemented to calculate the shaft resistance Qs using Eq. 4.20

Chapter 5

Conclusions and Recommendations

5.1 General

The conclusions drawn from the present investigation are summarized herein. Recommendations for future work are also presented in this chapter.

5.2 Conclusions

The experimental results of this investigation were used to develop a semi-empirical model in order to examine the mechanism that governs the development of shaft resistance of driven piles in overconsolidated sand. The following can be concluded:

1. The effects of stress history of sand on the shaft resistance of driven piles are ignored by conventional design methods in the literature.
2. The relative depth (L/D) has an effect on the average unit shaft resistance of driven piles in overconsolidated sand since the unit shaft resistance increases with an increase of L/D for a given insitu state of stress.
3. The relative depth has an effect on the coefficient of earth pressure K_s developed around the pile's shaft.
4. The stress history of the sand mass has a significant effect on the shaft resistance of driven piles. For a given relative depth (L/D) the shaft resistance increases without a significant increase in friction angle as the OCR increases.
5. The stress history of the sand mass has an effect on the coefficient of earth pressure, K_s, developed around the pile's shaft during driving.

6. An axisymmetric theoretical model which takes into account the variable mobilization of shear resistance and the inclination along the terminal radial surface was developed to predict the shaft resistance of driven piles in overconsolidated sands.
7. Considerations of the effects of stress history of sand can have a significant economic impact when designing driven piles in cohesionless soils

5.3 Recommendations for Future Research

The effect of stress history has been at large excluded from conventional formulations for computing the skin resistance of driven piles in sand due to the complexity of the mechanisms which govern the development of stresses surrounding the pile shaft. The work presented herein serves as a starting point for the development of a method of analysis that incorporates the effects of locked in stresses in a soil mass on the coefficient of earth pressure (K_s) around the shaft of a driven pile. In order to arrive at a general bearing capacity theory for deep foundations in sand that incorporates stress history, the following is recommended for future research:

1. Aside from the pile load tests presented in this thesis, series B tests where pushed to L/D values of 23 where the plots of Beta vs. OCR began to show non-linarites. It is recommended to study the effects of overconsolidation on the critical depth.
2. The model proposed in this study utilizes an empirical method derived from the experimental data to determine the angle Beta and it is found independently from the mechanism below the terminal radial surface. However, a link between shaft and tip resistance is evident since both mechanisms share the terminal radial surface. It is recommended to extend the present study to incorporate the effects

of stress history on tip resistance and to develop a theory which treats shaft and tip resistance as one single mechanism with variable failure surfaces.

REFERENCES

1. Alpan, I. (1967). "The Empirical Evaluation of the Coefficient K_O and K_{OR}, "Journal of Soils and Foundations, Tokyo, Japan, Vol. 7, No. 1, pp. 31-40.
2. Berezantzev, V. G. (1965). "Load Bearing Capacity and Deformation of Piled Foundations" Proceedings, 5th International Conference of Soil Mechanics and Foundation Engineering, Vol. 2, pp. 11-15.
3. Broms, B.B and Silberman, J.O. (1964), "Skin Friction Resistance for Piles in Cohesionless Soils", Sols-Soils No. 10, pp. 33-43.
4. Brooker, E. W., and Ireland, H. O. (1965). "Earth Pressure at rest Related to Stress History," Canadian Geotechnical Journal, Vol. 2, No. 1, pp. 1-15
5. Coulomb, C. A., (1776). "Essai sur une Application des Regles des Maximum et Minimum a quelques Problemes de Statique," Memoire Academie Royale des Sciences, 7. Paris.
6. Donath, A. (1891). "Untersulchengen Uber den Erdruck auf Stutzwande." Zeitsghrift fur Bawesen, 41 pp: 491-518.
7. Dorr, H. (1922). "Die Tragfaehigkeit der Pfaehle", Verlag W. Ernst & Sohn, Berlin.
8. Duncan, J. M., and Seed, R. B. (1986). "Compaction-Induced Earth Pressure under Ko Conditions," Journal of Geotechnical Engineering Division, ASCE, Vol. 112, No. GT1, pp. 1-22

9. Durgunoglu, H.T. and Mitchell, J.K. (1973), "Static penetration resistance of Soils", Space Science Laboratory, Series 14, Issue 24, University of California, Berkeley, CA.
10. Hanna, A. M. and Afram, A. (1986). "Pull-out Capacity of Single Piles in Sand", Canadian Geotechnical Journal, Vol. 23, No.3, pp 387-392.
11. Hanna, A. M. and Al-Romhein, R. (2008). "At-Rest Pressure of Overconsolidated Cohesionless Soil" Journal of Geotechnical and Geoenvironmental Engineering, ASCE, Vol. 134, No. 3, pp. 408-412.
12. Hanna, A. M. and T. Q. Nguyen (2002). "An Axisymmetric Model for Ultimate Capacity of a Single Pile in Sand", Soils and Foundations, Vol. 42, No.2, pp. 47-58.
13. Hanna, A. M., and Ghaly, A. M. (1992), "Effects of Ko and Overconsolidation on Uplift Capacity," Vol. 118 No.9 SEP, pp. 1449-1469
14. Hanna, A. M., and Khoury. A. (2005). "Passive Earth Pressure of Overconsolidated Cohesionless Backfill", Journal of geotechnical and Geoenvironmental Engineering, ASCE, Vol. 131, No. 8,pp.978-986.
15. Hendron, A, J. (1963), "The Behaviour of Sand in One-Dimensional Compression", PhD Thesis, University of Illinois at Urbana Campaign, Urbana,III.
16. Jaky, J. (1944). "The coefficient of Earth Pressure at Rest," Journal of the Society of Hungarian Architects and Engineers, pp. 335-358.
17. Jaky, J. (1948). "Prssure in Soils," Proceedings. 2nd International Conference on Soil Mechanics and Foundation Engineering, Vol. 1, pp. 103-107.

18. Janbu, N. (1976), “Static Bearing Capacity of Friction Piles”, Proceedings, 6th European Conference of Soil Mechanics and Foundation Engineering, Vol. 1.2, pp. 479-488.
19. Janbu, N. and Senneset, K. (1974), “ Effective Stress Interpretation of In-Situ Static Penetration Tests”, Proceedings, European Symposium on Penetration Testing, Stockholm, Vol. 2.2, pp.181-193.
20. Mayne, P.W (1995) “CPT determination of OCR and lateral stresses in clean quartz sands" Proceedings, International Symposium on Cone Penetration Testing, Vol. 2. Linkoping, Swedish geotechnical Society, pp. 215-220.
21. Mayne, P.W., and Kulhawy, F.H. (1982). “K_O-OCR Relationship in Soil,” Journal of Geotechnical Engineering Division, ASCE, Vol. 1080 No. GT6, pp. 851-872.
22. McClelland, B. et al (1967). “ Problems in Design and Installation of Heavy Loaded Pipe Piles”, Proc. Conf. Civil Engr. In the Oceans, ASCE, pp.601-634.
23. Meyerhof, G. G. (1951). “The Ultimate Bearing Capacity of Foundations”, Geotechnique, Vol.2, pp 301-322.
24. Meyerhof, G. G. (1973). “Uplift Resistance of Inclined Anchors and Piles”, Proceedings, 8th International Conference on Soil Mechanics and Foundation Engineering, Moscow, Vol.2.1, pp. (167-172).
25. Meyerhof, G.G. (1976), “Bearing Capacity and Settlement of Pile Foudations”, Jnl. Geot. Engr. Div., ASCE, Vol. 102, No. GT3, pp. 195-228.
26. Mueller, R. (1939), “Modellversuche ueber das Zusammenwirken von Pfaehlen”, Veroeff. Des Inst. Der Deutschen Forschungsges. f. Bodenmech. (Degebo) an der Techn. Hochsch. Berlin, Vol. 7, pp. 9-27.

27. Nguyen, T. Q. (1991), “A Three Dimensional Model for Vertical Piles in Sand. PhD Thesis, Concordia University, Canada.

28. Rankine, W. J. M, (1857). “On the Stability of Loose Earth,” Trains Royal Soc., London, Vol. 147.

29. Sarma, S.K (1979), “Stability Analysis of Embankments and Slopes”, Jnl. Geot. Engr. Div., ASCE, Vol. 105, No. GT12, pp.1511-1524.

30. Schmidt, B. (1966). Discussion of “Earth Pressure at Rest Related to Stress History,” Canadian Geotechnical Engineering Division, ASCE, Vol. 3, No. 4, pp. 148-161.

31. Sherif, A. M., and Mackey, R. D. (1977). “Pressure on Retaining Walls with Repeated Loading,” Journal od Geotechnical Engineering Division, ASCE, Vol. 103, No. GT11, pp.1341-1345.

32. Skempton, A. W. et al (1953). “Theorie de la Force Portante des Pieux”, Annales de l’Institut Technique du Batiment et les Traveaux Publics, No. 63-64, pp. 285-289.

33. Terzaghi, K. (1943). “Theoretical Soil Mechanics” Wiley, New York, NY.

34. Terzaghi, K. (1948). “Theoretical Soil Mechanics in Engineering Practices”. Wiley New-York.

35. Tomlinson, M. (2008), “Pile Design and construction Practice” Taylor and Francis, New York, NY.

36. Vesic, A. S. (1967). “Design of Pile Foundations”, Synthesis of Highway Practice No. 42, Transportation Research Board, National Research Council, Wachington, USA.

37. Wroth, C. P. (1975). “In Situ Measurements on Initial Stresses and Deformations Characteristics,“ Proceedings, In Situ Measurements of Soil Properties, ASCE, Vol. 2, pp. 181-230.

Appendix A

Soil Properties

Specific Gravity of Soil Solids

Applicable ASTM Standard: ASTM D-854

Note to the Reader: The experiments conducted in the determination of sand properties and presented herein comply with ASTM standards to the extent permitted by the equipment available in the facilities at Concordia University.

Equipment:

1. Volumetric flask (500ml)
2. Balance sensitive to 0.1 g
3. Vacuum Pump
4. Thermometer sensitive to 0.1 °C

Definition:

The Specific gravity (G_s) of a soil sample is defined as the ratio of the weight of a given volume of soil solids to the weight of an equal volume of water at 20° C.

Procedure:

The weight of a volume of water equal to that of soil solids was obtained, with the use of a scale, by displacement. A flask is filled with de-aired water so that the bottom of the meniscus is at the 500ml mark and then weighted. A sample of soil between 100 and 120 grams in mass is placed in the flask containing water. The soil-water mixture is de-aired

once again and the volume is adjusted to the 500ml mark. The soil-water mixture is weighed and the specific gravity of soil solids can be obtained from the following correlations.

$$G_s = \frac{\gamma_s}{\gamma_w} = \frac{\frac{W_s}{V_s}}{\frac{W_w}{V_w}}$$

Since the volume of water equals the volume of soil solids, the above relation reduces to the following:

$$G_s = \frac{W_s}{W_w}$$

The weight of water is determined as follows:

$$W_w = W_{f+w} - \left(W_{f+w+s} - W_s\right)$$

The values for specific gravity are usually reported on the value of density of water at 20°C. A correction factor α is used to obtain the specific gravity of soil solids at the reference temperature in the following correlation:

$$G_{s@20^\circ C} = \alpha \times G_{s@T}$$

The correction factor corresponding to the temperature can be obtained by interpolation on Table A1.

Table A. 1 Correction factor vs. temperature

Temperature (T°C)	α
16	1.0007
17	1.0006
18	1.0004
19	1.0002
20	1.0000

The experimental results for Silica Sand 4010 are shown on Table A2.

Table A. 2 Experimental Results for Silica Sand 4010

Item	Test No. 1	Test No. 2
Mass of flask + water, W_{f+w} (g)	654.16	654.26
Mass of flask + soil + water, W_{f+w+s} (g)	723.19	727.84
Mass of soil solids, W_s (g)	112.02	118.83
Mass of water, $W_{f+w} - \left(W_{f+w+s} - W_s\right)$ (g)	42.99	45.25
Temperature of soil + Water (°C)	18.7	18.8
Correction factor, α	1.00023	1.00021
$G_{s(T)}$	2.606	2.626
$G_{s(20^\circ C)} = \alpha \times G_{s(T)}$	2.607	2.627

$$\text{Average } G_{s@20^\circ C} = \frac{2.607 + 2.627}{2} = 2.62$$

Relative Density

Applicable ASTM Standard:

- ASTM D 4254- Standard Test Methods for Minimum Index Density and Unit Weight of Soils and Calculation of Relative Density
- ASTM D-4253-Standard Test Methods for Maximum Index Density and Unit weight of Soils Using a Vibratory Table

Note to the Reader: The experiments conducted for the determination of sand properties presented herein complied with ASTM standards to the extent permitted by the equipment available in the facilities at Concordia University.

Equipment:

5. Compaction mold
6. Surcharge weight
7. Surcharge plate
8. Balance sensitive to 1 g
9. Vibrating table
10. Caliper

Definition:

Relative density is the ratio of the difference between the void ratios of a cohesionless soil in its loosest state and existing natural state to the difference between its void ratios in the loosest and densest state.

$$D_r = \frac{e_{\max} - e}{e_{\max} - e_{\min}} \times 100$$

Corresponding to a given void ratio, a dry unit weight can be found and the above relation can be rewritten as follows:

$$D_r = \left(\frac{\gamma_d - \gamma_{d\_\min}}{\gamma_{d\_\max} - \gamma_{d\_\min}} \right) \times \frac{\gamma_{d\_\max}}{\gamma_d}$$

Procedure:

The purpose of this test is to determine the dry unit weights of Silica Sand in its loosest and densest states. To obtain the minimum unit weight (loose condition) the mold was filled with soil as loosely as possible by pouring the soil through a funnel from a height of one inch above the soil surface in a gentile circular fashion. After trimming the excess soil with a straight edge, the unit weight was obtained from the mass and volume of the sample. The procedure is depicted and results are summarized herein.

Table A. 3 Mold Dimensions

Item	Measurement			Average
Diameter of Mold (mm)	151.12	151.27	152.24	151.5433
Height of Mold(mm)	152.75	152.58	152.53	152.62

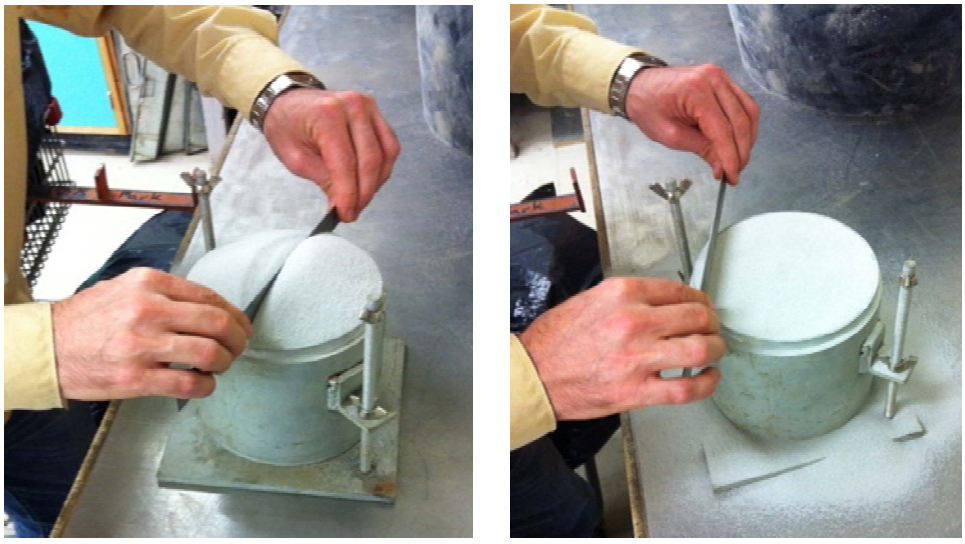

Figure A- 1 Relative density Tests (minimum

Table A. 4 Data and Results

Item	Silica 4010
Mass of mold (kg)	6.654
Mass of mold plus soil (kg)	10.577
Mass of soil (kg)	3.923
Volume of soil (m^3)	0.0027527
Area of mold (m^2)	0.018
Minimum Unit Weight (kN/m^3)	**13.98**

In order to determine the maximum dry unit weight (densest state), the mold was filled once again to the rim but this time, the sides of the mold were struck with a rubber mallet to settle the soil and give room for the loading plate and surcharge load placement. Once assembled, the set up was clamped to the vibrating table and allowed to run for 8 minutes. A record of the settlement was measured with the use of a caliper so that volume calculations could be done. The set up was vibrated again and subsequent measurements of settlement were taken thereafter at 4 minute intervals. A plot of Unit weight vs. time shaken was developed which resulted on an asymptotical approach to the value of maximum dry unit weight. After the maximum settlement was obtained the mold-soil mass was recorded and the maximum dry unit weight was determined. It should be noted that the duration of vibration was increased in by minute intervals from that of 8 minutes recommended by the ASTM standard due to slight differences in the equipment available, such as frequency of vibration of the shaking table and surcharge load applied. Illustrations of the setup as well as results are shown below.

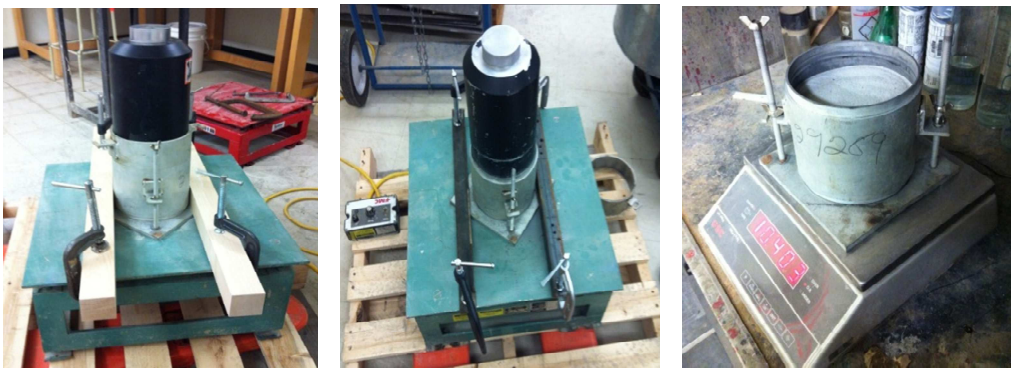

Figure A- 2 Relative Density Test (maximum)

Table A. 5 Initial measurements

Item	Silica 4010
Surcharge Mass (kg)	13.03
Surcharge Plate Mass(kg)	1.81
Surcharge Plate Thickness (mm)	
Initial Height of Sample (mm)	139.7367
Mass of Mold plus Soil (kg)	10.403
Mass of Mold (kg)	6.654
Mass of Soil (kg)	3.749
Initial Unit weight	14.62182

The height of the sample at the end of each vibration cycle was measured by subtracting the readings from the top of the mold plus the thickness of the surcharge plate, which was placed between the surcharge and the soil, from the height of the mold. The results are tabulated on Table 4.

Table A. 6 Maximum Dry Unit Weight Data and Results for Silica 4010

Duration of Vibration (min)	Height of sample (mm)	Volume (m^3)	Unit weight (kN/m^3)
0	139.74	0.002515	14.62
8	122.26	0.002201	16.71
12	120.68	0.002172	16.93
16	119.48	0.002151	17.10
20	119.16	0.002145	17.15
25	119.04	0.002143	17.16

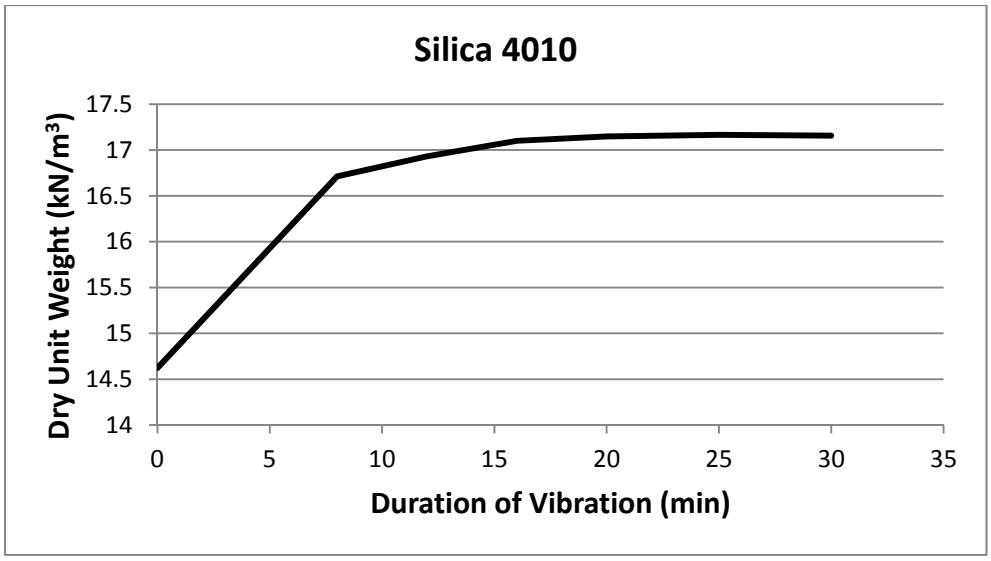

Figure A- 3 Maximum unit weight vs. duration of vibration

Table A. 7 Maximum Dry Unit Weight Data and Results for Silica 4010

Duration of Vibration (min)	Height of sample (mm)	Volume (m^3)	Unit weight (kN/m^3)
0	139.7367	0.002515	14.48532
8	118.3367	0.00213	17.10484
12	118.0642	0.002125	17.14432
16	117.6092	0.002117	17.21065
21	117.5417	0.002116	17.22053

Sieve Analysis

Applicable ASTM Standard:

- ASTM C136- Test for sieve or screen analysis of fine and coarse aggregates.

Note to the Reader: The experiments conducted for the determination of sand properties presented herein comply with ASTM standards to the extent permitted by the equipment available in the facilities at Concordia University.

Equipment:

1. Stack of sieves including pan and cover

2. Balance sensitive to 0.1g
3. Mechanical sieve shaker

Scope:

The standard sieve analysis test determines the grain size distribution present, among certain ranges, on a representative sample of soil. Grain size analysis is widely used in classification of soils.

Procedure:

The sieves to be used were weighted individually and then properly stacked with the sieves with larger openings above the ones with smaller openings with the pan being at the bottom. A representative sample of soil was weighted and placed in the top sieve. With the cover on, the stack was set to run in the mechanical shaker for ten minutes. The amount retained by weight on each sieve was recorded with the use of a balance. The following figures and tables depict the results.

Table A. 8 Sieve Analysis Results for Silica Sand 4010 (test 1)

U.S Sieve #	Opening (mm)	Mass of each Sieve (g)	Mass of each Sieve plus Soil Retained (g)	Mass of Soil Retained on each Sieve (g)	Cummulative Mass Retained above each Sieve (g)	Percent Finer
30	0.6	422.6	425.4	2.8	2.8	99.55
40	0.425	404.8	475.6	70.8	73.6	88.06
50	0.3	379.1	548.1	169	242.6	60.65
80	0.18	362	641.2	279.2	521.8	15.36
100	0.15	360.3	405.7	45.4	567.2	7.99
140	0.106	348.7	383.8	35.1	602.3	2.30
200	0.075	342.5	352.8	10.3	612.6	0.63
Pan		379.9	383.8	3.9	616.5	0

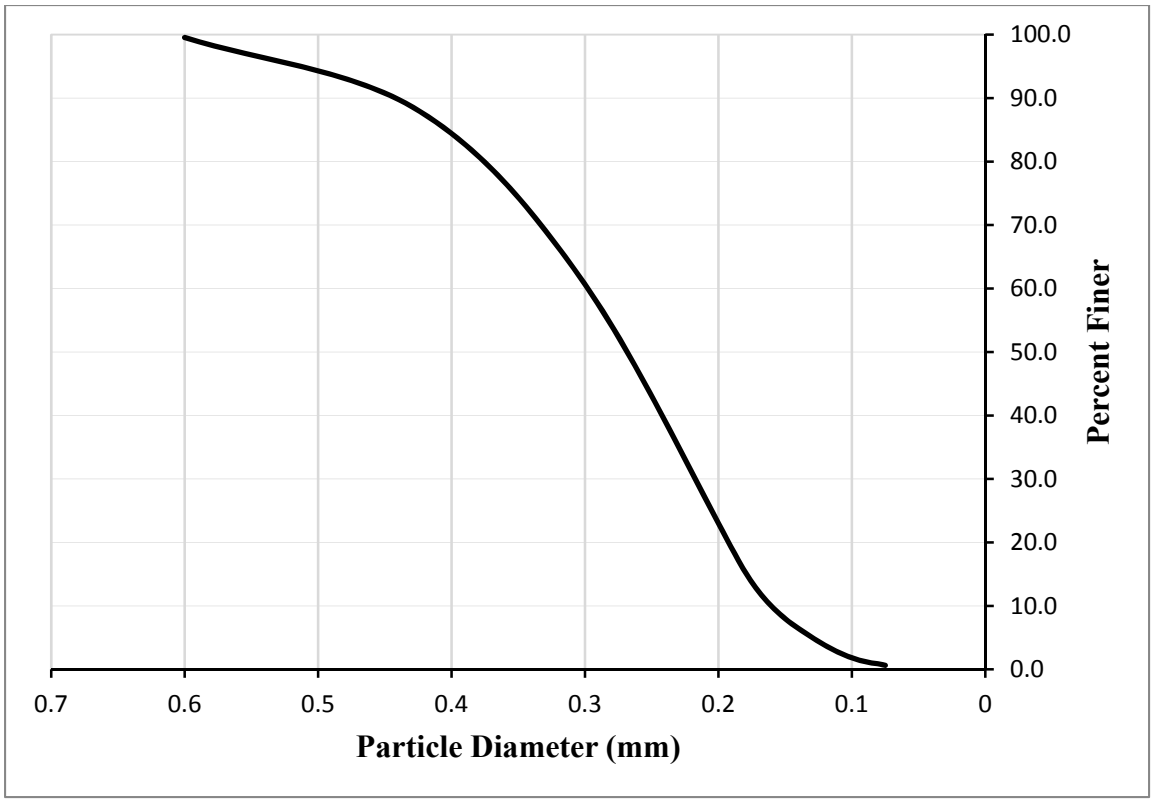

Figure A- 4 Particle Size Distribution for Silica Sand 4010

Table A. 9 Sieve Analysis Results for Silica Sand 4010 (test 2)

U.S Sieve #	Opening (mm)	Mass of each Sieve (g)	Mass of each Sieve plus Soil Retained (g)	Mass of Soil Retained on each Sieve (g)	Cumulative Mass Retained above each sieve (g)	Percent Finer
30	0.6	422.6	425.1	2.5	2.5	99.65
40	0.425	404.8	473	68.2	70.7	90.12
50	0.3	379.1	553.1	174	244.7	65.81
80	0.18	362	697.4	335.4	580.1	18.95
100	0.15	360.3	420.8	60.5	640.6	10.49
140	0.106	348.7	400.2	51.5	692.1	3.30
200	0.075	342.5	358.8	16.3	708.4	1.02
Pan		379.9	387.2	7.3	715.7	0

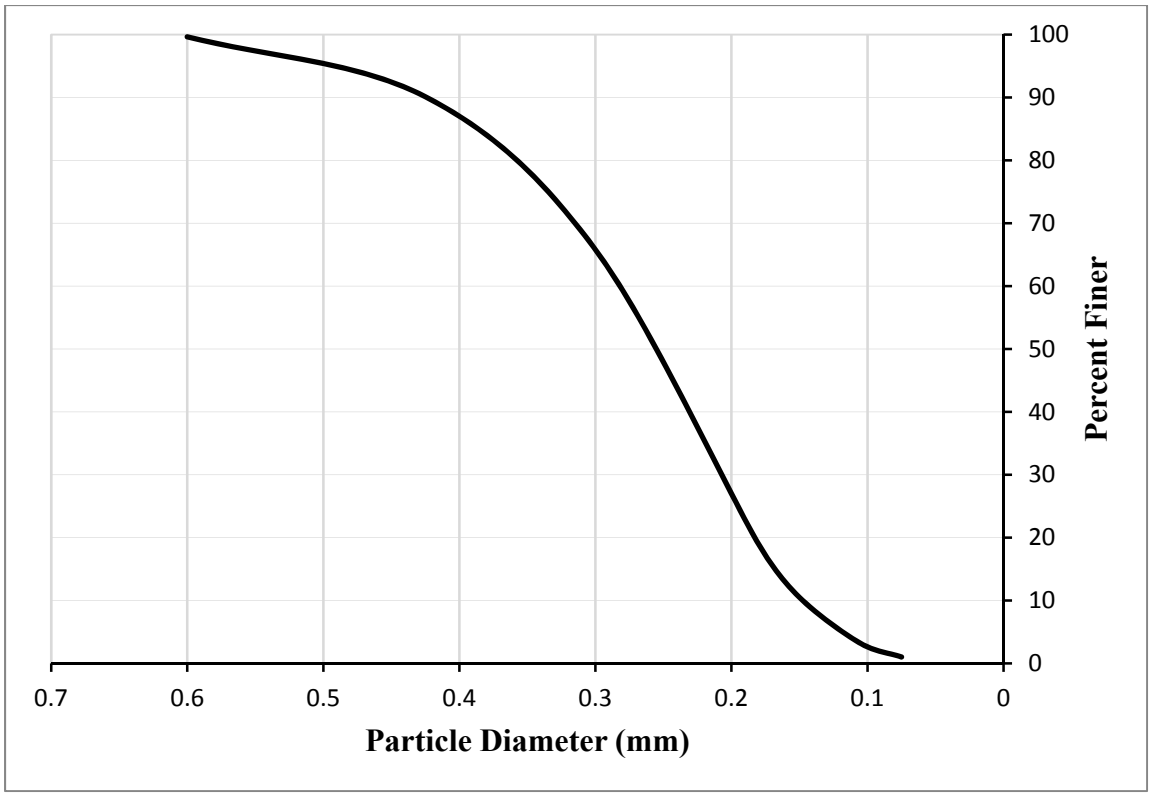

Figure A- 5 Particle size Distribution for Silica sand 4010 (test 2)

Table A. 10 Properties of Silica 4010

Property	Test 1	Test 2	Average
D_{10} (mm)	0.160	0.149	0.155
D_{30} (mm)	0.218	0.207	0.213
D_{50} (mm)	0.27	0.255	0.26
D_{60} (mm)	0.299	0.282	0.291
Coefficient of uniformity (C_u)	-	-	1.88
Coefficient of curvature (C_c)	-	-	1.01
Soil Classification (USCS)	-	-	SP

Appendix B

Program S-PILE

```
// S-PILE.cpp : Defines the entry point for the console application.
#include "stdafx.h"
#include "iostream"
#include "math.h"
using namespace std;
//The following program computes the total shaft resistance on a driven pile in
overconsolidated sand//
 int main(int argc, char* argv[])
{
       double D;
       double L;
       double Phi_Ave;
       double OCR_Ave;
       double Gamma_Ave;
       double Beta;
       double Rot_Angle;
       double R_inf;
       double Pi=3.14159265;
       double Phi_L;
       double Seg_DE;
       double Seg_CD;
       double Area_ACDE;
       double Centroid_X_onACDE;
       double Centroid_Y_onACDE;
       double Dist_centroid_X_to_axis;
       double Gamma_centroid_Y;
       double Ko,Kt,Ko_ocr,Ks;
       double Phi_Beta;
       double W3;
       double Delta_E1;
       double R_radial_component;
       double R;
       double Delta_E2_1;
       double Delta_E2_2;
       double Delta_E2_3;
       double Denominator;
       double Delta_E2;
       double Qs;
        std::cout<<"Enter the nominal depth, L \n";
        std::cin>>L;
        std::cout<<"Enter the pile Diameter\n";
        std::cin>>D;
        std::cout<<"Enter the average friction angle of the sand mass down to the
nominal depth\n";
        std::cin>>Phi_Ave;
        Phi_Ave=(Pi*Phi_Ave)/180;
        std::cout<<"Enter the friction angle of the sand mass at the nominal
depth\n";
        std::cin>>Phi_L;
        Phi_L=(Pi*Phi_L)/180;
        std::cout<<"Enter the average overconsolidation ratio down to the nominal
depth\n";
```

```
        std::cin>>OCR_Ave;
        std::cout<<"Enter the average unit weight down to the nominal depth\n";
        std::cin>>Gamma_Ave;
        std::cout<<"Enter the central angle of rotation in degrees\n";
        std::cin>>Rot_Angle;
        Rot_Angle=(Pi*Rot_Angle)/180;
        std::cout<<"Enter the  angle Beta\n";
        std::cin>>Beta;
        Beta=(Pi*Beta)/180;
        R_inf=(0.5*(1+((exp(((Pi/2-Phi_Ave/2))*tan(Phi_Ave/2)))/(sin((Pi/4-
Phi_Ave/2))))))*D;
        Seg_DE=R_inf-(D/2);
        Seg_CD=L+(Seg_DE*tan(Beta));
        Area_ACDE=0.5*(L+Seg_CD)*Seg_DE;
        Centroid_X_onACDE=((Seg_DE/3)*(L+(2*Seg_CD)))/((L+Seg_CD));
        Centroid_Y_onACDE=(1/3)*((pow(Seg_CD,3))-(pow(L,3)))/((pow(Seg_CD,2))-
((pow(L,2))));
        Dist_centroid_X_to_axis=Centroid_X_onACDE+(D/2);
        Gamma_centroid_Y=Gamma_Ave; //(approximately the same)
        Ko=1-sin(Phi_Ave);
        Ko_ocr=Ko*(pow(OCR_Ave,(sin(Phi_Ave)-0.18)));
        Kt=Ko;
        Phi_Beta=Phi_Ave/2;
        W3=Area_ACDE*Dist_centroid_X_to_axis*Gamma_centroid_Y*Rot_Angle;
        Delta_E1=0.5*Ko_ocr*Gamma_Ave*(pow(Seg_CD,2))*R_inf*Rot_Angle;

R_radial_component=0.5*Gamma_Ave*Kt*Seg_DE*((((pow(L,2)))+(L*Seg_DE*tan(Beta))
              +(1/3*(pow(Seg_DE*tan(Beta),2)))));
        R=2*(R_radial_component)*(sin(Rot_Angle/2));
        //Sarma
        Delta_E2_1=Delta_E1*(cos(Phi_Beta-Beta)*cos(Phi_Ave));
        Delta_E2_2=W3*(cos(Phi_Ave))*(sin(Phi_Beta-Beta));
        Delta_E2_3=-R*(cos(Phi_Ave))*(cos(Phi_Beta-Beta));
        Denominator=1/(cos(Phi_Beta-Beta+Phi_Ave));
        Delta_E2=(Delta_E2_1+Delta_E2_2+Delta_E2_3)*Denominator;
       Qs=(2*(Pi)/Rot_Angle)*Delta_E2*tan(Phi_Ave);
       Ks=(2*Qs)/(Gamma_Ave*L*tan(Phi_Ave)*L*2*Pi*(D/2));

       std::cout<<"Qs= "<<Qs/0.00980665<< " Kgf"<<endl;
       std::cout<<"\n";
       std::cout<<"Ks= "<<Ks<<endl;
       std::cout<<"\n";
return 0;
}
```